Retrofit modeling for green ships

A data-driven design approach for emission reduction using bunker delivery notes

J. J. M. Hermans

TU Delft

Retrofit modeling for green ships

A data-driven design approach for emission reduction using bunker delivery notes

by

J. J. M. Hermans

to obtain the degree of Master of Science
at the Delft University of Technology,
to be defended publicly on Friday March 1, 2024 at 03:00 PM.

Report number:	MT.23/24.021.M	
Student number:	4486110	
Thesis committee:	Dr. A.A. Kana,	TU Delft, supervisor
	Ir. J. L. Gelling,	TU Delft
	Dr.ir Y. Pang,	TU Delft
	B. O .M. Noble,	TU Delft

An electronic version of this thesis is available at http://repository.tudelft.nl/.

TU Delft

Abstract

Keywords: Retrofit, alternative power and energy, wind-assisted ship propulsion, bunker delivery notes, gray-box modeling

This thesis presents a data-driven design approach for emission reduction using bunker delivery notes (BDNs) to help support the revised IMO strategy to achieve net-zero greenhouse gas emissions by international shipping close to 2050. This research supports the Horizon Europe's Digital Twin for Green Shipping (DT4GS) project which focuses on the development of digital twins (DTs). Part of this project involves the development of a DT-supported method for the design and retrofit of ships. DTs are a promising approach for supporting maritime decarbonization efforts due to their simulation and big data handling capability. Despite the abundance of shipping data and growing digitalization, the potential of using ship operational data for decarbonization efforts remains not fully exploited. A data-driven method such as a DT could fill this gap. However, as DTs, by definition, require real-time connection between a physical entity and the digital representation, developing a true DT for new-build alternatively fueled ship designs remains a challenge. This research thus starts by looking into retrofitting using data from existing ships.

A design framework is proposed to construct digital models to support a DT for retrofitting purpose. The proposed framework is tested on a case-study using a 300-meter bulk carrier. Since January 2019, operational ship data is collected through BDNs, a mandatory data collection method for ships of 5000 GT and above, adopted by the IMO. Constructing a DT based on BDNs is considered to be convenient as it provides a solid source of operational data in the future.

First, the available data from the BDNs is preprocessed using an adopted framework based on data science literature. The resulting 5,678 data points are used for the construction of a model representing the bulk carrier and a model representing the green ship technologies part. A fuel consumption model is constructed to represent the bulk carrier. It utilizes a gray-box modeling approach, consisting of a white-box resistance model and a black-box artificial neural network. Both models incorporate environmental-dependent inputs. The investigated green ship technologies for the potential retrofit are represented by various wind-assisted ship propulsion (WASP) systems, namely a towing kite, a DynaRig sail, and a Flettner rotor. These systems are modeled using a white-box modeling approach, together with available wind data. Using an adopted integration framework, based on the propeller-engine matching procedure, both representations are combined into one green ship digital model.

An environmental assessment is performed using the IMO's EEXI and CII assessment tools, respectively evaluating the design and operational aspects of the potential retrofit. Additionally, a financial assessment is conducted using the payback period. Results showed the design implications and emissions reduction potential of implementing such systems which will guide the retrofit decision by the ship's owner.

Acronyms

AI Artificial intelligence

ALS Air lubrication systems

ANN Artificial neural network

AR Augmented reality

BBM Black-box model

BDA Big data analytics

BDNs Bunker delivery notes

BPNN Backpropagation neural network

CAD Computer aided design

cf Correction factor

CFD Computational fluid dynamics

CII Carbon Intensity Indicator

DBB Design building block

DBSE Document-based systems engineering

DCS Data collection system

DL Deep learning

DLAs Deep learning algorithms

DM Digital model

DS Digital shadow

DT Digital Twin

DT4GS Digital twin for green shipping

DWT Deadweight tonnage

EC European Commission

EEA European Economic Area

EEDI Energy Efficiency Design Index

EEOI Energy Efficiency Operational Indicator

EEXI Energy Efficiency Ship Index

ELMs Extreme learning machines

ESD Energy saving device

FC Fuel consumption

FCM Fuel consumption model

FPSO Floating Production Storage and Offloading

GBM Gray-box model

GHG Greenhouse gas

GP Gaussian process

GPR Gaussian process regression

GS Green ship(ping)

GT Gross tonnage

HF High-frequency

HFO Heavy fuel oil

ICCT International Council on Clean Transportation

IMO International Maritime Organization

IoT Internet of Things

LLs Living Labs

LNG Liquefied natural gas

LPG Liquefied petroleum gas

MAE Mean absolute error

MAPE Mean absolute percentage error

MBSE Model-based systems engineering

MEPC Marine environmental protection committee

MSE Mean squared error

OPEX Operational expenses

ReLU Rectified Linear Unit

ROI Return of investment

ROPAX Roll-on/roll-off passenger

RQ Research question

rs Random state

RMSE Root mean squared error

SE Systems engineering

SLR Systematic literature review

VR Virtual reality

WASP Wind-assisted ship propulsion

WBM White-box model

WHRS Waste heat recovery system

Contents

List of Figures

List of Tables

1
Introduction

1.1. IMO GHG strategy

During the United Nations Climate Change Conference near Paris in 2015, the Paris Agreement was adopted by the 196 parties present which stated that global warming must be limited to below 2°C (EC, 2015a). Unfortunately, international shipping together with international aviation were not taken into account in this agreement. As a reaction the International Maritime Organization (IMO), the specialized maritime organization of the UN, adopted in 2018 an initial strategy in order to reduce the greenhouse gas (GHG) emissions by international shipping (IMO, 2018). The goal of this initial strategy is set on a reduction of GHG emissions by 50% in 2050 compared to emission levels of 2008. During their annual meeting in July 2023, the strategy was revised to **net-zero GHG goal close to 2050**, addressing the IMO's environmental ambitions (IMO, 2023a). In order to reach the goal of the revised IMO GHG Strategy, the following checkpoints were adopted, all relative to 2008 levels:

- a minimum of 20% reduction of the total GHG emissions for total international shipping by 2030
- minimum 5% of energy used by international shipping is produced with zero or near-zero GHG emission technologies by 2030
- a minimum of 70% reduction of the total GHG emissions for total international shipping by 2040

The shipbroker firm Simpson Spence & Young estimated that global shipping emitted approximately 833 million tonnes of CO_2 in the year 2021 (Bockmann, 2022). This relates to 3.0% of CO_2 emissions on a global scale (Bockmann, 2022), which would make global shipping the world's 6^{th} largest CO_2 emitter if it were a country (Tiseo, 2023). Figure 1.1 visualizes the distinction of the CO_2 emissions per ship type in the year 2021 operating in the European Economic Area (EEA), showing the ship types that pollute the most. It also shows that general transport vessels, mainly covered by tankers, bulk carriers, and container ships, have a large contribution to total international shipping (Sinay, 2022). This all emphasizes that the reduction of CO_2 within the maritime transport industry, is a key factor in achieving the goal of the set GHG strategy.

1.2. The potential within shipping data

Shipping generates an extensive volume of data every minute, which includes information about the vessel's operations, like sailing speed and fuel consumption, as well as data concerning the route taken, such as weather updates and traffic reports (Figure 1.2). Additionally, data is generated beyond the ship's boundaries, including details about port fees and cargo handling times (Container XChange, 2020). Despite the abundance of data and growing digitalization, most of it is still collected in various formats, processed manually, and used on a short-term history basis, e.g., incident assessment or current routing (Marine Digital, 2020; Swider et al., 2018). Moreover, operational data that is collected during voyages is often used for only one purpose, for example, bunker delivery notes or voyage data records that are utilized to measure the ship's environmental impact. Therefore, the potential of the available shipping data is not being fully utilized (Mouzakitis et al., 2023). This is due to the involvement of various stakeholders, such as ship owners, ship operators, and ports, and the complexity of modern vessel design and operation linked to the growth

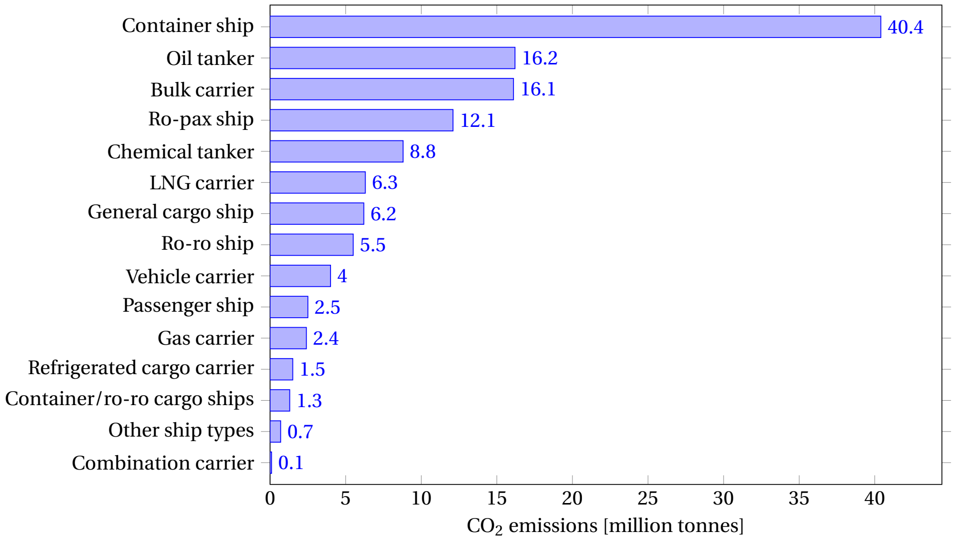

Figure 1.1: Total CO_2 emissions in the EEA per ship type in 2021 (EC, 2023)

of global trade, increasing advanced technologies, and growing importance of environmental sustainability (Container XChange, 2020; Mouzakitis et al., 2023; Swider et al., 2018).

To overcome this data challenge, Swider et al. (2018) suggest focusing on research and innovation linked to the digitalization of the shipping industry and usage of shipping data. Exploring new algorithms, tools, and platforms in the fields of artificial intelligence (AI), augmented reality (AR), virtual reality (VR), high-performance computing, and big data analytics (BDA) can unlock possibilities for various maritime applications (Sánchez-Sotano et al., 2020; Swider et al., 2018). These include vessel traffic monitoring and management, ship and ship energy system design & operation, autonomous shipping, fleet intelligence, route optimization, and more (Mouzakitis et al., 2023; Swider et al., 2018). While the transition towards more digitalization of manufacturing and engineering processes is ongoing, also known as Industry 4.0, the maritime industry is still lagging behind in this transformation (L. Huang et al., 2022). Maritime engineering processes, e.g., new ship & retrofit design or integrating energy-efficient technologies, are complex processes affected by international rules, regulations, and stakeholders. Therefore, available data is not as extensively used in maritime engineering (L. Huang et al., 2022) as it has in other engineering fields, such as aerospace (Shafto et al., 2010) or chemistry (Montáns et al., 2019). Nevertheless, utilizing shipping data could provide beneficial developments in the field of marine engineering, transitioning forward towards more digitalized processes (Mouzakitis et al., 2023; Swider et al., 2018).

1.3. DT4GS project

After the Paris Agreement, the EC introduced the European Green Deal in 2021. This initiative includes a series of project proposals aimed at achieving the EU's goal of reducing GHG emissions by at least 55% by 2030 compared to 1990 levels, with the ultimate target of achieving net-zero GHG emissions by 2050. By achieving this goal, the EC wants to become the first climate-neutral continent in the world, hence zero emission for international shipping (EC, 2021a, 2021b). One of these projects is **The Digital Twin for Green Shipping** (DT4GS[1]) project, funded by the European Union's Horizon research program. The vision of this project, as stated in the proposal, is: *"To develop and demonstrate low-emission solutions for all main ship classes and associated shipping services by 2030, in turn enabling shipping companies to implement strategies for achieving zero-emission waterborne transport by 2050".*

The vision of the DT4GS project focuses on the digitalization of the maritime transport sector, especially the development and application of Digital Twins (DT) together with the abundance of produced shipping data. A DT is the virtual representation of a physical model where real-time data is flowing in both ways (Mauro & Kana, 2023). This real-time data interaction between the physical and virtual model should be ca-

[1] https://dt4gs.eu/

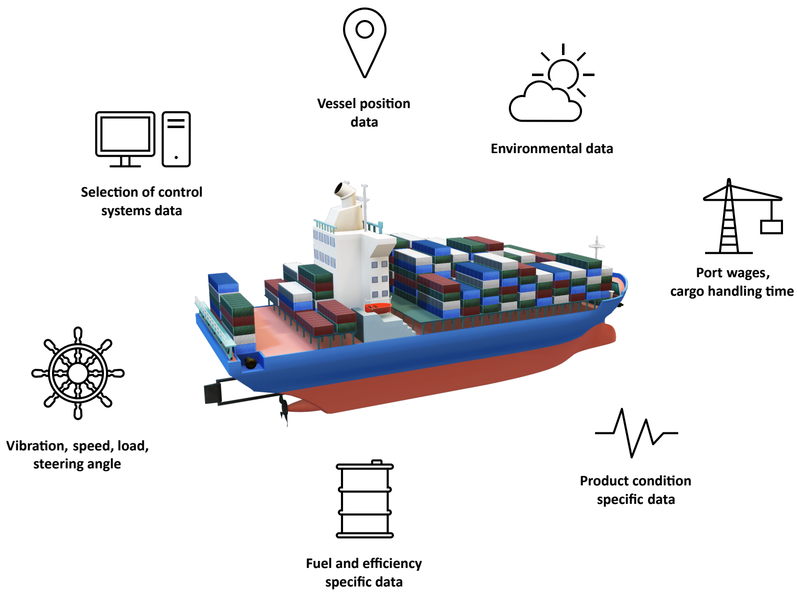

Figure 1.2: Overview of produced shipping data, based on Swider et al. (2018)

pable of evaluating and re-coordinating behavior for future decisions regarding the linked physical system. DTs, firstly developed and used by NASA, have already proven to have a significant and positive impact on the aerospace and automotive industry (Shafto et al., 2010; Van Os, 2018). During space missions, DTs have been used to evaluate and predict vehicle and system conditions to estimate mission success (Shafto et al., 2010). During the development of the Joint Strike Fighter jets, DTs are applied for the ongoing validating and verification of hardware and software, resulting in reduced time and costs (Land, 2022). A recent DT application in the automotive industry is the continuous and virtual digital testing of digital systems of modern hybrid-electric vehicles (Land, 2022; Saber, 2022).

Recently, Mauro and Kana (2023) performed a critical systematic literature review on DT maritime applications, especially regarding the ship's life cycle. This showed that DTs are scarce in the shipping industry, indicating the potential benefits of DT application in the maritime industry in the near future. Mauro and Kana found that a major challenge lies in determining a design methodology for new ships by applying DT-models. Within the DT4GS project, this challenge is tackled by the collaborating companies and institutions that investigate the feasibility and application of DTs in the optimization of green ship operations and design. Green shipping refers to the transportation of people or goods by ships while minimizing the use of resources and energy, with the aim of safeguarding the environment against the pollutants emitted by the ships while maintaining safe operational conditions (Container XChange, 2019). In a report published by the International Council on Clean Transportation (ICCT), several examples of emission reduction strategies are provided, such as shifting towards alternative fuels, ship speed reduction (slow steaming), and real-time weather routing. Some of those strategies could also potentially be included in the design of new-build ships or retrofit design (Wang & Hon, 2011). However, these emerging green ship technologies introduce various new risks into ship design and operation, risks that are often overlooked. For instance, alternative fuels bring zero-carbon, low flash point properties, posing significant safety hazards if not handled with care. Additionally, the adoption of emission reduction technologies may lead to an increase in onboard chemicals. Research by Reinhold et al. (2019) underscores these concerns. Employing DTs can aid in identifying and simulating these safety hazards, thereby helping to mitigate risks due to their digital nature, as highlighted by Van Os (2018).

The goal of DT4GS is to eventually accomplish zero emissions by 2050 for the ship types of the collaborating companies within the DT4GS project; represented by an oil tanker, a container ship, a bulk carrier, and a ROPAX vessel. These are also the most polluting ship types as depicted in Figure 1.1. The collaborating vessels function as so-called 'Living Labs' (LLs), where operational data is collected and stored for future use throughout the project. In order to accomplish this goal, the project is divided into three phases. During the first phase, a method is proposed for the application of DT in the design of green ships. With the application of a DT a CO_2 emission reduction of 20% is been set as a goal during this phase. The second phase involves the use of operational data originating from the collaborating ships, which is the input for the proposed DT, that will drive the ship design for new-builds and retrofits of the green transport vessels. The goal of the second phase is a minimum CO_2 emission reduction of 50% by 2030. Phase three captures the final goal of the project to have no harmful emissions by 2050. These project phases are depicted in Figure 1.3.

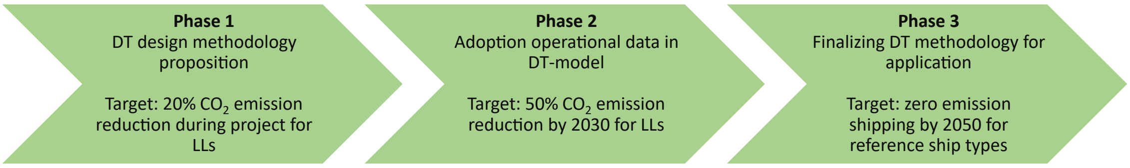

Figure 1.3: DT4GS project phases (DT4GS, 2022)

1.4. Research objective and questions

This master thesis will focus on the second phase of the DT4GS project, where available operational data is used to investigate design possibilities with regard to DT.

From the previously addressed environmental and data challenges, the following main research question is adopted:

"To what extent can available operational ship data be used to improve future green ship design by reducing CO_2 emissions?"

In order to answer the main research question, the following research questions (RQs) are specified:

Chapter 2 **RQ1** What is the state-of-the-art in data-driven ship design for green ships?

Chapter 3 **RQ2** Which steps are involved in constructing a DT for retrofit design?

Chapter 4 **RQ3** What is the most suitable green ship digital model using bunker delivery notes for CO_2 reduction?

Chapter 5 **RQ4** To what extent can data from bunker delivery notes be incorporated into the selected digital models?

Chapter 6 **RQ5** To what extent can the output of the digital models be integrated into one green ship DM?

Chapter 7 **RQ6** To what extent does the output of the green ship DM directly impact the retrofit design?

Chapters 2 and 3 will elaborate on the steps involved with constructing a DT for retrofit purposes, together with the current development status of such a DT. Chapter 4 presents the adopted methodology for the construction of a green ship digital model. Next, Chapters 5 and 6 elaborate on the constructed models and the adopted integration framework used to derive the resulting green ship digital model. Chapter 7 presents the results from the performed case-study. Finally Chapters 8 and 9 provide the conclusions and discussion on the research questions and adopted methodology including recommendations for future work.

2

Data-driven green ship design

This chapter elaborates on and aims to answer RQ1: *'What is the state-of-the-art in data-driven ship design for green ships?'*

In order to sufficiently investigate RQ1, firstly, the process of ship design in general is discussed, including the different stages within the design process and distinctive design methods. The design methods are examined with regard to green shipping and their ability to data use. Also, retrofit design is discussed compared with the general design process. Secondly, common green ship technologies identified in ship design literature are addressed. These technologies are explored in relation to their incorporation into both new-build designs and retrofit projects, with a particular emphasis on their compatibility with data-driven ship design approaches. Finally, the study investigates the current status and applications of Digital Twins (DTs), a data-driven method, in the design process for both new-build vessels and retrofits. This exploration aims to identify any existing literature gaps that this thesis seeks to address.

2.1. General ship design

The design process of a ship is an iterative process that typically consists of several stages aimed at ensuring the vessel meets the required specifications, performance criteria, and safety standards provided by the shipowner. While the exact distinction may vary depending on ship type and shipyard, in general, the design stages are divided as follows (Ni & Zeng, 2019):

- Concept & preliminary design (basic design)
- Contract design
- Detail design

These stages (Figure 2.1) generally hold for the design of a new-build vessel. The process of retrofit design slightly differs, especially within the concept & preliminary design (Carl Fredrik, 2018). First, the general stages of new-build designs are discussed, followed by the retrofit design.

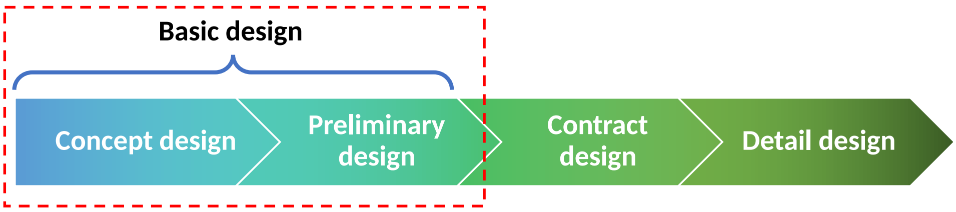

Figure 2.1: Ship design process in general (Ni & Zeng, 2019)

Concept & preliminary design

The design process begins with defining the purpose and requirements of the ship. This includes determining its intended use, cargo & passenger capacity, ship speed, range, and any other specific operational considerations. The defined requirements are then translated to design characteristics which will drive the first concept designs. A concept exploration is conducted for these concept designs through a feasibility study, and is characterized by innovation as it necessitates the pursuit of the most cost-effective solution while also considering whether the client's requirements can be fulfilled or not (Ni & Zeng, 2019; Papanikolaou, 2002).

There is no hard line between the concept design and the preliminary design as both stages are intertwined with each other, often simultaneously referred to as the basic design (Ni & Zeng, 2019). The preliminary design is the more refined version of one or two feasible concept designs including the first versions of the major technical documentation, e.g., lines plan, general arrangement plan, and list of main equipment. During this stage, the preliminary design is presented to the client for review and feedback. This feedback is essential in refining the design and incorporating any necessary modifications or adjustments based on the client's preferences, operational requirements, or budget constraints. The final preliminary design meets regulatory standards and will form the basis of the contract design.

When considering the application of green ship (GS) systems, those decisions are made during this stage (basic design), as power and emission characteristics of the ship become evident and the right GS-equipment can be chosen (Shi et al., 2018). Nowacki (2010) discusses the influence of digitalization and computer-aided design (CAD) on ship design and states that the use of computers influences mostly the concept design stage. By using digital applications and processes, multiple design variations are considered and evaluated faster and more efficiently.

As this thesis investigates the implementation of GS systems in ship design, it will focus on the concept & preliminary design stage (red-dashed box in Figure 2.1), where the decisions with regard to those systems are made.

Contract design

The contract design stage of shipbuilding involves the development and finalization of the contractual agreement between the shipowner and the shipyard. This stage focuses on capturing all the technical, commercial, and legal aspects of the shipbuilding project, ensuring that both parties are in agreement and have a clear understanding of their rights, obligations, and expectations (Ni & Zeng, 2019). The precise description of the hull form is determined, together with the final general arrangement, weight & center of gravity estimation, and calculations regarding the hydrodynamic performance.

Detail design

The detail design is the final stage within the ship design process where the final contract design is further refined and translated into detailed engineering drawings, specifications, and instructions that serve as the blueprint for the shipyard. The detail design and start of ship production in the shipyard are often simultaneously developed as a concurrent engineering process, where the production engineering plays an essential role in impacting the production schedule and integrating the most recent technologies (Elvekrok, 1997; D. Huang, 2013).

2.2. Retrofitting

Retrofitting involves enhancing a vessel and its onboard systems to extend its operational life while meeting current and upcoming energy and emission standards, thereby transforming it into a greener vessel (EC, 2015b). Retrofitting is often performed as a cost-effective procedure linked to the development of new technology and the degradation of onboard equipment in need of replacement, ultimately lowering the operational costs of a vessel (Chirica et al., 2019). Because a retrofit design involves the improvement of an already existing vessel, consequently the design stages and decisions slightly differ from those of a new-build vessel (Carl Fredrik, 2018). The feasibility study of the possible retrofit throughout the concept & preliminary designs becomes more important due to existing structures and available space (Chirica et al., 2019). Technical drawings will only include the newly implemented equipment and the systems that will be affected by the retrofit. However, these affected systems can be of a major scale in the case of the retrofit design impacting a large part of the ship. The contract and detail design stages mostly follow the procedure as that of a new-build vessel, with their focus on only the retrofit and affected systems instead of the whole ship (Carl Fredrik, 2018; Chirica et al., 2019).

Given the fact that the concept & preliminary design stage is most important within a retrofit design, this design stage (red-dashed box in Figure 2.1) will also be referred to when addressing retrofitting or retrofit design further on in this thesis.

2.3. Ship design methods

When designing a ship, various methods can be applied which all embrace their own philosophy. Traditionally the design process can be described as the design spiral introduced by Evans (1959), involving continuous iterations of the ship design. But throughout the years more methods were adopted, each with their own pros and cons. Several design methods with potential to green shipping are briefly discussed including their main philosophy and data-driven capability.

Ship design spiral

The ship design spiral, developed by Evans (1959), describes the iterative process of ship design over multiple stages. As depicted in Figure 2.2, it involves a cyclic approach of continuous evaluation starting with the concept design phase. By going further toward the spiral center, computations become more detailed, driving the level of design refinement. The focus lies on refining the adopted design from the initial phase, resulting in a single solution by the final detailed design phase. This approach underlines a point-based, solution-driven methodology, encouraging multiple teams to specialize in distinct design aspects and utilize various design tools. These teams continuously iterate over time by evaluating the current design at that stage. Due to the fact that ship design has become more complex over time, the data produced and used during the design also increased in complexity (Mosedale, 2020). Because of the continuous evaluation within the design spiral, the time of the evaluation increases with more data. Therefore, the ship design spiral is not considered an efficient method when dealing with (big) data (Radosavljevic, 2022).
Philosophy: iterative, point-based, solution-driven, continuous evaluation

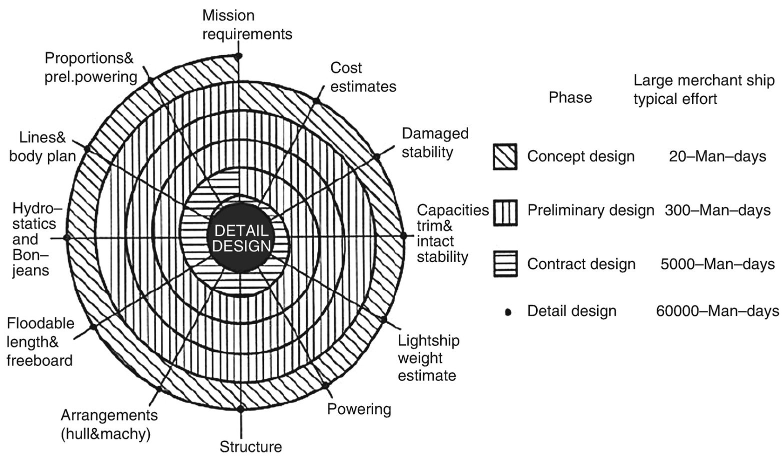

Figure 2.2: Ship design spiral (Evans, 1959)

Set-based design

Set-based ship design is an approach that emphasizes exploring and evaluating a broad range of design alternatives concurrently in separate design spaces or sets, rather than prematurely converging on a single solution (Singer et al., 2009). In the final stage of the design, designers systematically analyze and compare the different design alternatives by identifying similarities. Ultimately converging to one final design through trade-offs between the competing alternatives. The different design sets, mainly large data sets generated during the conceptual design stage, are convenient to be analyzed with data-driven methods, such as AI (Fitzgerald & Ross, 2019).
Philosophy: iterative, multiple design spaces, parallel exploration, trade-off analysis

Holistic design

Holistic ship design is an approach that considers the ship as a whole, taking into account various interconnected factors and their interdependencies. It uses an optimization algorithm where the main particulars and load cases of the ship are known, and through exploration diverges towards design solutions (Papanikolaou, 2010). The holistic design approach can effectively be enhanced through data-driven techniques by improving the optimization algorithms and predictive modeling (Kondratenko et al., 2023; Nikolopoulos & Boulougouris, 2020).
Philosophy: ship as one product, optimization through algorithm, fixed main particulars

Design building block

The ship design building block (DBB) method is an approach that breaks down the ship design process into individual building blocks or modules supported by CAD, allowing for a systematic and flexible approach to ship design. It involves developing and integrating pre-defined modules that represent various ship components, systems, and functionalities (Andrews, 2006). Due to the CAD-basis within DBB, Andrews (2006) indicates the potential big data handling capabilities of the DBB approach when acceptable ict facilities are available and the (pre)processing is performed carefully.
Philosophy: modular, CAD, ship is a combination of subsystems, iterative over system blocks

Model-based systems engineering

Model-based systems engineering (MBSE) is an approach within systems engineering (SE) that employs models as a central tool for conducting SE processes, e.g., representing, analyzing, and designing complex systems (Shevchenko, 2020). It is an alternative to traditional document-based systems engineering (DBSE), where diagrams and textual documents are used to describe system requirements, design, and architecture (Tepper, 2011). Both MBSE and DBSE follow the philosophy SE where the total (complex) system is decomposed into smaller sub-systems and processes (Van Bruinessen et al., 2014). Papanikolaou (2014) showed by decomposing a ship into interdependent subsystems and processes, optimal performance and efficiency requirements can be achieved. With the model-centric approach, multiple design teams with different disciplines can work within the same model which is capable of handling the different data and integrating data-driven techniques (Estefan et al., 2007; Kooij, 2022; Tepper, 2011). MBSE does not represent a design method itself but has an assisting role within the design process by performing design exploration supporting data-driven techniques (Maimun et al., 2019).

Digital twin supported design

A representative MBSE approach is the use of a digital twin (DT), which fulfills a supporting role throughout the design process. W. Li (2023) concluded that a DT-based design method is the most suitable approach regarding green ship design, due to its capability of life-cycle evaluation and larger capability of tackling design challenges introduced by GS design, compared to the various examined design methods. When a DT is used during the ship design process, it allows ship designers to analyze and optimize the ship's design based on operational simulations performed with the DT (Arrichiello & Gualeni, 2020; Lo et al., 2021).

A DT is not solely used for supporting the ship design, but can also exist throughout the ship's lifetime as a data-driven support system, performing complex simulations, and providing future operational decisions based on those simulations (Erikstad, 2017; Lo et al., 2021; Tao et al., 2018; Zhang et al., 2022). As briefly mentioned earlier in Chapter 1, a DT is a virtual product representing a physical product including a real-time data flow between both products. A simple schematic representation of a DT is depicted in Figure 2.3. Chapter 2 will elaborate furthermore on the description and construction of a DT itself.

A DT-based design is not a design method itself, but an enhancement of other ship design methods by applying a MBSE approach. Nikolopoulos and Boulougouris (2020) and Mouzakitis et al. (2023) have suggested the integration of a DT with a holistic design approach. As Nikolopoulos & Boulougouris presented a conceptual DT-framework, they were only able to illustrate the potential of this framework by demonstrating a reduction of the ship's operational costs (OPEX) and emissions rate (EEOI) during their first results. Bucci et al. (2021) presented that their newly adopted design methodology, where a DT is combined with a system-based approach in the early-stage of ship design (basic design), will accelerate the assessment and evaluations during that stage, and hence, speed up the design process itself.

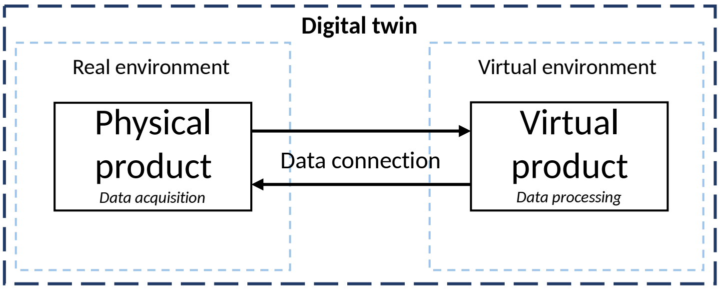

Figure 2.3: Schematic representation of a digital twin based on definition by Grieves (2014)

Nevertheless, a paradox emerges when incorporating the design of a new-build ship with the true definition of a DT, stated by Kritzinger et al. (2018). The authors emphasize that a true DT has a real-time, automated data flow between the physical product and the virtual product. In the case of a new-build ship, a physical ship does not yet exist, hence no real-time data is available. Therefore, the virtual product can not be labeled as a true DT. In the case of retrofit design, a true DT can exist as there is a physical ship present, and possibly collecting data using installed sensors. The question that arises here is to what extent the virtual model supports the new-build design and up to what level of detail the virtual product represents the new design. Unfortunately, no literature currently elaborates on this. During a discussion on this problem with a consortium within the DT4GS project, they shared their vision that a DT should grow and develop parallel with the design of a new vessel. The level of detail of the virtual representation is equal to the design of the vessel at that moment. This enables the possibility of performing simulations and evaluating the design concept in the early-stage of ship design at the same level of accuracy as those concept designs. When the new-build design further increases in the level of detail (e.g., transitions to the next design stage), the virtual representation also increases in the level of detail together with its simulation capabilities and associated accuracy.

In conclusion, a DT-supported design is selected for this research. Due to the integration of operational data, a DT has the ability to perform simulations to be used to evaluate green ship design technologies. This is also in line with the research conducted by (W. Li, 2023), where DT-supported design is identified as the most suitable approach with regard to green ship design together with its capability of handling big data.

2.4. Green ship design

This section discusses relevant innovations linked to the design of green ships found in recent literature. Green shipping (GS), refers to the safe marine transportation of people and goods while aiming to protect the environment against pollutants from ships by means of minimizing energy usage and reducing harmful emissions (Container XChange, 2019). With environmental regulations in place, innovations that reduce harmful emissions become more essential for the design of future green ships. The green ship technologies discussed in this context are classified based on the general categorization outlined by de Kat and Mouawad (2019):

- Hull form optimization
- Power & propulsion system
- Alternative fuels
- Renewable energy
- Air lubrication

This thesis focuses on the design of green ships, other aspects, such as GS operations (Sherbaz & Duan, 2012a), ship recycling (Sunaryo & Pahalatua, 2015), and adaptation of GS practices by shipping firms (Lai et al., 2011) are left out of consideration. First, an overview of the environmental regulations adopted by the IMO linked to the assessment of GS is provided. Following this, the aforementioned green ship design technologies will be examined in terms of their potential for implementation in both new-build projects and retrofits, as well as their capabilities in leveraging data-driven approaches.

2.4.1. IMO's environmental measurement tools

During the annual meetings of IMO's Marine Environment Protection Committee (MEPC), environmental regulations are proposed and adopted in order to improve the energy efficiency of global marine traffic and reduce their GHG emissions. Within these regulations, environmental measurement tools are proposed to quantify these GHG emissions and evaluate the ship's energy efficiency, for both new-builds and existing ships. These tools compare the environmental impact on society with the benefits to society, respectively in terms of CO_2 emissions and transport work. The following measurement tools will be discussed in the next sections: EEDI, EEXI, CII, and EEOI.

EEDI (IMO, 2022b)

The Energy Efficiency Design Index (EEDI) is a mandatory regulatory measure that applies to **new-build ships** engaged in international voyages. The primary objective of EEDI is to promote the use of energy-efficient technologies and designs for the construction of new vessels. The EEDI sets specific energy efficiency targets that vary based on the type and size of the ship, considering factors such as deadweight tonnage (DWT) and ship type. The index is calculated based on the amount of CO_2 emitted per unit of transport work, typically measured in grams of CO_2 per metric tonne per nautical mile (mt-nm). The EEDI of new-build ships must meet or exceed the required EEDI to be considered compliant with the regulations (Equation 2.1). The required EEDI is represented by reference lines, depending on the ship type, DWT, and a reduction factor based on the aforementioned characteristics and the year of build. The EEDI measurement is a one-time certificate addressing the technical state of the vessel and does not apply to icebreakers and ships with non-conventional propulsion. A simplified version of the attained EEDI formula is provided below (Equation 2.2).

$$EEDI_{attained} \leq EEDI_{required} \tag{2.1}$$

$$EEDI_{attained} = \frac{\text{Design } CO_2 \text{ emissions}}{\text{Design transport work}} = \frac{P_{engine} \cdot sfc \cdot C_f}{DWT \cdot V_s} \tag{2.2}$$

Herein the product of the total engine power (P_{engine}), the total specific fuel consumption (sfc), and the conversion factor from fuel to CO_2 emissions (C_f) is divided by the product of the DWT and ship's design speed (V_s).

EEXI (IMO, 2022b)

The Energy Efficiency Existing Ship Index (EEXI) is a regulation focusing on **existing vessels** above 400 gross tonnage (GT), unlike the EEDI which applies to new ships. The purpose of EEXI is to assess and improve the energy efficiency of existing ships by setting certain carbon intensity limits. The same formula is used to determine the EEXI of a ship as for the EEDI (Equation Ref. 2.2), together with the same complaint requirement (Equation 2.2). To obtain the required EEXI a reduction factor (X) based on the ship type and carrying capacity (DWT) is used together with the EEDI-reference line (Equation 2.4). Existing ships are required to undergo an assessment of their energy efficiency and demonstrate compliance with the adopted EEXI limits. Ships that fall short of meeting the required standards will need to implement energy-saving measures or technologies to achieve compliance, e.g., retrofitting. As with the EEDI, the EEXI is a one-time technical certificate of the vessel. Existing ships that are excluded from the EEXI measurement are icebreakers, FPSOs, and drillships.

$$EEXI_{attained} = EEDI_{attained} = \frac{\text{Design } CO_2 \text{ emissions}}{\text{Design transport work}} = \frac{P_{engine} \cdot sfc \cdot C_f}{DWT \cdot V_s} \tag{Ref. 2.2}$$

$$EEXI_{attained} \leq EEXI_{required} \tag{2.3}$$

$$EEXI_{required} = (1 - \frac{X}{100}) \cdot EEDI_{ref,line} \tag{2.4}$$

CII (IMO, 2022a)

The Carbon Intensity Indicator (CII) is the newest regulation introduced by the IMO in November 2020. It is part of the IMO's efforts to further reduce greenhouse gas emissions from international shipping. The CII is designed to be a complementary measure to the existing EEDI and EEXI regulations. The CII measures the ship's annual operational carbon intensity, which is represented by the amount of CO_2 emitted per unit of transport work. It takes into account the actual operational efficiency of the ship, including factors such as the ship's design, engine power, speed, and cargo carried. The CII is calculated as a value in grams of

CO_2 emitted per mt-nm. Unlike EEDI and EEXI, the CII applies to **both new and existing ships**. Shipowners and operators are encouraged to reduce their vessels' carbon intensity by adopting more energy-efficient practices, improving operational procedures, and implementing technological upgrades. The attained CII of a ship is calculated annually with the fuel consumption and distance traveled over that year (Equation 2.5). The required CII (Equation 2.6) comprises ship type-dependent parameters (CII_{ref}, a, c), vessel carry capacity (DWT) and an annual reduction factor (Z).

$$CII_{attained} = \frac{\text{Operational annual } CO_2 \text{ emissions}}{\text{Operational annual transport work}} = \frac{FC_{1year} \cdot C_{f_{CO_2}}}{DWT \cdot D_{1year}} \tag{2.5}$$

$$CII_{required} = CII_{ref} \cdot (\frac{100 - Z}{100}) = a \cdot DWT^{-c} \tag{2.6}$$

$$CII = \frac{CII_{attained}}{CII_{required}} \tag{2.7}$$

The CII is calculated by dividing the attained CII of a vessel by the required CII (Equation 2.7). The CII is then assigned a ranking label from among the five grades (A, B, C, D, or E) depending on the ship's carrying capacity and the current year (Figure 2.4). Grade C represents the value of the required CII. In case the vessel has a D rating for three consecutive years or an E rating for one year, the ship owner is obliged to take measures to improve the energy efficiency of the ship for the coming year.

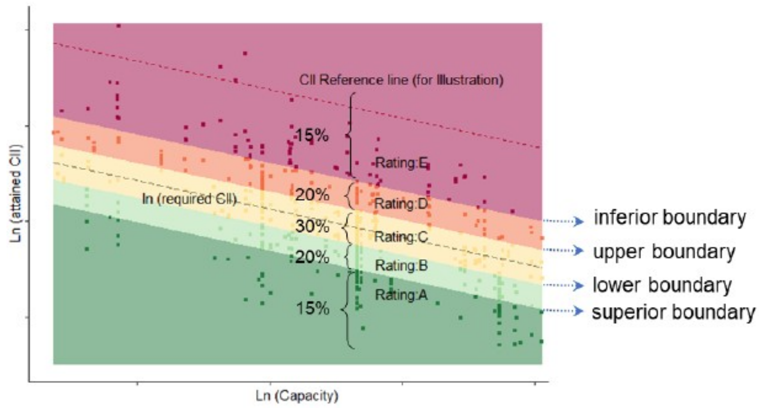

Figure 2.4: CII rating grades (IMO, 2022a)

EEOI (IMO, 2009)

The Energy Efficiency Operational Indicator (EEOI) is a measurement tool equal to the attained CII (Equation 2.5). Instead of assessing the yearly environmental impact, the fuel consumption and distance traveled over a specific distance are measured, often one voyage. The EEOI serves as a ship's performance indicator for the ship owner per voyage, to be used voluntarily. The calculation for the EEOI is provided in Equation 2.8.

$$EEOI = \frac{\text{Operational } CO_2 \text{ emissions}}{\text{Operational transport work}} = \frac{FC \cdot C_{f_{CO_2}}}{m_{cargo} \cdot D} \tag{2.8}$$

The choice of which measurement tool(s) will be used, will be made later on as first the research gap needs to be identified. This will indicate which tools will be applicable to this research. The aforementioned green ship technologies will be discussed in the next sections.

2.4.2. Hull form optimization

When a ship is sailing through water, it experiences resistance. The hull of the ship experiences the most resistance as being submerged most of the time, compared to the other parts (e.g. superstructure). This hull resistance can be divided into three main components: viscous, wave-making, and air resistance (Bateman, 2019). This resistance division is depicted in Figure 2.5. The viscous resistance is composed of frictional losses due to the interaction between the water and the ship's hull and is therefore a function of the total wetted surface area, surface roughness, and viscosity (Bateman, 2019). When sailing at low speeds, the viscous resistance is the dominant component, accounting for between 50% up to 80% of the total hull resistance (Toossi, 2013). This is the case for transport vessels in general which sail at relatively low speeds (Agarwal, 2019). De Kat and Mouawad (2019) state that by optimizing the hull form of the vessel energy efficiency can be achieved which decreases the energy consumption and lowers the ship's emissions. Although energy savings devices (ESDs) and hull coating also influence the interaction between the water and the ship's hull, only optimizing the hull form is examined here. Hull coating is not considered in this thesis, however, ESDs will be discussed separately. Within hull optimization, de Kat and Mouawad (2019) provide a distinction between three major options for the vessel's owner to decide:

1. Accept a standard, readily available hull form and propulsion system offered by the shipyard.

2. Modify an existing and preferably well-optimized hull form to address the expected operating profile.

3. Develop a new hull form design based on the expected operational profile.

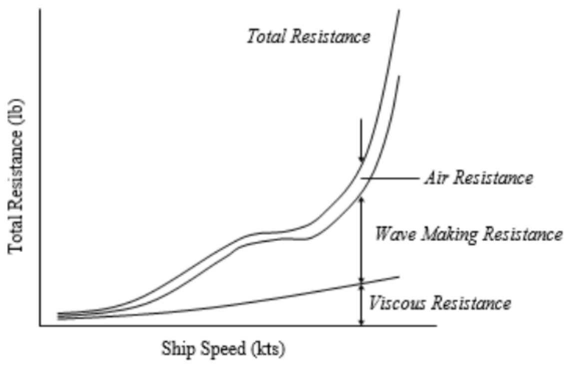

Figure 2.5: Components of hull resistance as a function of ship speed (Bateman, 2019)

The first option offers cost savings in vessel construction by adopting a shipyard's parametric design. Improving the ship's fuel consumption efficiency is already been done for more than a century (Endresen et al., 2007), resulting in standard hull designs that are well-optimized for common design conditions. Off-design conditions are often not covered in these hull shapes due to significant changes in the hydrodynamic capabilities of a vessels with varying ship speed, trim, and drafts (Perera & Mo, 2016). Demo et al. (2021) presented in their research a data-driven framework using machine-learning algorithms for the hull shape optimization of a standardized post-panamax container ship. By successfully applying Gaussian process regression as a model order reduction technique, a 1.2% total resistance coefficient reduction was obtained with respect to the original hull form.

Option 2 allows for design optimization based on specific service conditions, including expected operating draft, different trim conditions and various speeds. This option mostly involves alterations in the forebody of the ship and propeller area (Brenner et al., 2013; de Kat & Mouawad, 2019). M. Kim and Park (2015) have applied option 2 on an ultra large container ship (new-build) with constant dimensional parameters and various speeds with promising results. By investigating various bulbous bow configurations a reduction in hull resistance up to 2% was found. Kim and Park used throughout the iterative optimization process, CFD calculations for verification and validation, which is common practice with hull form optimization (Gao et al., 2016; H. Kim & Yang, 2010; Peri et al., 2001). In the work of Wei et al. (2023) a machine-learning based model is used for the optimization of a Wigley hull, a well-known hull form with good seakeeping qualities and fuel efficiency widely used for experimental studies (Matsui, 2022).

The third option enables the optimization of main ship dimensions in combination with the propeller and power plant choices linked to the operational profile of the respective ship. Hochkirch et al. (2013) applied this third option on a large container ship (new-build) by optimizing for the operational profile together with parametric hull design. Out of CFD validation of various configurations they found a potential reduction in fuel consumption of 3.7%. W. Sun et al. (2022) proposed a framework including the use of AI to generate the hull shape for a bulk carrier with a defined operational profile. With research still ongoing, the first results show that this framework could successfully generate a prototype hull and is able to optimize the hull form further on with given constraints.

Even though it is not commonly performed, the main dimensions of a ship's hull can also be altered for efficiency and environmental gains when applying hull optimization (Hochberg, 2020). As this involves the modification of an already existing ship's particular (e.g., length, breadth, depth), it is labeled as a retrofit operation (Hochberg, 2020; Moore, 2018; Nissen, 1989; Schuler, 2015). The cruise ship 'Song of Norway' was cut in half in order to lengthen the ship for mainly economical benefits (Hochberg, 2020). Two cruise ferries built by the Italian yard Grimaldi underwent retrofitting for both financial and environmental reasons (Moore, 2018). The ferries were lengthened to accommodate more vehicles & passengers and to be able to install multi mega Watt battery systems for green ship operations during port visits. Both a Canadian icebreaker vessel (Nissen, 1989) and a container ship (Schuler, 2015) were lengthened and widened to create space for new equipment and increase the ship's lifetime. However, since these retrofit operations require model basin tests and new sea trials, no publications are found directly linked to examples of data-driven methods used for retrofit hull form optimization.

2.4.3. Power & propulsion system

The power and propulsion system of a vessel represent the second main aspect of green shipping (Tadros et al., 2023). Figure 2.6 presents the typical power losses in the propulsion system of a ship. It shows that on average the engine has a 40% power output (net energy engine), and after accounting for the propeller losses, only 24% of the initial power is generated into net thrust considering marine fuel oil (Bateman, 2019). This indicates a potential for green power and propulsion designs to improve power efficiency by addressing areas such as optimizing engine performance to reduce losses and enhancing propeller design together with the combined hydrodamic coupling with the rudder, to maximize net thrust generation (Tadros et al., 2023; Voermans & Cales, 2020).

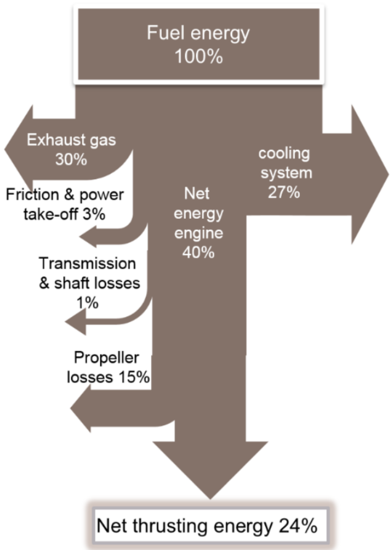

Figure 2.6: Typical energy losses in shipboard propulsion system (Bateman, 2019)

Research into green ship technologies with regard to the ship's power system have increased over the last decade (Tadros et al., 2023). By improved 1D (e.g., considering one system's characteristic over time) and 3D modeling software, new engines have successfully been developed by optimizing individual parts of an engine and achieving a reduction of exhaust emissions (Tadros et al., 2023). Also various engine techniques have enjoyed improvements in their performance and applicability, such as turbocharging reducing the power-to-size ratio of an engine (Tadros et al., 2015; Woodyard, 2009), fuel injection timing reducing harmful emissions (Cong et al., 2022; X. Sun et al., 2022), exhaust gas recirculation improving fuel consumption efficiency and achieving economical benefits (Zhao et al., 2021), and dual-fuel engines capable of supporting alternative fuels achieving lower exhaust emissions (Benvenuto et al., 2017; S. Park et al., 2017; Wu et al., 2023). Such improvements regarding the power system can successful be applied to new-build vessels, whereas in the new ship design the improved power system can be taken into account relatively easy (Tadros et al., 2023). In the case of existing vessels, spatial constraints become more critical since modifications to the power system can be more complex (Tadros et al., 2023). Nevertheless, if it deems to be feasible, existing vessels can also enjoy such improvements (Tadros et al., 2023).

One method applicable for new-build and retrofit design is installing a waste heat recovery system (WHRS). A WHRS is a technology designed to capture and utilize the excess heat generated during the ship's operation, which would otherwise be wasted, and convert it into useful energy (Baldi & Gabrielii, 2015; de Kat & Mouawad, 2019). Ships, especially large ones like cargo vessels and naval vessels, produce a significant amount of heat as a byproduct of their engines and other onboard systems. WHRS helps improve the overall energy efficiency of the ship and reduce fuel consumption, leading to cost savings and environmental benefits (Baldi & Gabrielii, 2015; Tadros et al., 2023). In the work of Baldi and Gabrielii (2015) a method is proposed to estimate the potential of installing a WHRS to be used within the early stages of (retrofit) ship design. By making use of data collected from onboard measurements with their performed case-study of a chemical tanker, Baldi and Gabrielii (2015) found achievable fuel savings from 4% to 16% together with a payback time of 5 years.

Within the propulsion system, the propeller is a crucial component as it propels the vessel by converting the engine power into thrust. Propeller choice, and therefor propeller design, is making the delicate trade-off between propulsion efficiency and cavitation behaviour (Vesting et al., 2016). A propeller of a general transport vessel has an efficiency between 50% and 60% (MAN, 2018), and suffer from power losses around 15% of the total engine power input (Figure 2.6). The total propeller loss can be categorised into an axial loss, a frictional loss and a rotational loss which all represent energy losses (Breslin & Andersen, 1994). In order to reduce power consumption and energy losses in the propulsion train, four main strategies are adopted in general: optimizing hull form, optimizing propeller, optimizing rudder for given propeller and applying ESDs (Voermans & Cales, 2020).

Optimizing the hull form, which improves the water flow towards the propeller, is already discussed in the previous section. By optimizing the propeller design, a reduction of axial and rotational losses can be achieved (Voermans & Cales, 2020). Examples of this are applying contracted loaded propeller tip design (Leaper et al., 2014) or designing for multiple operational conditions (Tadros et al., 2021). Those optimizations are performed in general with numerical methods based on CFD (Gaggero et al., 2022) or empirical models based on the Wageningen B-series (Leifsson et al., 2008). However, with the increment of applying machine learning for SE (Patzer, 2021), methods such as artificial neural networks (ANNs) (Rudzki & Tarelko, 2016) and Gaussian optimization processes (Gaggero et al., 2022) begin to demonstrate their time reduction advantages within design optimization. Besides the propeller itself, also the rudder design for a given propeller can be improved. By recovering the energy in the wake of the propeller by a rudder optimized in rudder profile and type, a reduction in fuel consumption between 2% and 8% can be achieved (Hochkirch & Bertram, 2010; J. Liu & Hekkenberg, 2017). Both the propeller and rudder are relatively easy accessible when a ship is taken out of service and placed in a dry-dock, in the case of retrofitting (Aronietis et al., 2014; de Kat & Mouawad, 2019).

As where the three propulsion optimizing strategies are mostly applied for new-build ship designs, ESDs are largely applied as retrofitted structures (Voermans & Cales, 2020). An ESD is a piece of equipment that can be attached to the hull, propulsion system, rudder or stern, which reduces the fuel consumption of the vessel at a given sailing speed and draught by improving the water-hull (e.g. fluid-structure) interaction and recovering energy losses (Sherbaz & Duan, 2012b; Voermans & Cales, 2020). Mewis and Deichmann (2013) found a 3.8% power reduction by retrofitting large container vessel with a Mewis duct (Figure 2.7). In the research of Spinelli et al. (2022), various ESD retrofit applications on the stern of bulk carriers, tankers and general cargo ships are investigated. Spinelli et al. found a potential energy saving rate ranging between 2% and 14% (depending on ESD type) during both model tests and sea trials. Prins et al. (2016) focused their research on the early performance assessment of ESDs, taking into account the installation processes in a shipyard. The authors found the beneficial feasibility of installing ESDs with regard to retrofitting, due to relatively high ROI and installation convenience when the ship is in dry-dock.

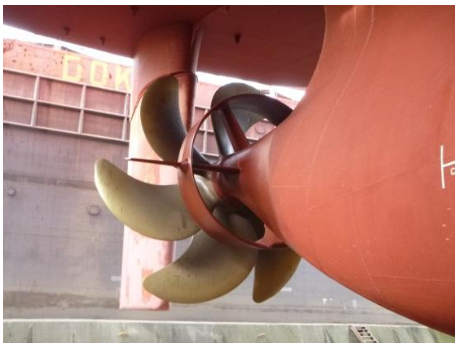

Figure 2.7: Mewis duct installation on 7090 TEU container vessel (Mewis & Deichmann, 2013)

2.4.4. Alternative fuels

Switching from conventional fuels (e.g., MDO or HFO) to alternative fuels (e.g., ammonia or methanol) is a highly effective strategy for reducing GHG emissions (Atilhan et al., 2021). Alternative fuels contain lower carbon concentrations than HFO, and therefor produce less pollutant emissions than HFO (Gilbert et al., 2018). However, alternative fuels have a lower power density (figure 2.8) and substantial chemical differ compared to current marine fossil fuels (Foretich et al., 2021). This poses engineering challenges regarding onboard ship infrastructure, including the transition to alternative engine types (Feng et al., 2022), and introduces risks associated with storage facilities (Boulland, 2021).

Biofuels have a relatively high energy density and would be good candidates as an alternative fuel because they are compatible with several existing marine diesel engines (H. Kim et al., 2020; Noor et al., 2018), making it a feasible candidate regarding retrofitting (Kesieme et al., 2019). However, the manufacturing of biofuels comes with a higher cost compared to traditional fossil fuels, accelerates soil degradation more rapidly, eventually competing with the production of food (H. Kim et al., 2020).

LNG and LPG have as advantage of having generally low fuel costs and can potentially achieve a CO_2 reduction of up to 26% due to the low carbon quantities (H. Kim et al., 2020). The lower fuel costs indicate economic benefits, but the required LNG and LPG infrastructure (e.g., storage facilities) result in a trade-off in terms of payback time regarding retrofitting investments (Wang, 2014). Ritari et al. (2023) found in their recent research that the economic benefit for the ship owner can be increased up to 40% when the ship's power and energy system is modified together with the switch to alternative fuels during retrofitting.

When considering hydrogen as an alternative fuel, current research indicates its potential to be with new-builds due to existing engine infrastructures (Atilhan et al., 2021). Even though when hydrogen is combined with fuel cell technology, the ship can reach a fuel reduction up to 60% (H. Kim et al., 2020), the higher price and complex facilities compared to HFO make it less feasible for retrofitting (Atilhan et al., 2021; H. Kim et al., 2020).

2.4.5. Renewable energy

One obvious strategy regarding green shipping is the use of renewable energy. In the shipping industry, the use of renewable energy is concentrated towards wind power, due to its history with shipping and availability at sea (de Kat & Mouawad, 2019). Nevertheless, the potential of using wave and solar power for shipping are also extensively being investigated (de Kat & Mouawad, 2019; B. Li et al., 2023; Pan et al., 2021; Rutkowski, 2016). Wind, wave, and solar power are all dependent on environmental conditions and do not produce the amount of power for to be used as main propulsion power, therefore to be labeled as auxiliary power sources for a ship (de Kat & Mouawad, 2019).

Wind-assisted ship propulsion (WASP[1]) systems have proven to achieve significant power reductions under favorable wind conditions: Thies and Ringsberg (2023) achieved a reduction between 10% en 14% by applying a Flettner rotor during the retrofitting of a ROPAX vessel, providing new-build design parameters

[1]Various designations are used throughout literature for wind propulsion systems, in this research 'WASP' will be adopted

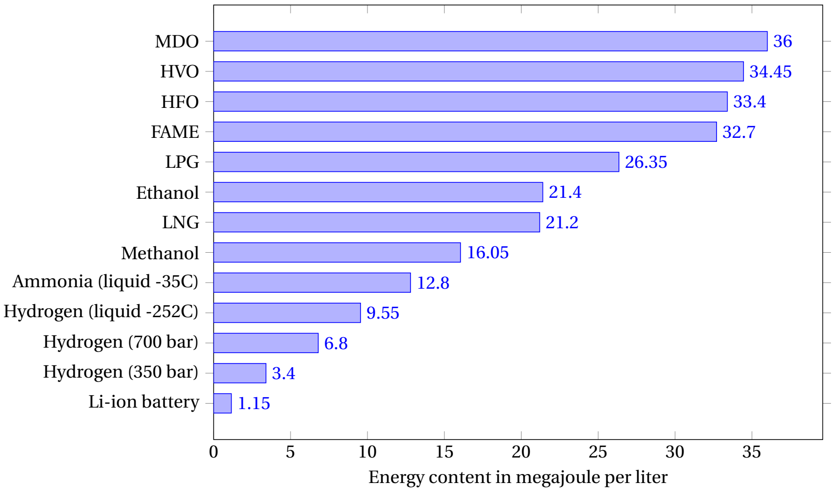

Figure 2.8: Energy density of maritime fuels in 2020, by fuel type (Statista, 2021)

for future ships with this WASP system. Lindstad et al. (2022) investigated the influence using a WASP configuration on the hull form and achieved through a case study with a bulk carrier design a 40% emission reduction by applying 5 Flettner rotors together with a slender hull form. Besides Flettner rotors, other WASP systems such as towing kites, hard sails, and (rigid-)wing sails also show promising results by means of power reduction (Bentin et al., 2018; Chou et al., 2021; Reche-Vilanova et al., 2021). Examples of these systems are depicted in Figure 2.9.

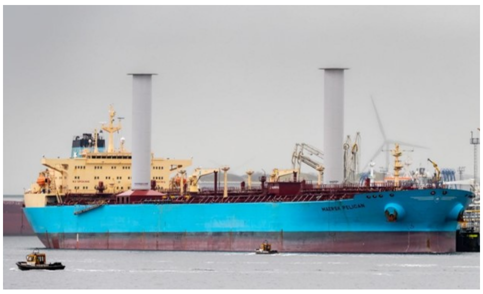

(a) Flettner rotor (Reche-Vilanova et al., 2021)

(b) Towing kite (Bentin et al., 2018)

(c) Rigid-wing sail (Reche-Vilanova et al., 2021)

(d) DynaRig sail (Reche-Vilanova et al., 2021)

Figure 2.9: Four distinctive types of WASP systems

For the feasibility study of retrofitting a towing kite to an oil tanker, Antai and Williams (2021) used wind data collected from wind reports along the sailing route of their performed case-study. Antain and Williams found a theoretical fuel saving of up to 40% in favorable wind conditions, and validated this by actually installing the towing kite through retrofitting. This is in line with the research of Naaijen et al. (2006), who estimated a theoretical fuel saving up to 50% for slow sailing transport ships (i.e. tanker vessels and bulk carriers). The same modeling with wind data can also be performed in order to evaluate other WASP technologies (Lu & Ringsberg, 2020; Pan et al., 2021). In the work of Lu and Ringsberg (2020) a wing sail, a DynaRig (hard sail), and a Flettner rotor are evaluated for an tanker by using available wind data related to the area of interest. Besides the feasibility case study, Lu and Ringsberg also showed the ability of performing a parametric study for these WASP systems in order to find the most optimal dimensions of these systems. The resulting fuel savings ranged from 5.6% to 8.9%.

Due to the fact that solar power has a relatively high capital costs and requires significant surface area to be of use for larger transport vessels (de Kat & Mouawad, 2019; Pan et al., 2021), it is left out of examination here. Wave energy conversion is also not on a suitable level to be implemented into industry, with research still going on (B. Li et al., 2023; Pan et al., 2021).

2.4.6. Air lubrication

Another method to achieve a reduction of friction resistance of the hull is by air lubrication. An air lubrication system (ALS) installed onboard of a ship lowers the contact area of the hull with the water, reducing the generated friction between hull and water (An et al., 2022). A schematic overview of an ALS is depicted in Figure 2.10.

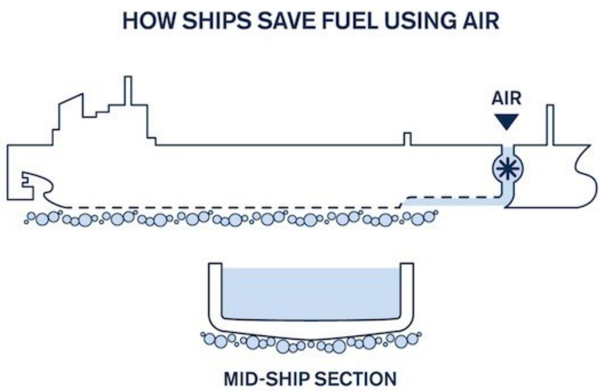

Figure 2.10: Schematic overview of an air lubrication system (gCaptain, 2012)

Fitzpatrick et al. (2017) investigated the applicability of an ALS considering the retrofits of an LNG carrier and heavy cargo carrier. Through first experimental model tests and later also sea trials and operational voyages of full-scale vessels, Fitzpatrick et al. (2017) achieved a 4.0% and 8.8% net power reduction for the LNG carrier and cargo carrier respectively. Due to high costs and low ROI regarding installing a complex system such as an ALS in an already existing ship, the ALS is considered to be more feasible for new-build ships (Fitzpatrick et al., 2017; Pavlov et al., 2020).

The data-driven applications within ALS are at this moment only found in the development of numerical assessment of an ALS (Giernalczyk & Kaminski, 2021; Kawakita et al., 2015). Giernalczyk and Kaminski (2021) used collected operational data of a chemical tanker with an installed ALS to address the benefits of such a system in terms of improved EEDI value. Nevertheless, Giernalczyk and Kaminski also found an increase in operational costs and high investment costs. Kawakita et al. (2015) proposed a CFD-based prediction technology for an ALS that utilizes operational data of ships with such a system installed to increase the simulation accuracy. Kawatika et al. address the challenges of simulation air bubbles together with the hydrodynamic effects on the respective vessel and emphasize the verification possibilities by using more extensive operational data.

2.4.7. Retrofit applicability green ship techniques

This section summarizes the applicability of the previously addressed green ship technologies with regard to ship design. When designing a new-build ship the design constraints are in general guided by economical perspective and customer requirements, and not by spatial constraints (Ni & Zeng, 2019). Spatial constraints become more important for retrofit design, as the existing ship forms the foundation for the new design. Therefore, this section exclusively focuses on assessing the feasibility of green ship techniques with regard to retrofitting. By assessing these techniques at a high level, a first evaluation is provided regarding the identification of possible green ship techniques for retrofit design purposes.

Optimizing the hull form involves alterations of a ship's main dimensions, aiming to reduce the viscous resistance of a vessel. As large alterations are linked to structural changes it is mostly applied for new-build ships were it is often impossible to apply on existing vessels. Even though examples can be found regarding retrofitting, it is not considered in this research. Retrofitting power systems might involve upgrading engines, adding hybrid or electric propulsion systems, or integrating waste heat recovery systems. Feasibility depends on the ship's layout and compatibility with new technologies. Propeller retrofitting is feasible and can be effective in improving propulsion efficiency. When a ship is in dry-dock, the propeller is relatively easily accessible to be replaced. As the propeller selection is linked with the ship's hull form and power system, all interconnecting dependent parts need to be compliant with possible changes linked to the propeller. Installing ESDs can often be applied when the ship's structure tolerates modifications involved with ESD installation. As is the case with propeller retrofitting, the ESD installation is relatively easily performed when dry-docked.

Switching to alternative fuels, such as transitioning from conventional fossil fuels to LNG or biofuels, might require modifications to the fuel system. Feasibility depends on infrastructure and cost considerations. Retrofitting WASP systems like sails or rotors is feasible, though it might involve adding new structures to the ship's superstructure as the installation is spatially dependent. Also, because the generated propulsion power of WASP systems is weather-dependent, the transport route of the sailing ship needs to be examined in terms of available wind. The installation of an ALS involves complex operations, such as adding air release mechanisms and air guidance structures. Since installing an ALS is also involved with relatively high costs, it is not considered in this research. Table 2.1 gives a brief overview of the aforementioned reasoning of energy efficient techniques regarding retrofit feasibility.

Table 2.1: Applicability green ship design techniques regarding a retrofit design

Green ship design techniques	Retrofit	Remarks
Hull form optimization	✗	Too complex and often impossible
Power system	✓	Feasible if within spatial constraints
Propeller optimization	✓✓	Feasible if compliant with hull form and installed engine
ESDs	✓✓	High ROI, easy to apply if within tolerable dimensions
Alternative fuels	✓	Dependent on onboard infrastructure
WASP	✓	Spatially and route-dependent
Air lubrication	✗	High costs, low ROI, complex installation

At first sight, applying propeller optimization and ESD installation is deemed to be the most favorable options regarding retrofitting. This high-level applicability analysis is mainly focused on spatial feasibility and level of complexity. Nevertheless, when considering the potential energy efficiency, applying such techniques will not result in the desired CO_2 reduction. Thus adopting combinations of multiple green ship technologies will be inevitable.

2.5. Current maritime DTs for design

In this section, the current status of DTs in the maritime sector is examined. A recently performed systematic literature review (SLR) is used as a guideline for investigation (Mauro & Kana, 2023). Mauro & Kana observed that research into maritime DT technology is now in a growth stage where at this point scientific publications are increasing exponentially including examples of DT application. This trend is also visible in the literature review performed by Tao et al. (2019) on DT technology in the overall engineering sector.

Mauro and Kana (2023) made a content classification in their SLR regarding the different phases throughout the total life-cycle of a ship, providing a clear visualization of publications of DT application over the last years as depicted in Figure 2.11. They found out of the 58 selected articles, most DT research focuses on the operational phase of a vessel, where the design and retirement phase experience a delay in the development of DT application and is considered to currently be in the formation and incubation stages of DT research (Tao et al., 2019).

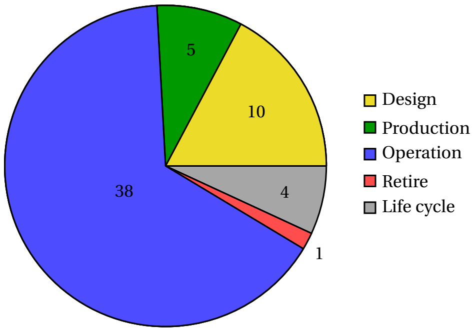

Figure 2.11: Division filtered papers from SLR per ship's life-cycle phase, by Mauro and Kana (2023)

The authors suggested that investigating design methodologies of new-build ships using DT technology is a logical direction for future research into this topic. This is also in line with the addressed potential benefits of applying DTs in the design and production process of new ships (Mouzakitis et al., 2023; Van Os, 2018). Van Os (2018) also discusses the implementation of a DT in the product life-cycle management of a ship, achieving a higher correct maintenance prediction rate and supporting future upgrades and conversions of the respective ship, hence retrofitting. As investigated by Hirdaris and Cheng (2012), the development of novel design methodologies, especially with the current digitalization of the marine industry, plays a key role in the development of green vessels. Hirdaris and Cheng state that the focus should be kept on the research and development of assessment tools for these new design methodologies, together with the complex on-board systems of ships. A DT can fulfill the role of such a newly applied technique in the design of green ships and simultaneously support the research of DT application in ship design.

Nevertheless, Mauro and Kana (2023) investigated publications up to August 2022, thus an additional literature investigation is conducted to retrieve and investigate recent publications to be of interest. For this additional investigation, the search engines Google Scholar and Web of Science are used. With alterations needed depending on the engine, the following search query was used:

"(marine OR maritime OR ship OR vessel) AND digital AND twin AND (design OR constructing OR construction OR model OR modeling OR modelling)"

This resulted, after filtering for ship design-related references, in three additional papers up to September 2023: one covering a proposed DT-design framework for a new-build vessel (Zhang et al., 2022), and two frameworks with regard to existing ships and ship virtual infrastructure (Mouzakitis et al., 2023; Xiao et al., 2022). The findings from both the SLR and additional literature search will be discussed in the next sections.

2.5.1. New-builds

As this thesis focuses on the ship's design phase, and especially the concept & preliminary design, it is important to have clear nomenclature between the literature regarding the ship's life-cycle phases and design phases. Table 2.2 shows which distinctive designs addressed in Section 2.1 correspond to the design and production phase adopted by Mauro and Kana (2023).

Table 2.2: Division of ship design and life-cycle phases

Ship design phases (Ni & Zeng, 2019)	**SLR ship life-cycle phases** (Mauro & Kana, 2023)
concept design preliminary design contract design	design phase
detailed design	production phase

The SLR only found 1 publication of a detailed maritime DT application, including a framework for its integration (Sapkota et al., 2021). Unfortunately, this article is not linked to the design of a whole ship but to a subsystem, namely the ship's structural integrity.

The remaining articles concern mostly subsystems of a vessel and relate to conceptional applications or only provide a general description of such an application (Arrichiello & Gualeni, 2020; Nikolopoulos & Boulougouris, 2020; Pérez Fernández, 2021; Stachowski & Kjeilen, 2017). Erikstad (2017) has also identified this trend of subsystem DT application but indicated the potential of getting closer to achieving a DT of a complete ship when such subsystem DTs are merged together. Nevertheless, with the search for recent publications, one article was identified that proposes a vertical-horizontal design idea incorporating the use of a DT for the total life-cycle of a ship, including the design phase (Xiao et al., 2022). Herein a comprehensive description of this design idea is provided including the construction and integration of the proposed DT. The life-cycle phases from design to operation are examined throughout a performed case study. Even though it provides promising conclusions, it is still a theoretical framework with in-depth research still being conducted as mentioned by the authors.

In conclusion, the literature search for recent publications and previously performed SLR shows 7 examples regarding DT application in the design of new-build vessels. However, they are still in the conceptual stage or cover only a subsystem of the total vessel considered. Since the research into DTs for maritime application is in the growth stage, as identified by Tao et al. (2019), it is expected the number of publications will increase in the near future. Nevertheless, with no concrete available publications on new-build vessels by DTs, a potential research gap is identified. By making use of already conducted research on DT subsystems and merge them together, a possible method of a DT design method for new-build vessels can be adopted.

2.5.2. Retrofits

Even though it is not performed for every ship and therefore not considered as a general life-cyle phase, retrofitting is common to perform when aiming to reduce emissions or to improve the onboard systems, especially with the increasing digitalization linked to Industry 4.0 (RINA, 2020; Wilkins, 2016). When analysing a ship's life-cycle, Mauro and Kana (2023) suggest to incorporate retrofitting into the retire phase of a ship. The authors identified only one DT article related to the this phase (Kamath et al., 2019). This can be explained by the fact that the retire phase is the last stage of a ship's life-cycle and subsequently will also be the last stage to be fully investigated with regard to DTs. By incorporating retrofitting, which has as its goal to increase the total life-time of a ship with due regard to the ROI, an increment of research for this phase could be accomplished throughout the coming years (Mauro & Kana, 2023). Nevertheless, when searching publications regarding ship retrofitting and DT application, no articles are available at this point. This indicates a potential research gap.

After the retrofit of a vessel is successfully completed, the ship returns to service. Therefore, it is suggested to review the available DT research regarding the implementation of a DT during the operational phase of a ship which focuses on the total vessel or multiple subsystems simultaneously, not a single subsystem. With knowledge from the actual ship operating, improvements could be identified which in turn can result in design decisions for a possible retrofit.

Zhang et al. (2022) propose the construction of a DT for an already existing research vessel, 'Gunnerus'. Although the project is still ongoing, the article provides a comprehensive DT architecture including the data-driven DBB method using the Open Simulation Platform[2], an open-source simulation platform which is publicly available. Even though here a unique vessel is being considered, the authors' aim is to provide a standardized DT concept for the maritime industry.

Another recently published article regarding a DT framework is linked to the EU-funded project *'VesselAI'* (Mouzakitis et al., 2023). Mouzakitis et al. address the importance of using high performance computing together with big data analytics in order to develop and therefore contribute to high-level digital products for the maritime industry, i.e. DTs. The article presents a novel holistic DT framework that makes use of digital technologies linked to Industry 4.0, such as Deep learning algorithms (DLAs), AI, and big data together

[2]https://opensimulationplatform.com/

with their potentials (Papanikolaou, 2019). The DT architecture includes a proposed data integration into the existing unified system within the *'VesselAI'* project. The project is now in the phase where the initial tasks and requirements are completed and further technical requirements are finalized together with validation through four case studies.

As a conclusion, the literature search showed no available publications linked directly to DT application for ship retrofitting. It is suggested to incorporate retrofitting into the retire phase of a ship, in order to boost the research regarding this life-time phase. Nevertheless, this indicates a research gap. In order to fill this gap it is proposed to examine research done on DTs in the operational phase which will provide sufficient information on design decisions linked to retrofitting. Ultimately, a retrofit is performed with a goal of extending the life-time of the vessel. With ship data acquired during the operational phase of the respective vessel and processed by a DT, design decisions for this retrofit can be derived throughout the DT. Two articles are identified which both present a conceptual framework to integrate DTs with an existing ship (Zhang et al., 2022) or virtual system (Mouzakitis et al., 2023).

2.5.3. Summary & research gap

In the previous sections, the current status of DTs for new-build and retrofit ships is discussed. In literature reviews previously conducted, it has been noticed that research into (maritime) DT application finds itself in the growth stage whereas the number of publications is now rapidly growing. This resulted in, at this point, mostly articles containing conceptual DT applications that focus on parts of a ship instead of the total ship itself. Only two available publications are found that address a DT theoretical framework considering new-build methods, and of which only one is associated with the design of the whole ship (Xiao et al., 2022). This article discusses a DT framework proposing the use of a vertical-horizontal design method of a new-build regarding the total ship throughout all its life-cycle phases (Xiao et al., 2022). This framework, part of an EU-funded project, is still under development, with promising expectations. Nevertheless, no articles are available regarding concrete applications of DTs linked to new-build design methods, only for theoretical and conceptual cases.

Concerning DT application for retrofit methods, no publications are available directly linked to DTs and retrofitting, indicating a potential literature gap. With the fact maritime DT application is still heavily being researched, it is logical to assume publications regarding retrofitting will become available in the future. It is suggested to examine research of DTs in the operational phase to support information regarding a possible retrofit, given the fact retrofitting is being performed to extend the life-time (e.g., operational phase) of a ship. Two recent articles are found, providing a conceptual DT framework to integrate with existing systems (Mouzakitis et al., 2023; Zhang et al., 2022).

Concluding, for both new-build designs and retrofit designs a literature gap is identified regarding the application of DTs. It is chosen to investigate the DT retrofit design for this thesis. As operational data is available from the LLs of the DT4GS project, green ship design decisions based on this data can be investigated to be applied to the vessel respectively. Moreover, this thesis argues for a DT design framework that requires starting with a DT retrofit design, resulting in a DT-enabled design for new-build ships. This overall design framework will be discussed in Section 9.5. The choice for DT retrofit investigation automatically results in the use of the EEXI as an environmental measurement tool assessing the ship design. Besides the EEXI, the CII will also be taken into account since it is mandatory for vessels and involves the continuous assessment of the vessel's operations. Nevertheless, the EEXI will function as the main assessment tool throughout further research as it addresses the technical state of the vessel.

2.6. Conclusion on current data-driven green ship design

This chapter has elaborated on the design process of new-build ships and retrofits and their current data-driven status, aiming to answer RQ1: *'What is the state-of-the-art in data-driven ship design for green ships?'*

As this thesis is investigating green ship design, the focus within the design process lies on the concept & preliminary design stage, often also referred to as the basic design. During this stage, the design choices regarding green ship technologies are made. Traditionally the philosophy of the design spiral (Evans, 1959) is applied when designing a ship, but with digitalization and the abundance of shipping data, the use of document-centric designs (DBSE) shifts towards the use of more computer-based models to support the design (MBSE). Green ship design refers to the goal of designing environmentally friendly ships while maintaining safe operational conditions. The design of green ships introduces new risks in terms of safety and logistics, compared to traditional ship design. Therefore, newly developed design techniques are required to mitigate these potential risks. A DT-supported design is identified as a favorable approach regarding green ship design, due to its capabilities of handling big data and performing complex simulations. These capabilities have the potential to mitigate the newly introduced risks within green ship design. DT-supported design is selected as the design method to be used and investigated further in this research.

With regard to green ship design, the environmental assessment tools adopted by the IMO are presented. Within these tools a distinction can be made between design and operational assessment, respectively EEDI & EEXI and CII & EEOI. Where the EEDI is mandatory for new-build vessels and the EEXI for most existing vessels. Several technologies regarding green ship design are discussed in terms of their data-driven capabilities. As the design of a new-build ship is in general guided by economical constraints, and less spatially dependent, a high-level analysis of these technologies is presented with regard to their retrofitting feasibility. This resulted in propeller optimization and installing ESDs being the most favorable options to be applied when retrofitting due to their relatively low installation complexity and high ROI.

When examining the current state-of-the-art of DTs for maritime design, the literature showed that scientific research into maritime DT applications is still in the early stages of development but rapidly growing. Regarding the design of new-build ships, publications only cover conceptual DTs or consider a subsystem of the ship, not the total ship. Furthermore, no available publications are found regarding DTs for retrofit design. Even though this is logical due to the fact maritime DT research is in the early stages of development. A research gap is identified for the DT application of both new-build design considering the total ship and retrofitting in general. This thesis investigates the development of a DT supporting green ship design for retrofitting purposes, because of the availability of operational data through the DT4GS project. As this data is collected on existing ships, the possible retrofit design decisions can be investigated for the respective ship.

With the state-of-the-art of maritime DTs discussed together with the design method and techniques of green ships, the theory and steps behind constructing a DT for ship design will be discussed in the next chapter.

3
Digital twin modeling

This chapter focuses on the construction of a DT model by addressing the different aspects involved in this process. By providing these different facets, RQ2 can be answered: *'Which steps are involved in constructing a DT for retrofit design?'*

Before going in-depth into the construction of a retrofit-related DT, a more thorough definition of a DT is provided.

3.1. Definition digital twin

In 2002, Grieves first publicly introduced the concept of a DT during the Society of Manufacturing Engineers conference as a physical product with a virtual counterpart which contains information on the physical part regarding its life-cycle management (Grieves, 2019). Later in a follow-up paper, he expands on this definition in the following way; a total DT model is composed of three main parts (Grieves, 2014):

1. A physical product in the real environment composed of information of itself
2. A virtual product in a virtual environment representing the physical product
3. And a data connection between these two products actively flowing in both ways as so-called mirroring or twinning

The function of this bi-directional data connection is to process the information from the physical product, update the virtual product, assess the current state, predict the future state, and provide further instructions for the physical product, all in an automated way.

Because of the fact DT modeling is still an extensively researched topic, and rather new in the engineering world as discovered by recent literature reviews on the topic (Jones et al., 2020; M. Liu et al., 2021; Mauro & Kana, 2023), the term 'Digital Twin' is not used correctly throughout literature. Often virtual/computer models are falsely labeled as a DT. In order to correct for this error in nomenclature, Kritzinger et al. (2018) distinct three different types of models:

- A *Digital Model* (DM) which is the virtual representation of the physical product, but without any form of exchange of automated data between both. Data exchange could occur but only be performed manually. The DM is mostly used for simulation and planning-based operations which does not require automatic data integration.
- A *Digital Shadow* (DS) which is an extended version of a DM including only an automated data flow from the physical product towards the virtual product by which it is actively updated.
- And lastly a *Digital Twin* (DT) is, as previously mentioned, composed of a physical and virtual product including an automated data flow between both entities.

Throughout the rest of this thesis, the previously addressed definitions by Kritzinger et al. (2018) will be used, and where a ship will fulfill the role of the product. A schematic representation of the three definitions is presented in Figure 3.1.

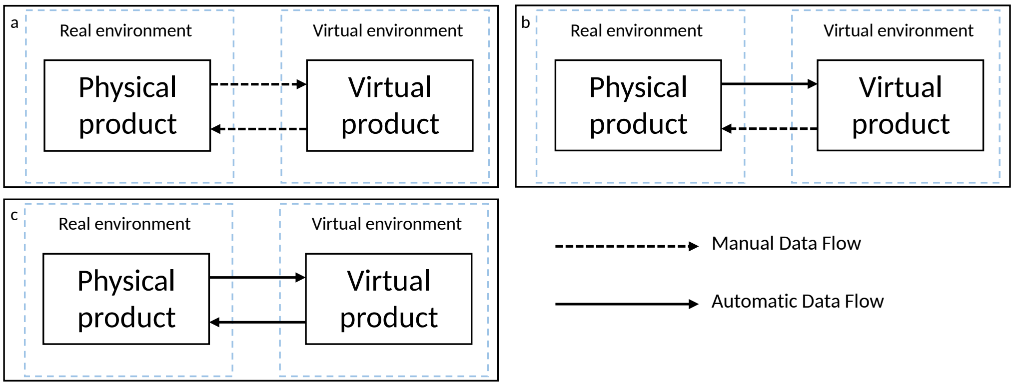

Figure 3.1: Schematic representation of a digital model (a), digital shadow (b) and digital twin (c), by Kritzinger et al. (2018)

3.2. Objective & feasibility of the DT

The objective of a DT determines the composition and modeling process of the DT (Giering & Dyck, 2021). As addressed in the conclusion of Chapter 2, the function of the DT will be to support the design process of green ships for retrofitting purposes. The objective of the DT is to generate output that will drive design decisions integrating energy-efficient technologies to lower CO_2 emissions. Consequently, the output of the DT will be linked to the emission determination and prediction of the physical vessel in order to provide information for these design decisions. As the fuel consumption of a ship is directly linked to its emissions, a fuel consumption model is an exemplary representation of a ship's emission prediction (Fan et al., 2022). Thus, the DT objective will indicate which virtual models are required for the DT (green circle Figure 3.2).

The DT output is based on performing simulations, using available operational data. The composition of the virtual part of the DT depends on this data, as this will determine the feasibility of modeling certain parts within the DT, and thus drives the modeling process (Giering & Dyck, 2021). By investigating the available data, the virtual models that are feasible to construct are identified (red circle in Figure 3.2).

Finally, the overlap between the required models (derived from the DT objective) and the feasible models (derived from the available data) will provide the models to be selected for the final DT (Figure 3.2).
After establishing the DT's objective and the model selection process, the modeling phase commences. The

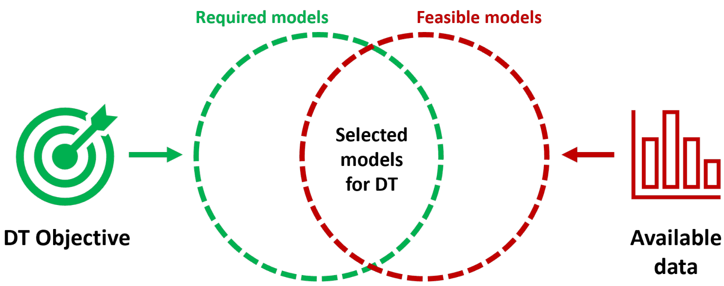

Figure 3.2: Selection process of digital models for DT

next sections will outline and discuss the general steps involved in this modeling process, as follows:

1. Set-up the data acquisition
2. Establish a preprocessing framework
3. Choose modeling approaches for the virtual models

4. Perform model training in case of statistical-based models
5. Verify and validate (V&V) the virtual models
6. Integrate the virtual part with the physical part

3.3. Data collection & acquisition

In order to acquire the data for the DT, a data acquisition system needs to be established. The data acquisition system will collect the information required to model the DT, and therefore function as the collector for the bi-directional data connection. This data collection can be done through various methods.

In the case of a ship, the data acquisition can be done by using onboard sensors together with the Internet of Things (IoT) (Chen et al., 2018). The IoT enables this data retrieval through the sensors as seen as a totally connected network of numerous different sensors. This (wireless) network is then linked with the integrated automation and monitoring system of the ship where the data is stored. The operational data is later on delivered to monitoring centers ashore where it can be analyzed and used for further operations. Traditionally operational data is provided with a noon report. Often manually prepared by the chief engineer on a ship, a noon report contains the average ship performance features on a daily basis, consisting of one data point representing the respective day (Anish, 2021).

With the increase of data handling capability and collection through the IoT, the use of high-frequency (HF) data reports become more common which contain values of ship performance on a minute-scale (Abbas et al., 2022). During the MEPC in 2016, the IMO adopted the Data Collection System (DCS) for the ship's fuel oil consumption. Since 1 January 2019, the DCS has been mandatory for ships of 5000 GT and above, which are required to collect consumption data for each type of fuel oil they use. Besides fuel consumption data, also voyage and environmental data are collected as specified by the IMO. The IMO's DCS typically includes (IMO, 2023b):

- Bunker delivery notes (BDNs)
- Voyage data records
- Electronic record books
- Fuel flow meters
- Emission control systems
- Hourly fuel oil consumption data
- Traveled distance

The IMO utilizes this information to establish further environmental measures in order to reduce GHG emissions from ships (IMO, 2023b). Constructing the DT-models based on data collected with IMO's DCS guidelines would be convenient for the future as the DCS is mandatory for most ships. With this solid and standardized data source, the reliability of the DT is increased throughout the ship's life-time with this continuous data abundance. Following the definition in Section 3.1, for a DT this data flow needs to exist in an automated way.

3.4. Data preprocessing

With the operational data accessible, it needs to be preprocessed in order to be of use as input for the virtual model(s). Depending on the input format of the constructed DT, the data undergoes certain preprocessing steps, such as data cleaning and normalization. García et al. (2016) discuss key data preprocessing techniques in the field of computer science, consequently related to DT modeling. An overview of these techniques is depicted in Figure 3.3.

There is no one-truth preprocessing order for these techniques. A preprocessing framework depends on the chosen modeling approach, and consequently on the type of data. By establishing an effective framework, redundancies are reduced regarding all connected features within the DT (Autiosalo et al., 2019).

With regard to ship operations, Zwart (2020) has adopted a framework based on the techniques by García et al. (2016) for ship's trim optimization. This proposed framework is used with a gray-box modeling approach (GBM) to estimate fuel consumption during sailing. In this framework (Figure 3.4), the sequential order preprocessing steps are established based on the quality and format of the available data (noon-reports), and

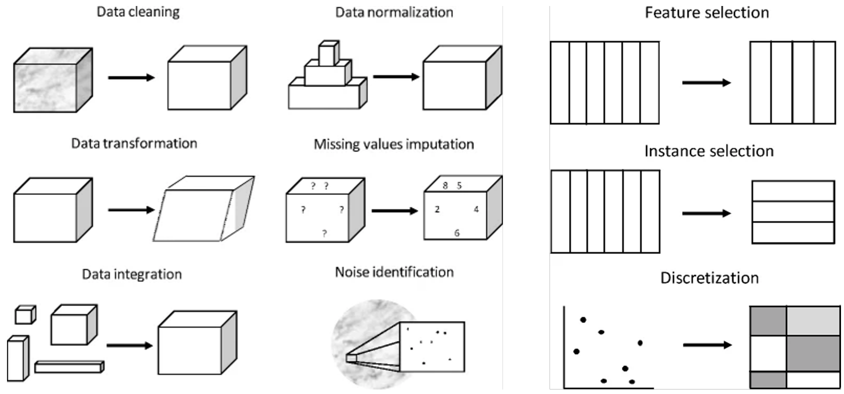

Figure 3.3: Data preprocessing techniques by García et al. (2016)

the intermediate outputs within this framework.

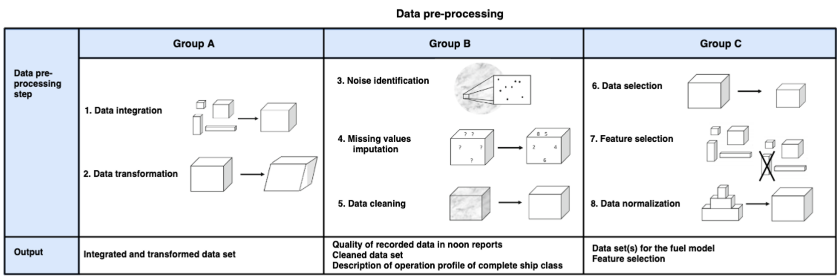

Figure 3.4: Data preprocessing framework for GBM by Zwart (2020), based on García et al. (2016)

In the work of W. Li (2023), a preprocessing framework is proposed for DT supported design process of green transport vessels. As with the framework of Zwart (2020), this framework is also based on García et al. (2016). Although it is part of a proposed design framework regarding DT for green transport vessels, and therefore is not been validated yet, it provides a basis for DT-supported ship design. This proposed framework is depicted in Figure 3.5.

3.5. Modeling approaches

When the virtual models are selected, the modeling approach can be determined. This section will elaborate on three different modeling approaches adopted in standard data-science literature, namely: black-box modeling, white-box modeling, and gray-box modeling (Ehmer & Khan, 2012).

Black-box models

A black-box model (BBM) is a digital model purely based on statistical techniques in order to find relationships between a set of empirical input data and a set of desired output data (Ehmer & Khan, 2012). No prior knowledge is required of how the system works or any physical relevance regarding the considered system. The emphasis is entirely on the relationship between the input and output. Examples of applied techniques are various regressions methods and ANNs (Mjalli et al., 2007). Hu et al. (2019) investigated the feasibility of modeling a ship's fuel consumption with environmental data using a BBM. BBMs have proven to achieve a high level of accuracy due to their ability to identify complex patterns between the provided data sets (Yasar & Wigmore, 2023). Hu et al. (2019) demonstrated that both a backpropagation neural network (BPNN) method and a Gaussian process regression (GPR) are capable of predicting fuel consumption within acceptable accuracy. On the other hand, BBMs have shown that they require a significant amount of high-quality data and lack poor extrapolation properties, hence predicting inaccurate off-design conditions (Pedersen & Larsen, 2009). When data scarcity is a fact, a pure BBM will not be the preferred choice (Parkes et al., 2018).

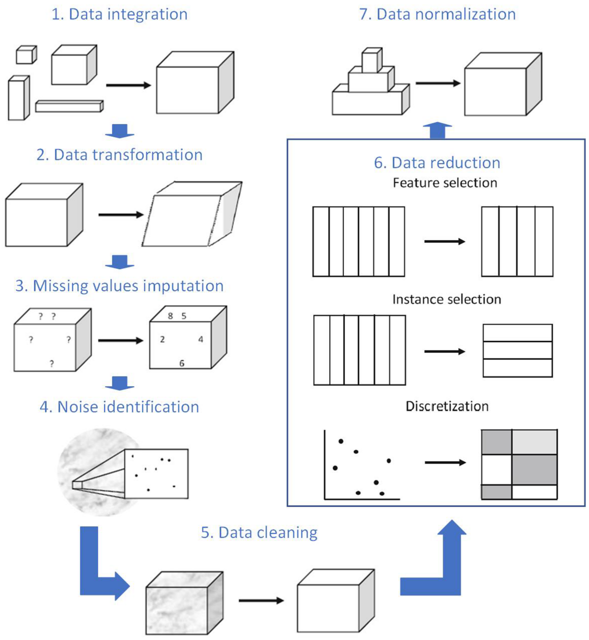

Figure 3.5: Data preprocessing framework of DT for new-build ship design by W. Li (2023), based on García et al. (2016)

White-box models

A white-box model (WBM) is the exact opposite of a BBM. Instead of using statistics, it is constructed based on physical principals, a theoretically derived set of equations, and experimentally derived data (Ehmer & Khan, 2012). By means of this derivation, the WBM achieves comprehensive levels of fidelity within the defined space but increases the level of complexity of the total model (Zwart, 2020). The main idea of the white box modeling for ship performance evaluation can be summarized as follows; the ship's total resistance is divided into components like still-water resistance and added resistance due to wind, waves, shallow water, and maneuvering (Haranen et al., 2016). An established ship performance model can consequently be used for evaluating the respective ship and investigating potential gains through retrofitting. Fan et al. (2020) established a WBM based on the ship resistance regression method by Holtrop and Mennen (1982) to predict the fuel consumption of a bulk carrier with an average accuracy of 93.54%. Even though a WBM approach provides insight into the correlation between the various parameters (Mauro & Kana, 2023), it also increases the complexity of the model as these internal parameters are closely connected and easily affected, resulting in errors (Fan et al., 2022; Haranen et al., 2016). A simple representation of a BBM and a WBM is depicted in Figure 3.6.

(a) Black box model (BBM)

(b) White box model (WBM)

Figure 3.6: Schematic representation of a BBM and a WBM (Ehmer & Khan, 2012)

Gray-box models

A combination of a BBM and WBM is the gray-box model (GBM), aiming to achieve the advantages of both model types. A GBM consists of the analytically and experimental driven methods of a WBM to achieve physical accuracy, together with the statistical techniques of a BBM to identify patterns and eventually lower the computational time (Ehmer & Khan, 2012; Fan et al., 2022). As mentioned in Section 3.4, Zwart (2020) developed a GBM for trim optimization of a sailing ship to predict fuel consumption, using operational data from noon reports. By using a GBM approach, Zwart was able to take into account dynamic factors related to environmental conditions. Even though GBMs offer promising benefits, for example, they require fewer data than BBMs and have a lower level of complexity than a WBM, it also has some disadvantages. GBMs have limited transparency due to the fact a part of the model is still related to a BBM and have a lower overall accuracy than WBMs (Zwart, 2020). But if these limitations are acceptable for its application, then the GBM is a good candidate.

A GBM can be constructed in two ways: by combining the BBM and the WBM either in parallel or in series. Leifsson et al. (2008) used a GBM to predict the fuel consumption of an ocean-going cargo vessel. Also, the difference between using a parallel or serial-coupled BBM-WBM was investigated. As Leifsson et al. (2008) found a higher accuracy by the GBM than using a BBM and better extrapolation capabilities than a WBM, there was no major difference between the parallel and serial gray-box modeling approach. Figure 3.7 illustrates the possible composition of a GBM coupled parallel and in series.

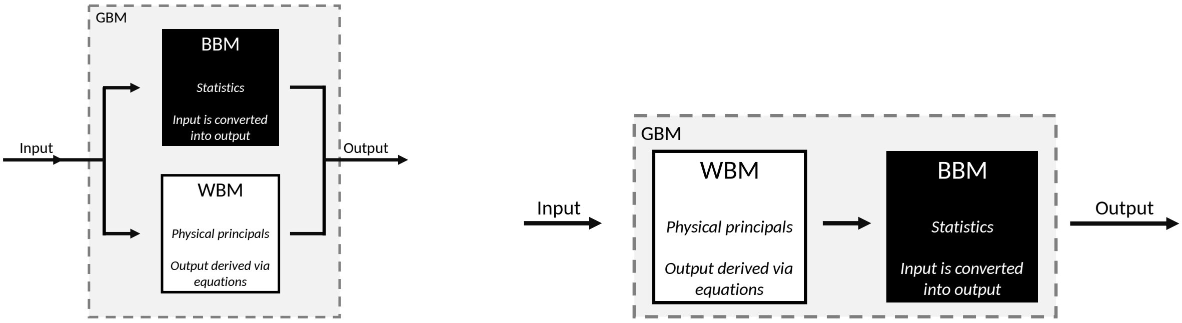

(a) Parallel GBM (b) Serial GBM

Figure 3.7: Parallel and serial coupled gray-box model (Leifsson et al., 2008)

Summarizing, the modeling approach will depend on the objective of the DT, available data, and acceptable accuracy range. With each modeling type having its own advantages and disadvantages, a trade-off has to be made to determine the modeling approach.

3.6. Model training

After the data is preprocessed it is applicable to the virtual model. Through training, the model is calibrated in order to achieve acceptable accuracy. For model training, which is required for a BBM and the black-box part within the GBM, several options are possible. By using machine learning algorithms, and especially DLAs, the model is able to learn from the provided data and predict future states. DLAs are a preferred choice for data-driven models together with an abundance of data (Brunton & Kutz, 2022; Dairi et al., 2019). Several DLAs, used for computer modeling with known maritime applications are discussed further on.

Within deep learning, ANNs are commonly been used, and especially with gray-box modeling for maritime applications (Duan et al., 2023; Parkes et al., 2018; Pedersen & Larsen, 2009; Skulstad et al., 2023; Yoo & Kim, 2023; Zwart, 2020). ANNs are inspired by the structure and functioning of the human brain. They are computational models composed of multiple layers of interconnected nodes, called artificial neurons, that work together to process and learn from input data. ANNs have the ability to recognize complex patterns in order to make predictions (Tibco, 2023). A neuron receives at least one input value, applies weights to the input, and passes the weighted sum through an activation function to produce an output. The first layer in an ANN is the input layer, receiving the initial data. The last layer is the output layer, which produces the final output. In between are so-called hidden layers, which perform intermediate computations. In Figure 3.8 a basic layout of an ANN is presented.

The training process consists of providing the network with a selected training dataset with known input and output values. The network adjusts the weights of its neurons through an iterative process called back-propagation. This training process aims to minimize the difference between the predicted outputs and the true outputs, enabling the network to generalize and make accurate predictions on newly provided data (Y.-S. Park & Lek, 2016). ANNs have been successfully applied by Pedersen and Larsen (2009) in order to predict the

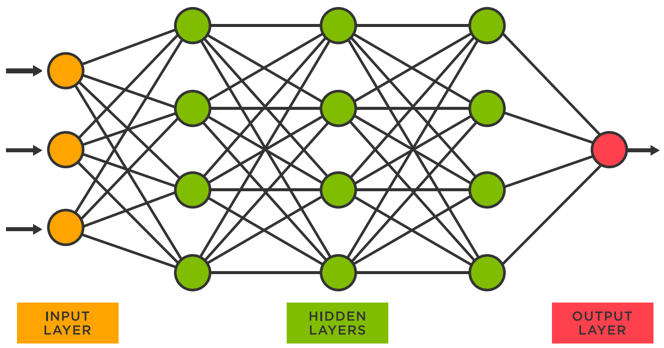

Figure 3.8: Basic layout of an ANN (Tibco, 2023)

ship speed and propulsion power of container vessels. Parkes et al. (2018) have proposed and successfully demonstrated a prediction method for the shaft power of large transport vessels, achieving a high accuracy by using ANNs.

Another training method is by applying a combination of Gaussian processes (GPs) together with ANNs. A GP is defined by a prior normal distribution over mathematical functions, allowing to derive the most likely functions that fit the observed data (Natsume, 2021). These functions follow the predicted output variables from the input data of the model. The combination of ANN with GP aims to address the limitations of traditional deep learning models by providing uncertainty estimates and handling small data sets more effectively (Natsume, 2021). Petersen et al. (2012) presented a comparison between applying ANNs and GPs for model training in order to predict the ship propulsion efficiency, discussing the draw-backs of GPs regarding their poor scaling abilities and the advantage of recognizing and quantifying the uncertainty within the applicable model.

Research done by Coraddu et al. (2019) made use of Extreme Learning Machines (ELMs) for investigating and predicting the ship's speed loss due to fouling effects. ELMs are similar to ANNs but apply feedforward neural networks. The feedforward training process consists of randomly assigning the weights between the input and typically one hidden layer, instead of applying the iterative, backward propagated process of an ANN (Tissera & McDonnell, 2016). By this arbitrary assignment and direct computation of output, the computational and training speed of the model is faster for an ELM than for an ANN. However, due to the lower complexity of ELMs with a single hidden layer, the generalization performance is lower than that of an ANN. Complex datasets with high dimensionality, and thus complex patterns, prefer ANNs over ELMs.

In summary, deep learning algorithms like ANNs have proven effective, as seen in applications like ship speed and propulsion power prediction by researchers such as Parkes et al. (2018) and Pedersen and Larsen (2009). Additionally, combining GPs with ANNs offers valuable uncertainty estimates and better handling of smaller datasets, as highlighted in the work of Petersen et al. (2012). On the other hand, ELMs present a faster computation alternative, but their simplicity may limit their performance on complex, high-dimensional datasets. Selecting the most suitable modeling method should be guided by the specific requirements and characteristics of the maritime application at hand, ensuring optimal performance and decision-making support.

3.7. Model verification & validation

When the chosen models are constructed, and trained in the case of a BBM or GBM, they need to be verified and validated. The verification and validation processes are critical to ensure the accuracy and reliability of the chosen modeling approaches.

Verification involves assessing whether the outputs of the constructed models align with the available data (Tao et al., 2018). It serves as a quality check to confirm that the models faithfully represent the underlying systems they aim to emulate. Additionally, the training phase, for especially BBMs and GBMs, plays a vital role in their initial validation, where the models are evaluated using dedicated testing datasets that were not used during the training phase to ensure their effectiveness (Ehmer & Khan, 2012; Haranen et al., 2016).

In contrast, the validation process goes beyond mere consistency with data and focuses on evaluating whether the models produce the desired output, as determined by the initial objective (Ehmer & Khan, 2012; Tadros et al., 2023). For BBMs and GBMs, this assessment occurs after training and may involve comparing the model outputs with real-world data (Haranen et al., 2016). Meanwhile, WBM validation involves evaluating the internal components of the model against onboard ship data (Haranen et al., 2016).

Furthermore, a case-study approach can be employed during both validation and verification, wherein the model's outputs are compared to predefined objectives to ensure they meet the intended goals (Sapkota et al., 2021). This comprehensive verification and validation process is essential for the successful integration of models into the DT for retrofit design, ensuring the DT provides accurate insights and supports informed decision-making.

3.8. Virtual - physical integration

After the models have been verified and validated, they can be integrated into the DT infrastructure. Following the aforementioned DT definition by Grieves (2014), the output of the virtual models needs to be sent in an automated way to the physical ship.

When a DT is constructed for ship operational purposes, the output will be related to monitoring and predicting of performance and maintenance (Mauro & Kana, 2023). Also, virtual tests can be performed by the DT to safely investigate off-design conditions for possible future situations (Mauro & Kana, 2023). As it is related to the physical vessel, this output can directly be received and used by the respective vessel.

In the case of a DT for retrofit design purposes, the output will relate to recommendations regarding design decisions. This has no value to be sent directly to the vessel as it will not result in instant retrofitting. It is considered that the output of the models will drive the retrofit design, and after the retrofit is successfully been performed, the virtual models will represent the modified vessel. Thus, after the retrofitting the virtual-physical integration can take place. With the integration completed, the DT is established and can be used for operational purposes, such as performance monitoring.

Figure 3.9 shows a schematic representation of the transition towards a DT for retrofitting. The previously mentioned integration step is performed at the end and can occur simultaneously with the completion of the retrofit (step V). The final retrofit DT originates from a digital model which represents the ship (step I), and which is further investigated for possible retrofit options (step II). The chosen retrofit design (step III) will then be used for the actual retrofitting of the respective vessel (step IV).

3.9. Summary of DT construction for retrofit design

This chapter elaborated on the modeling process of a DT for marine design purposes, aiming to answer RQ2: *'Which steps are involved in constructing a DT for retrofit design?'*

Computer models are often falsely labeled as DT. In order to correct for this error a clear definition of a DT is established, namely the combination of a physical and virtual product connected through a two-way automated data flow. The steps involved in constructing a DT are identified as:

1. Determining the DT objective
2. Set-up the data acquisition
3. Establish a preprocessing framework
4. Choose modeling approaches for the virtual models
5. Perform model training in case of statistical-based models
6. Verify and validate (V&V) the virtual models
7. Integrate the virtual part with the physical part

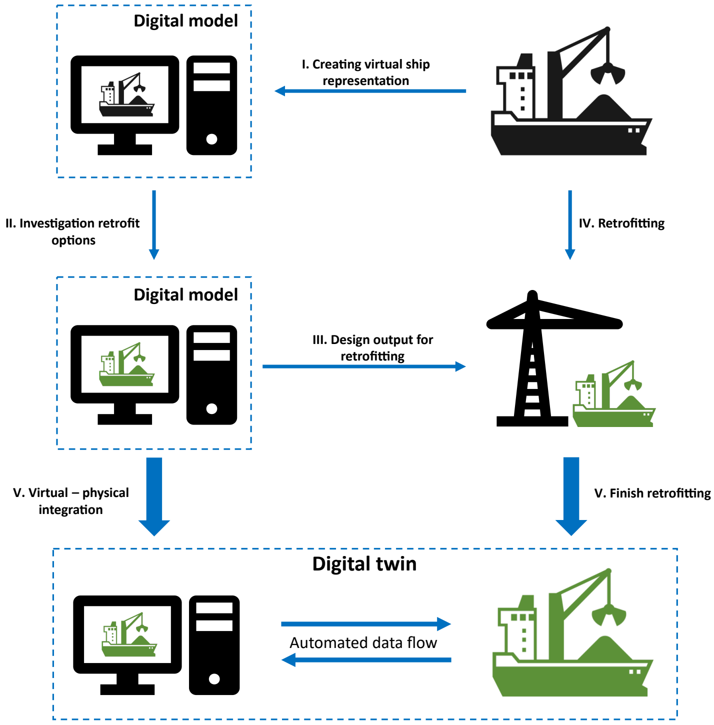

Figure 3.9: The development of the digital twin for retrofitting, based on the adopted DT definition

The previously mentioned steps are all linked with each other through dependency of the available data and, consequently choices made during the modeling process are based on the data.

By formulating the DT objective, the virtual models can be identified which are required to assess the DT. These required models have to comply with the models that are feasible to construct. The feasible models are dependent on the available data, as the data indicates the modeling possibilities.

The data acquisition system determines the availability and quality of the data being used for the DT. From January 2019, the IMO established their DCS which is mandatory for most ships. Constructing a DT based on IMO's DCS is considered to be convenient as it provides a solid source of operational data in the future, especially taking into account the life-cycle evaluation capabilities of a DT.

It is essential to establish an effective data preprocessing framework when operational data is available. After preprocessing, the data is suitable as input for the chosen models. Prepossessing steps involve techniques, such as data cleaning, normalization, and noise identification. Depending on the collected data, the respective framework is established.

When the virtual models are selected, the modeling approach can be determined. From standard data-science three main modeling approaches are provided: BBM, WBM, and GBM. BBMs rely solely on statistical relationships between inputs and outputs, requiring no prior knowledge of the system. They excel in accuracy under design conditions but may struggle with extrapolation and demand ample data. In contrast, WBMs employ physical principles and mathematical equations, increasing model complexity. However, they can introduce significant errors due to random events, such as environmental conditions. A GBM combines both approaches, offering reasonably high accuracy while benefiting from reduced computational time compared to BBMs. A trade-off should guide the choice between BBM, WBM, or GBM.

In the case of statistical-based models (BBM or GBM), model training is required in order to calibrate and achieve acceptable accuracy. Model training is preferably been performed with DLAs, such as artificial neural networks, Gaussian processes, extreme learning machines, or combinations of multiple algorithms.

Before integrating the virtual models with the physical part, the models need to be verified and validated. The V&V is critical to ensure the accuracy and reliability of the total system can be attained. Model training can be considered as part of the V&V as it calibrates the systems and increases accuracy. Although the actual validation will use different datasets as the sets used to train the model. A case-study or performing model tests can also be done as a V&V-procedure.

As a final step, the virtual-physical integration can take place. With a design orientated DT, the virtual model output will relate design decisions that have no direct value for the respective vessel. After the retrofitting of the vessel is completed, based on the derived output, the integration can take place as the virtual part will represent the modified physical vessel.

With the construction and modeling process of a DT for retrofit design purpose being discussed, a DT objective needs to be chosen in order to present the addressed DT method. The next chapter will elaborate on this regarding a defined DT objective and available operational data, which will form the basis of the adopted methodology of this research.

4

Green digital model methodology

This chapter elaborates on how a digital model for a green ship is constructed by answering RQ3: *'What is the most suitable green ship digital model using bunker delivery notes'.*

First, by following the aforementioned definition of a DT, the argumentation for constructing a digital model is provided. Secondly, the available data is discussed and the case-study is introduced. Then, the environmental assessment of the case-study is presented which together with the data will result in the identification of the models that will be constructed. This will represent the methodology of this research. A conclusion is provided summarising the process of constructing a green DM and answering RQ3.

4.1. Green ship digital model

As discussed in Section 3.8, a DT for retrofit purpose starts as a digital model which becomes a DT after the retrofitting is completed. This thesis will focus on the modeling of virtual part within the DT environment which will lay the basis for a green ship DT using this operational ship's data. Thus, using the definition by Kritzinger et al. (2018), this research will work on a green ship **digital model** (DM), supporting the process of constructing the digital twin (Figure 4.1). This will be addressed as the green ship DM.

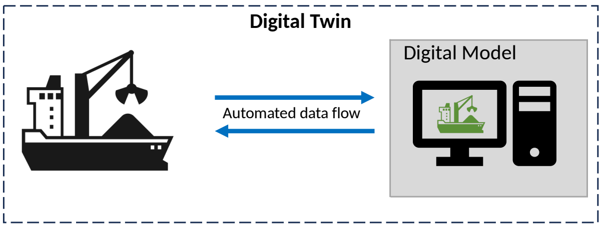

Figure 4.1: Focus of this research: representation of the green ship digital model (gray) within final digital twin

4.2. Available data & case-study

The DM will be strongly dependent on the available data with which it will be built. Within the DT4GS project, HF operational data is collected through four Living Labs (LLs) which cover four distinctive operating ship types (oil tanker, container vessel, bulk carrier, and ROPAX vessel) of the collaborating shipping companies. Currently, this collected HF data is manually sent from the ships to a digitally accessible platform. The HF data of the 300-meter bulk carrier is chosen to be used for this thesis, as this has the most extensive data available at this moment. This data is collected following IMO's approved guidelines regarding their adopted operational data collection, namely IMO's DCS method A: BDNs[1]. The BDNs contain ship and voyage data, such as engine rpm, ship speed, fuel consumption, water depth and wind speed. An overview of all the different data types is provided in Appendix A. The available BDNs of the bulk carrier contain over 129,000 data points, with a time interval of 5 minutes during the following periods:

[1] https://www.imo.org/en/MediaCentre/PressBriefings/Pages/01-MARPOLamendments01012019.aspx

- Q2 2022: 02/06/'22 - 30/06/'22
- Q3 2022: 01/07/'22 - 30/09/'22
- Q4 2022: 01/10/'22 - 31/12/'22
- Q1 2023: 01/01/'23 - 24/02/'23
- Q2 2023: 01/04/'23 - 30/06/'23
- Q3 2023: 01/07/'23 - 30/09/'23

From here on, these periods will be referred to with their corresponding year and quarter.

4.3. Environmental assessment

The next step is to link the available data to the environmental goal of the main objective. As discussed in Section 2.5.3, the EEXI will be used as the main measurement tool to assess the desired CO_2 reduction, together with the CII. Both the attained CII and attained EEXI are measures that compare the environmental impact on society with the benefits to society, respectively in terms of CO_2 emissions and transport work. Here the CII follows an operational approach and the EEXI a technical (design) approach (Equations 2.5 & 2.2).

$$CII_{attained} = \frac{\text{Operational annual CO}_2\text{ emissions}}{\text{Operational annual transport work}} = \frac{FC_{1year} \cdot C_{fCO_2}}{DWT \cdot D_{1year}} \tag{Ref. 2.5}$$

$$EEXI_{attained} = \frac{\text{Design CO}_2\text{ emissions}}{\text{Design transport work}} = \frac{P_{engine} \cdot sfc \cdot C_{fCO_2}}{DWT \cdot V_s} \tag{Ref. 2.2}$$

The environmental aspect of the thesis' main objective is to investigate and achieve CO_2 reduction. By investigating the formulas of the CII and EEXI, the factors within both measures can be identified that drive the emission reduction goal. Because this thesis focuses on ship design, the yearly sailing distance (D_{1year}) is kept the same. Also, the dead-weight tonnage (DWT) of the ship is kept the same in order to restrict potential retrofit design decisions not to being too extensive and resulting in significant changes in cargo capacity.

Equations 4.1 and 4.2 are respectively the improved CII and improved EEXI. The term 'improved' refers to the identification of ship parameters linked to the CO_2 reduction goal, highlighted in red. In the improved CII the emission reduction is solely linked to the fuel consumption of the ship. This means in order to achieve CO_2 reduction, the fuel consumption (of the same fuel type) of the ship needs to be reduced over the same distance and DWT.

$$CII_{attained-improved} = \frac{\text{Operational annual CO}_2\text{ emissions}}{\text{Operational annual transport work}} = \frac{FC_{1year} \cdot C_{fCO_2}}{DWT \cdot D_{1year}} \tag{4.1}$$

$$EEXI_{attained-improved} = \frac{\text{Design CO}_2\text{ emissions}}{\text{Design transport work}} = \frac{P_{engine} \cdot sfc \cdot C_{fCO_2}}{DWT \cdot V_s} \tag{4.2}$$

In the EEXI the CO_2 reduction is linked to the specific fuel consumption (sfc) and total engine power (P_{engine}), as these are the factors directly contributing to the produced CO_2 emissions. Here the DWT and C_{fCO_2} are also kept the same in order to restrict the impact of retrofit modifications on the cargo capacity and fuel type. This is also in line with the guidelines of the IMO (2021) elaborating on how to treat innovative energy efficiency technologies (green ship design) for the EEXI calculation of a ship, indicating the environmental influence of these factors in the formula. Besides the sfc and P_{engine}, these guidelines also identify a possible shift in the power curve of a vessel due to the implementation of certain green technologies. This shift then results in a change in the combination of engine power and design speed. For that reason, the design speed is also identified to be possibly affected when applying green ship technologies.

Concluding, the main parameters which are identified to contribute to the assessment of the CO_2 emission reduction goal, or to be affected by green ship technologies are:

- annual fuel consumption (FC_{1year})
- specific fuel consumption (sfc)
- total engine power (P_{engine})
- design speed (V_s)

4.4. Models

In this section, the different models are presented which will be used for the green ship DM. The parameters identified in the assessment tools in the previous section will guide the identification of the models required for the environmental assessment. The available operational data determine which models are feasible to construct. The overlap between both outcomes provides the models that will be selected for the green ship DM of the bulk carrier case-study (Figure 4.2).

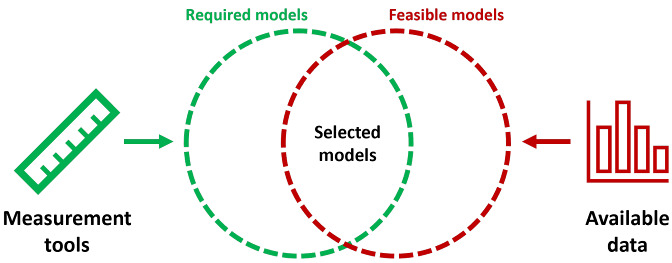

Figure 4.2: Process of model selection for green ship DM

The goal is to make a virtual representation of the ship itself, in this case, the bulk carrier, and to implement green ship technologies through modeling in order to be able to assess potential benefits for retrofit to achieve the CO_2 reduction goal. This entails constructing a model representing the ship and another model representing the green ship technologies, as illustrated in Figure 4.3.

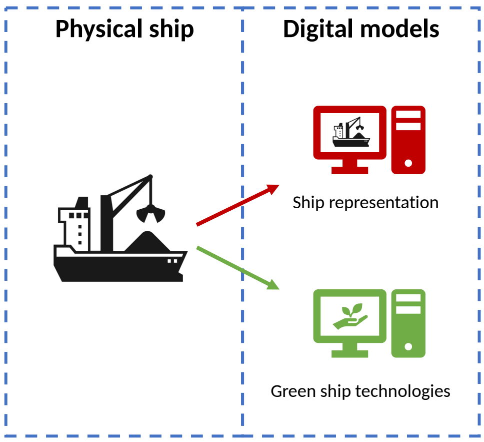

Figure 4.3: Adopted modeling approach: part representing the ship and part representing green ship technologies

4.4.1. Ship representation

Addressed in Section 4.3, in both the equations of the CII and the EEXI, the (specific) fuel consumption is identified as an important parameter. This suggests that a fuel consumption model (FCM) can be of use for the DM. These models have already extensively been utilized to represent an operational ship and achieve accuracy above the 90% (Fafoutellis et al., 2020; Fan et al., 2022; Hu et al., 2019; X. Sun, 2015). It is therefore chosen to use an FCM as a virtual representation of the bulk carrier. The review paper of Fan et al. (2022) showed that an FCM of a ship can successfully be modeled by using a WBM, BBM, or GBM. These three modeling approaches for an FCM will be discussed next.

In the aforementioned FCM of Fan et al. (2020) (Section 3.5) random environmental parameters were used to establish a WBM. With the combination of this data, the Holtrop & Mennen method, and applying the ship-engine-propeller principle, the fuel consumption could successfully be predicted with an acceptable accuracy of 93.5% regarding available real-time data of the respective vessel.

Besides a WBM, BBMs are also proven to successfully predict a ship's fuel consumption (Hu et al., 2019; X. Sun, 2015; Uyanık et al., 2020). In the work of Uyanık et al. (2020) multiple prediction methods (e.g., Ridge Regression, Tree-Based Algorithms, Multiple Linear Regression) are applied on a fuel consumption BBM for a container ship. The BBM was established from main engine characteristic inputs, such as the number of cylinders, scavenging air, cooling water temperature, and engine rpm. By only taking into account parameters from the engine room, Uyanık et al. (2020) found the highest accuracy by applying Bayesian ridge regression, Kernel ridge regression, Multiple linear regression, or Ridge regression on the BBM, all with a root-mean-square error of 0.0001. Both the work of X. Sun (2015) and Hu et al. (2019) successfully show that the BPNN method is able to predict ship fuel consumption within acceptable accuracy. In both researches, a BBM was developed based on environmental input, including wind speed, wind direction, water depth, water speed, and engine power. Hu et al. (2019) also compared the BPNN method with GPR, finding a slightly higher accuracy applying GPR but at the cost of more computational time. Hu et al. advise it is up to the final user to make the trade-off between computational time and accuracy.

Even though GBMs are not traditionally used to model ship's fuel consumption due to similar accuracy with most BBMs, they become more appealing to apply with current increasing accuracy improvement methods proposed by researchers (Fan et al., 2022). The benefit of a GBM is it can achieve accurate predictions with less data than a BBM and even with insufficient data coverage, consequently lowering the computational time (Fan et al., 2022). Yang et al. (2019) showed this benefit by using a GBM approach for the modeling of the fuel consumption of an oil tanker. Although basic principles regarding ship propulsion were applied and no hull-propeller effects were taken into account, the GBM mitigated the incomplete data coverage through integrated successive parameter estimation programs. In the work of Yuan and Nian (2018) a Gaussian process model was used to investigate the influence of environmental and operational factors on fuel consumption. With this type of GBM, the relationship between energy saving capabilities and fuel consumption reduction could be verified, resulting in a refining emission reduction strategy.

In order to determine which type of modeling will be used for the fuel consumption model, the available data needs to be investigated. In the BDNs of the bulk carrier case-study, environmental data that corresponds to the WBM of Fan et al. (2020) and BBMs of X. Sun (2015) and Hu et al. (2019) are present. This indicates the feasibility of developing both a WBM and BBM using environmental data extracted from the bulk carrier's BDNs. This approach is consistent with the GBM developed by Yuan and Nian (2018). By merging these models, a GBM can be constructed for fuel consumption. By adopting a GBM, the aforementioned benefit of less computational time can be enjoyed (Fan et al., 2022). Moreover, a GBM has a wider range maintaining acceptable accuracy with different engine speeds compared to a BBM (Coraddu et al., 2015). It is therefore chosen to develop a fuel consumption GBM using the available environmental data together with engine power based on the work by Fan et al. (2020) and Hu et al. (2019). This fuel consumption model will be the virtual representation of the bulk carrier case-study (Figure 4.4).

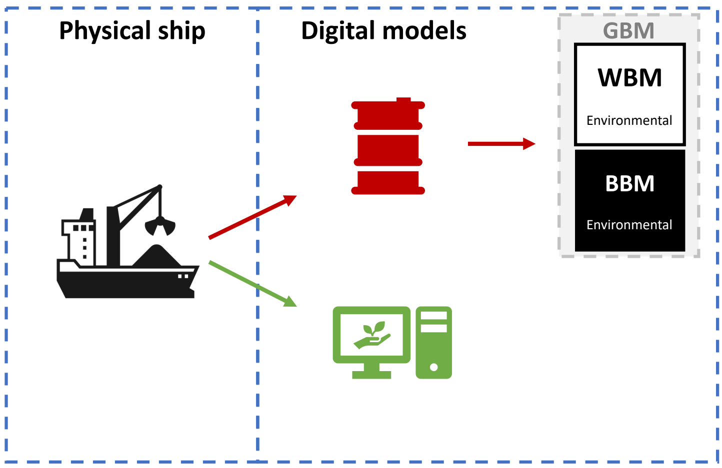

Figure 4.4: Schematic representation fuel consumption model (red oil barrel) modeled with a gray-box approach using environmental data

4.4.2. Green ship technologies representation

Next, the model selection of the green ship technologies is discussed. In the BDNs of the bulk carrier, the wind speed and wind direction are recorded. This indicates the potential for investigating the application of WASP technology. In Section 2.4.7, WASP technology is identified as applicable technology for retrofit. With wind data available its potential can be investigated and therefore chosen to apply as green ship technology for the model.

In the work of Bentin et al. (2018), the modeling of three different types of WASP systems (towing kite, Flettner rotor, and DynaRig sail) are discussed, and their energy saving potential in terms of ship's brake power. Bentin et al. (2018) use a WBM approach for their calculations, in which the wind speed and to be determined WASP system's effective wind surface are sufficient to provide a reliable estimation of the WASP power and its energy saving potential. Their WASP modeling is validated through a case-study with a multi-purpose carrier, bulk carrier, and tanker. These ship types were chosen because they identified them to be suitable for WASP installation without changing the ship's capacity and the cargo loading and unloading function of the ship (Bentin et al., 2018). This is also addressed by Reche-Vilanova et al. (2021), where tankers and bulk carriers are identified to be especially suitable for WASP system installation due to their available deck space. Reche-Vilanova et al. (2021) present a performance prediction program for three WASP types (Flettner rotor, rigid wing sails, and DynaRig sail) with only the ship's main particulars and general WASP dimensions as input data. Using a WBM approach together with a WASP aerodynamic database, a generic approach is established to assess WASP applicability as a design tool during early stage feasibility studies.

Both the work of Bentin et al. (2018) and Reche-Vilanova et al. (2021) successfully present a WBM approach for WASP technology. For that reason, a WBM approach is chosen to model a WASP system to represent the green ship part for the bulk carrier case-study (Figure 4.5). In this thesis, the following WASP systems will be investigated based on the research conducted by Bentin et al. (2018) and Reche-Vilanova et al. (2021): towing kite, Flettner rotor, and DynaRig sail.

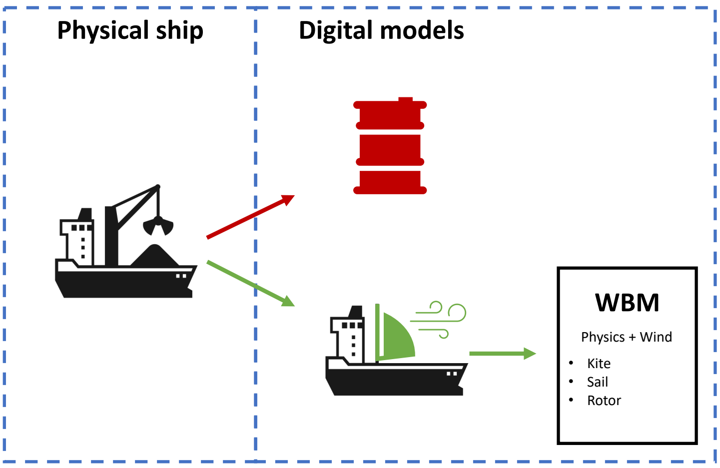

Figure 4.5: Schematic representation WASP model (green sail), representing a kite, sail, and rotor, modeled with a white-box approach using wind data

The available wind data will be used to indicate if it was beneficial to have a WASP installed on this ship in terms of potential fuel savings and CO_2 reduction during the period of data collection. A schematic representation of the total composition of the DM to identify retrofit design is depicted in Figure 4.6.

4.5. Model assessment

In order to validate the models and achieve the set CO_2 reduction goal, the models need to undertake an assessment. This will include an environmental assessment regarding the selected IMO's measurement tools EEXI and CII, and a financial assessment. A feasibility check, in terms of spatial availability, is conducted during the respective WASP configuration selection for the case-study.

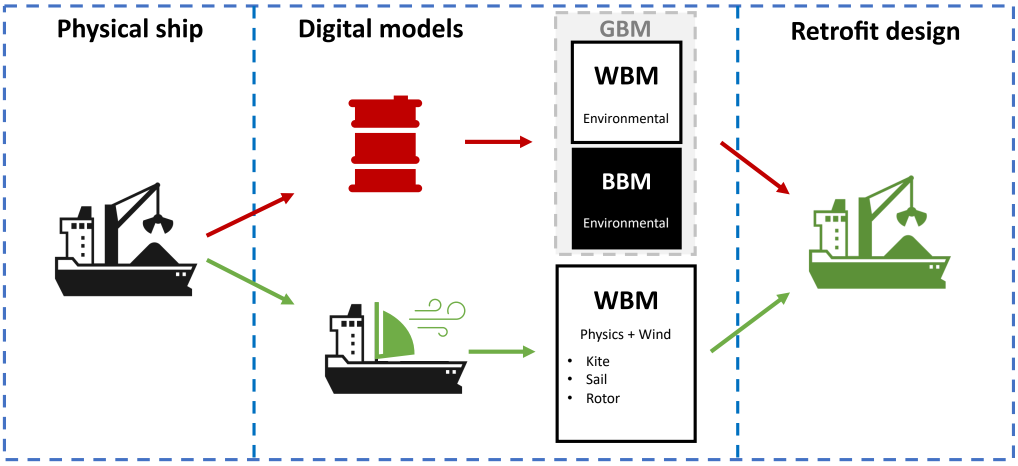

Figure 4.6: Overview of chosen modeling method toward constructing green ship DM for retrofit (green bulk carrier)

4.5.1. Environmental assessment

EEXI

The installation of WASP on a ship influences the total engine power of the respective ship (Chou et al., 2021). For that reason, WASP technology is taken into account in IMO (2021) innovative energy efficiency technology guidelines. Depending on the characteristics and effects of the EEXI formula, these technologies are allocated to category A, B-1, B-2, C-1, or C-2. WASP technology is allocated in category B-2. Whereas the B-category refers to technologies that reduce the propulsion power of the ship at the design speed without generating electricity. A distinction is made regarding the possibility of using the technology at its full output at any time (f_{eff} = 1) or only under limited conditions (f_{eff} < 1), respectively category B-1 and B-2. A small overview of the other categories is provided in Figure 4.7.

Innovative Energy Efficiency Technologies				
Reduction of Main Engine Power			Reduction of Auxiliary Power	
Category A	*Category B-1*	*Category B-2*	*Category C-1*	*Category C-2*
Cannot be separated from overall performance of the vessel	Can be treated separately from the overall performance of the vessel		Effective at all time	Depending on ambient environment
	$f_{eff} = 1$	$f_{eff} < 1$	$f_{eff} = 1$	$f_{eff} < 1$
– low friction coating – bare optimization – rudder resistance – propeller design	– hull air lubrication system (air cavity via air injection to reduce ship resistance) (can be switched off)	– wind assistance (sails, Flettner-Rotors, kites)	– waste heat recovery system (exhaust gas heat recovery and conversion to electric power)	– photovoltaic cells

Figure 4.7: IMO's innovative energy efficiency technologies categories, including WASP systems (red-dashed box) (IMO, 2021)

In order to determine the available effective power of the WASP, the IMO has set up Equation 4.3 (IMO, 2021). Herein the available effective power ($f_{eff} \cdot P_{eff}$) is represented as a matrix operation, containing the availability factor (f_{eff}) and the effective power (P_{eff}). By formulating the available effective power in this way, each wind condition is addressed with a probability and a specific wind propulsion system force. It should be noted that secondary effects due to applying WASP which might increase ship resistance are not taken into account in these guidelines. Without a significant loss of accuracy, the additional drag due to heel and rudder angle, leeway, or reduced propeller efficiency are ignored in light running conditions. Moreover, the forces generated during those conditions are considered to occur during unsafe operational conditions, thus automatically being avoided during sailing.

$$(f_{eff} \cdot P_{eff}) = \underbrace{\left(\frac{1}{\sum_{k=1}^{q} W_k}\right)}_{\text{Wind probability}} \cdot \left(\underbrace{\left(\frac{0.5144 \cdot V_{ref}}{\eta_D} \sum_{k=1}^{q} F(V_{ref})_k \cdot W_k\right)}_{\text{WASP power generation}} - \underbrace{\left(\sum_{k=1}^{q} P(V_{ref})_k \cdot W_k\right)}_{\text{WASP power demand}} \right) \tag{4.3}$$

The parameters highlighted in red (Equation 4.3) are the three different wind-dependent parameters that need to be determined for the WASP power calculation by the IMO, representing the following:

- the global wind probability matrix; W_k (3x)
- the force matrix of the respective WASP for a given ship speed; $F(V_{ref})_k$
- the WASP's power demand for a given ship speed; $P(V_{ref})_k$, with the same size as W_k and $F(V_{ref})_k$

For each of these parameters, the IMO has provided calculation guidance. Certain WASP systems require electric power input in order to generate propulsive force, an example of such a system is a Flettner rotor which needs to be rotating at a certain speed to generate this force. This power demand is usually provided by the manufacturer and is implemented as $P(V_{ref})_k$ in Equation 4.3.

In the force matrix $F(V_{ref})_k$, each element represents the propulsion force exerted by the WASP for the respective wind speed and angle. Various methods can be used to determine $F(V_{ref})_k$, of which the following three are briefly discussed in the guidelines: wind tunnel model test, numerical calculation, and full-scale test. Due to the data-driven nature of this thesis, numerical calculations through WBMs will be used to determine the force matrix of the respective WASP system (Section 4.4.2).

The global wind probability matrix W_k, which covers the average wind conditions of all main global shipping routes, is provided in the guidelines (IMO, 2021). Each matrix element represents the probability of the specific wind speed and angle relative to the ship. Along the routes from the main global shipping network (Figure 4.8), 106 wind conditions charts were used to determine W_k.

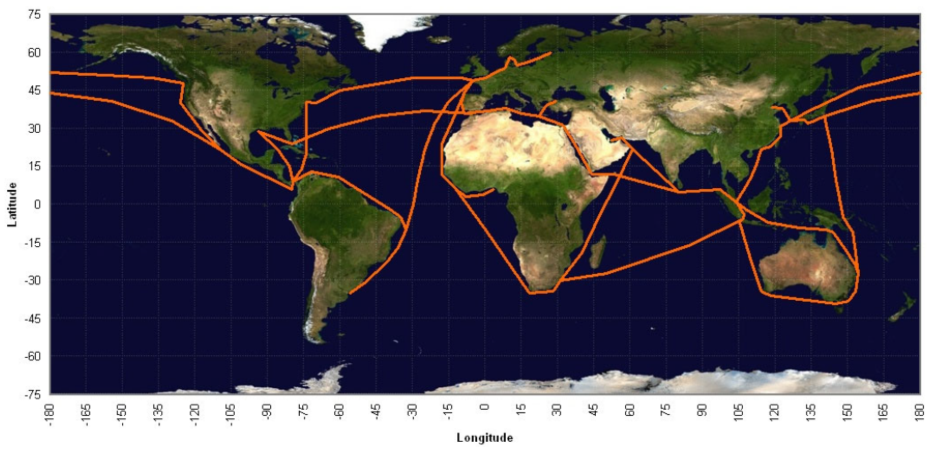

Figure 4.8: The main global shipping network used for the wind probability matrix (IMO, 2021)

When the $F(V_{ref})_k$ is properly modeled (WBM), together with the determination of W_k and $P(V_{ref})_k$, the available effective power of the WASP can be calculated using Equation 4.3. This result is then used as a power reduction in Equation Ref. 2.2 in order to calculate the new EEXI value of the ship. Hence, the design speed V_s is kept the same as only a power reduction at design speed is being considered (IMO, 2021).

Finally, the current ship's EEXI and the difference between the new EEXI value including a WASP configuration value determines the CO_2 reduction at the design level.

CII
For the environmental assessment with the CII, only the fuel consumption plays a role. The official attained CII value is calculated with Equation 2.5 using operational data of 1 full calendar year. Unfortunately, no full calendar year is available for the case-study. Moreover, a first investigation of the location-related data per period showed sensor failure of several days in Q3 2023. For this reason, this period is been disregarded for the CII calculation. Also, both Q2 2022 and Q3 2022 do not contain data for 3 months, indicating that a CII calculation of 1 year is not possible. However, one CII calculation will still be performed for the period Q3 2022 - Q2 2023 in order to show the applicability of this assessment tool, indicating the ship's environmental impact at an operational level. The major remark of the performed CII calculation is that it covers in this case-study the CII value of 11 months.

4.5.2. Financial assessment

Besides an environmental assessment of the possible retrofit, also a financial assessment is performed. It is unlikely that ship owners take their ships out of service to retrofit if it does not result in a profit. The financial assessment is performed by calculating the predicted reduction of the fuel costs and providing the payback period. As fuel costs are directly correlated with both fuel consumption and the bunker price of the specific fuel type, the payback period is affected by various factors, such as (Ammar & Seddiek, 2022; Bentin et al., 2018):

- Costs of time that ship is out of service for retrofitting instead of transporting
- Costs of installment retrofit systems
- Maintenance costs installed retrofit systems
- Desired lifetime extension of the ship
- Lifetime of installed retrofit systems
- Expected reduction of fuel costs

This research investigates WASP systems for the potential retrofit. The lifetime of a WASP system and the desired ship's lifetime extension depend on the shipowner. The other four financial parameters are used for WASP's payback period calculation (P). This calculation is performed with Equation 4.4, which is based on the financial assessments by Kiran (2022) and van der Kolk et al. (2019).

$$P = \frac{B + C}{A - D} \tag{4.4}$$

Where the financial parameters represent:

A: $-savings per sailing hour using WASP

B: Purchase & installation system

C: Out of service costs & dry docking

D: Hourly operational & maintenance costs WASP

Although the main objective is centered around environmental assessment, conducting a financial assessment provides valuable insights into the feasibility of the retrofit decision, taking into account factors such as time and cost considerations.

4.5.3. Feasibility assessment

During the WASP configuration selection, a feasibility assessment is performed in terms of the spatial and safety constraints related to the chosen bulk carrier. With the available drawings of the respective vessel, installations of the investigated WASP systems are evaluated regarding available deck space.

4.6. Conclusion on green ship digital model

This chapter has elaborated on how a green DM can be constructed, answering RQ3: *'What is the most suitable green ship digital model using bunker delivery notes?'* Because of the adopted DT definition, a green ship DM will constructed which will support the final DT. This DM depends on the available data which determines the models that are feasible to construct, and on the chosen environmental assessment tools which determine the required models (Figure 4.2).

For the introduced bulk carrier case-study, the selected digital models are an FCM and a WASP model, respectively representing the bulk carrier and green ship technology. Publications regarding modeling an FCM show that both a BBM approach and WBM approach are feasible, and their combined approach (GBM) also shows successful results. Within the case-study a GBM approach will be used for the FCM, as this is possible with the available data. The choice for a WASP model is the result of the available wind data found in the BDNs of the bulk carrier. In this study, three WASP systems will be explored based on existing literature: a towing kite, a DynaRig sail, and a Flettner rotor. The combined models will be verified with the data and validated throughout a performed case-study. Besides evaluating the emissions reduction potential, a financial and feasibility assessment will be performed to investigate if the proposed retrofit of the respective vessel can be achieved.

In conclusion, a green ship DM is composed of the combination of a model representing the ship itself and one or multiple models representing the green ship technologies which are used to investigate a potential retrofit. An overview of the adopted modeling approach is provided in Figure 4.9.

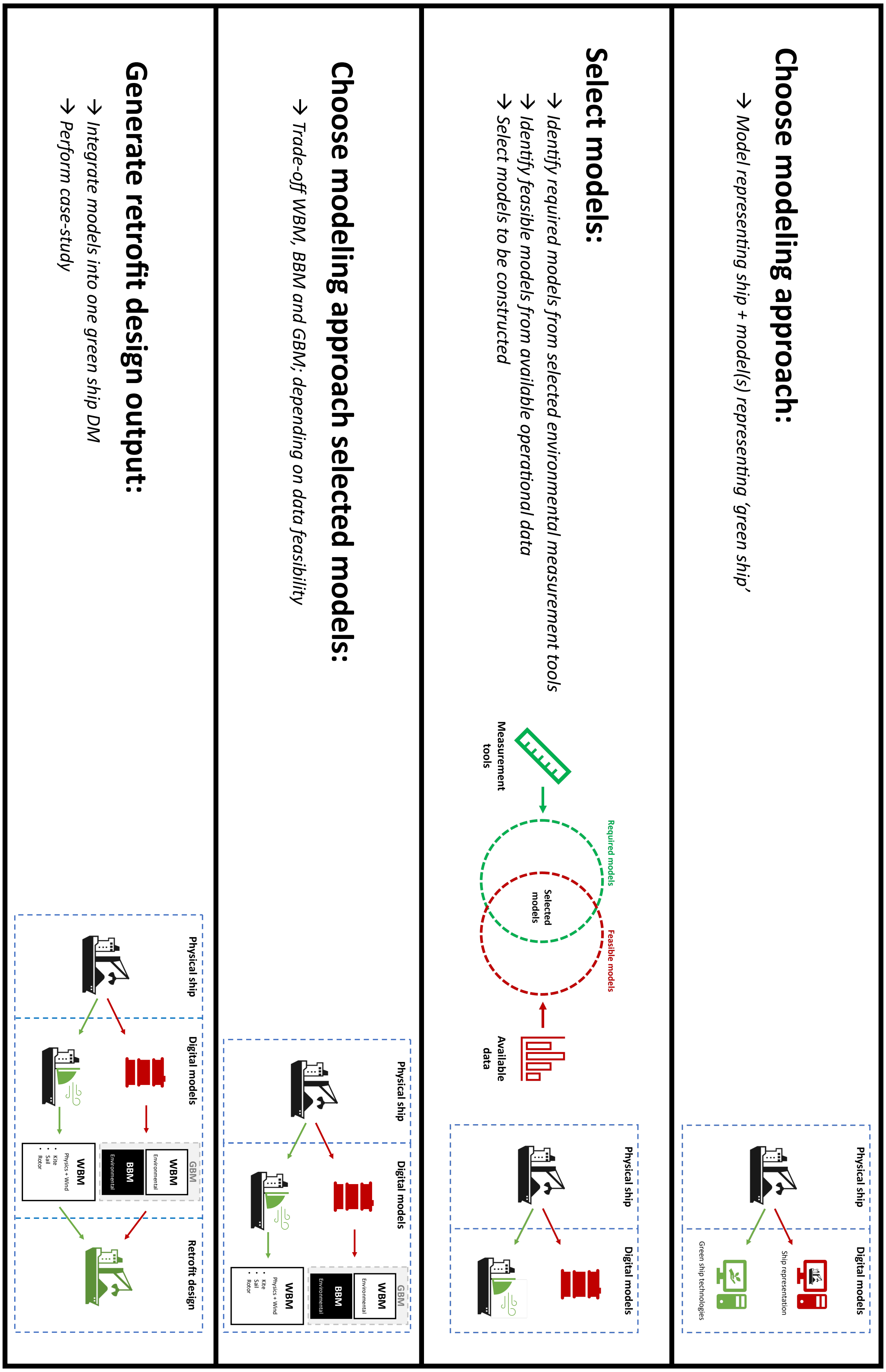

Figure 4.9: Overview modeling approach of green DM for retrofit, from top to bottom

5

Model construction

This chapter elaborates on the construction of the selected models. The adopted preprocessing framework is presented, together with an overview of the operational data. Next, the FCM and WASP models are discussed separately. By presenting the model construction, RQ4 can be answered: *'To what extent can data from bunker delivery notes be incorporated into the selected digital models?'*

5.1. Available data for the case-study

Data used for the construction of the models consists of the ship's main particulars, info regarding the propulsion, environmental characteristics, and the BDNs. An overview of these data is provided in the next sections.

5.1.1. Main particulars and environmental characteristics

Within the DT4GS project, the main particulars of the bulk carrier are provided as PDF-files. The parameters and other environmental characteristics used throughout the case-study are listed in Table 5.1. The bulk carrier does not have a gearbox, resulting in a gearbox efficiency η_{GB} of 1.

Table 5.1: Ship and environmental characteristics bulk carrier case-study

Ship/environmental characteristic	Symbol	Value
Length overall [m]	L_{oa}	300
Breadth (molded) [m]	B	50
Depth (molded) [m]	D	25
Deadweight tonnage (summer) [mt]	DWT_s	209,472
Diameter propeller [m]	D_p	9.5
Thrust deduction factor [-]	t	0.176
Wake fraction [-]	w	0.338
Blade area ratio propeller [-]	Ae/Ao	0.4077
Shafting efficiency [-]	η_S	0.99
Gearbox efficiency [-]	η_{GB}	1
Density sea water [kg/m^3]	ρ_{sw}	1025
Density air [kg/m^3]	ρ_a	1.225
Gravitational acceleration [m/s^2]	g	9.81

5.1.2. Bunker delivery notes

As mentioned in Section 4.2, the operational data is provided as BDNs, consisting of 129,174 data points of 6 periods between 02/06/'22 - 30/09/'23. Every 5 minutes, 107 different data types are recorded. One thing to notice here: in the BDNs the shaft power is present, but because the bulk carrier does not have a gearbox the shaft power is equal to the ship's brake power P_B, using Equation 5.1 (Klein Woud & Stapersma, 2002). From here on the recorded shaft power in the BDNs will be referred to as the ship's brake power.

$$\eta_{GB} = \frac{P_S}{P_B} \tag{5.1}$$

5.2. Data preprocessing

The abundance of operational data from the BDNs does not necessarily imply that all these data are of good quality and in the right format to be utilized. In order to be of use for the case-study, the data is first preprocessed. Figure 5.1 shows the performed steps of the adopted data preprocessing framework of this research, which is based on the techniques described by García et al. (2016). Each step will be briefly discussed in the next sections. The preprocessing and model construction are conducted in the Python (v3.11.5) IDE: Spyder v5.4.3. The presented preprocessing framework covers the steps performed towards the data implementation of the final digital model for the retrofit design. The next sections elaborate on these steps.

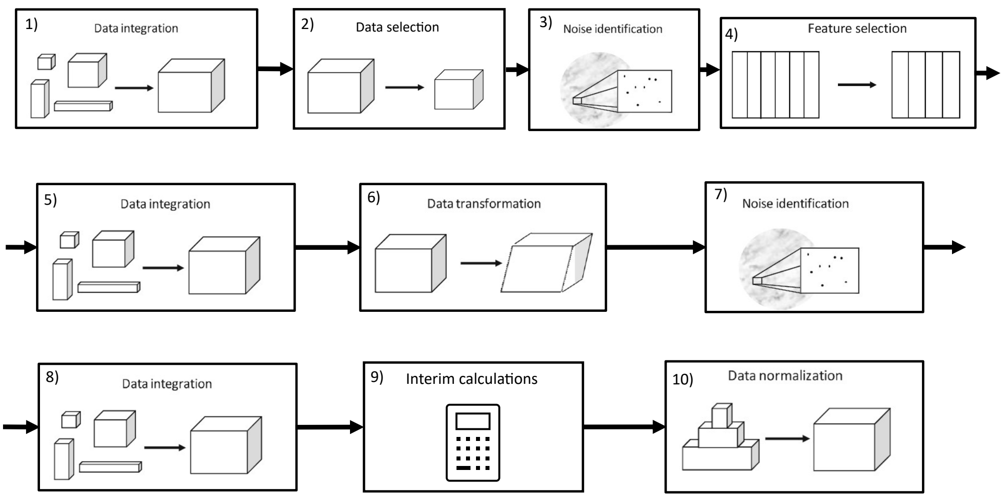

Figure 5.1: Adopted preprocessing data framework, based on García et al. (2016)

Step 1) Data integration

The BDNs are provided in a Microsoft Excel sheet, containing the different data labels as listed in Appendix A. The ship's main particulars, machinery information, and sea trial results, are found in several ship reports (written reports and digital PDF-files). All these data are integrated into one Python script to be used further on for the model construction.

Step 2) Data selection

With the data imported in the Python script, the first filtering can be performed: the data selection. For the case-study a ship in sailing conditions is considered. This means that only data points are used when the ship has a certain minimal speed. By investigating the bulk carrier during sailing conditions, the minimal ship speed (through water) of 6 knots is selected to filter out data points related to non-sailing conditions.

Step 3) Noise identification

The next step is to identify outliers within the data set. Outliers can corrupt the models when not identified and treated correctly. If possible, these values can be replaced by interpolating around the respective data points, or the whole data point is disregarded. In this research, the identified outliers are disregarded. The identification is based on the following criteria:

- Brake power is negative or zero
- The instant specific fuel consumption of the main engine is negative or zero (a result of a calculation)
- Sampling time is not 5 minutes
- Speed through water difference between 2 data points (= 5 min) is more than 3 knots, the second point is then disregarded

Step 4) Feature selection

In the BDN data set, 107 different data types are found. Not all of these data types are required for the models, hence the next filtering step is feature selection. Each model requires different data types. The selection for the BBM (ANN) is performed through a Spearman correlation analysis, and the WBM feature selection depends on which functions the models are based. The sampling time is selected because it will be used for noise identification (step 7). The speed over ground is selected to be used in the interim calculation for the speed difference (step 9). The main engine rpm will be used for the integration of the FCM with the WASP models (Section 6.4). The other 7 features are the result of feature selection per model. A more thorough discussion on this selection is provided in the model construction Sections 5.3 and 5.4. The selected features from the BDNs are:

- Sampling time
- Brake power
- Main engine rpm
- Rudder angle indicator
- Wind direction
- Wind speed
- Speed over ground
- Speed through water
- Sea water temperature
- Fuel consumption main engine

Step 5) WBMs WASP input (data integration)

The WBMs of the WASP systems only need relative wind speed and direction as input values. At this point, the data of those inputs is ready to be used with the WBMs and feasible to be integrated into the data set. The ship's brake power in the case of an operating WASP system is calculated per configuration per data point and added to the data set. The established integration framework is presented in Chapter 6. The main engine rpm is only required for this integration and will not be used further on in the preprocessing.

Step 6) Data transformation

The data, currently sampled every 5 minutes per data point, will be transformed to a more conventional sampling time of 1 hour. For each selected feature, the data covering an entire hour will be aggregated into a single value corresponding to that hour. In this step, three different methods are used depending on the feature type: a summation, the mean value, and the weighted average of the 1 hour. The aggregation method used per feature is listed below. Note that the main engine rpm is disregarded as it was necessary during the data integration (step 5) to calculate the brake power with a WASP system.

- Sampling time: sum
- Brake power: sum
- Rudder angle indicator: mean
- Wind direction: weighted average
- Wind speed: mean
- Speed of ground: mean
- Speed through water: mean
- Sea water temperature: mean
- Fuel consumption main engine: sum
- Brake power with WASP: sum

Step 7) Noise identification

A new noise identification step is performed after the hour conversion. For this step, the sampling time is selected as the main criterion. If the sampling time of an hour (resulting data point) is not 60 minutes, it is an indication that the data of the respective hour is incomplete and the data point is disregarded.

Step 8) WBM resistance model input (data integration)

The white-box part of the FCM is a ship resistance model calculating the sum of the calm water resistance and the wind resistance. The inputs of this model are ship speed, sea water temperature, wind speed, and wind direction. Section 5.3.1 provides a more thorough description of this model. At this point, the required inputs have the right quality and are in the correct format. The resistance sum, which represents the average value of the respective hour (data point), is calculated and integrated with the data set.

Step 9) Interim calculations

Before the data can be normalized, the speed difference needs to be calculated. The speed difference is an environmental parameter that represents the water current's speed. This difference is calculated by subtracting the speed over the ground from the speed through the water.

Step 10) Data normalization

The final step is the normalization of the data set. Except for the main engine fuel consumption, the selected data is normalized with the MinMaxScalar function which linearly scales the data down into a fixed range. In this case between 0 and 1. The largest occurring data point corresponds to the maximum value and the smallest one corresponds to the minimum value. This operation is represented by Equation 5.2. Normalizing the data improves the training process of an ANN. Because the input data is now on the same scale, the network can converge faster for a given learning rate (da Silva et al., 2017).

$$x_{norm} = \frac{x - x_{min}}{x_{max} - x_{min}} \tag{5.2}$$

The amount of data points reduced per preprocessing step is provided in Table 5.2. After performing the adopted data preprocessing steps, 5,687 data points are left. However, when inspecting the resulting data points per period it is noticed that Q2 2022 has a lot of anomalies and only provides 9 useful sailing hours. These 9 hours are just a tiny fraction of the resulting 5,687 hours (0.2%) and are therefore disregarded. This results in **5,678 data points**, representing 'pure' sailing conditions, to be used for model construction.

Table 5.2: Data preprocessing results of BDN data

	Data integration	Data selection	Noise identification				Data transformation
Period	Raw	$V_s \geq 6$ kts	$sfc_{ME} \leq 0$	$P_B \leq 0$	$T_s \neq 5$ min	$\Delta V_s \geq 3$ kts	Hour conversion
Q2 2022	8,267	3,165 (-5,102)	2,769 (-396)	148 (-2,621)	148 (0)	147 (-1)	9 (-39)
Q3 2022	26,488	15,582 (-10,906)	15,579 (-3)	15,572 (-7)	15,572 (0)	15,570 (-2)	1,284 (-162)
Q4 2022	26,493	18,281 (-8,212)	18,280 (-1)	18,280 (0)	18,279 (-1)	18,276 (-3)	1,514 (-108)
Q1 2023	15,697	9,756 (-5,941)	9,756 (0)	9,756 (0)	9,756 (0)	9,755 (-1)	802 (-131)
Q2 2023	26,207	12,586 (-13,621)	12,586 (0)	12,586 (0)	12,586 (0)	12,586 (0)	1,047 (-22)
Q3 2023	26,022	13,404 (-12,618)	13,353 (-51)	12,647 (-706)	12,645 (-2)	12,641 (-4)	1,031 (-269)
Σ	129,174	72,774 (-43.7%)				68,975 (-5.2%)	5,687 (-1.1%)

5.3. Fuel consumption model - GBM

In the next sections, the construction of the different models will be discussed, starting with the FCM. As presented in Section 4.4.1, the FCM will be modeled as a GBM. First, the resistance model representing the white-box part within this GBM is discussed, followed by the ANN representing the black-box part.

5.3.1. Resistance model - WBM

The WBM within the GBM (Figure 4.4) will calculate the calm water ship resistance and wind resistance of the ship. The approximation for the calm water resistance (R_{cw}) is performed in accordance with the Holtrop & Mennen method (Holtrop & Mennen, 1982). The wind resistance (R_{AA}) is calculated according to the method of Andersen (2013). Because no wave data is recorded in the BDNs, no additional wave resistance is calculated. This resistance output ($\Sigma(R_{cw} + R_{AA})$) will be used as one of the inputs for the BBM and represents the ship's sailing requirement for a given situation, depending on the desired ship speed and environmental conditions. As described by Holtrop & Mennen, the total calm water resistance of a ship is calculated with Equation 5.3:

$$R_{cw} = R_F(1 + k_1) + R_{APP} + R_W + R_B + R_{TR} + R_A \tag{5.3}$$

The calm water resistance R_{cw} is composed of: the frictional resistance R_F including the hull's form factor $(1+k_1)$; appendages resistance R_{APP}; wave-making and wave-breaking resistance R_W; additional pressure resistance due to the presence of a bulbous bow near the water surface R_B; additional pressure resistance of the ship's immersed transom stern R_{TR}; and, a model-ship correlation resistance R_A. The general procedure to calculate these resistance components is provided in Appendix B. Two things to address here are: R_B is set to zero due to the absence of a bulbous bow, and an interpolation for the kinematic viscosity (ν) of the seawater is performed depending on the seawater temperature. The ν is required for the calculation of the Reynolds

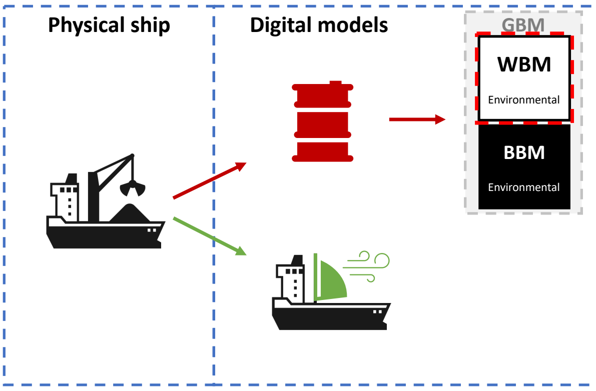

Ref. Figure 4.4: The white-box resistance model (red-dashed box) within the gray-box fuel consumption model

number (R_n). The seawater properties tables provided by the ITTC (2011) are used for this interpolation. Andersen (2013) derived Equation 5.4 to approximate the additional resistance due to wind.

$$R_{AA} = 0.5 C_X \rho_a V_a^2 A_T \tag{5.4}$$

The parameters in this equation are the wind force coefficient C_X; air density ρ_a; relative wind speed V_a and transverse projected area above the waterline A_T. C_X is determined from the interpolation of available sea trial results, depending on the relative wind direction. A_T is determined from the ship's drawings, depending on the draft. Table 5.1 in Section 5.1.1 provides the ship's main particulars and important environmental parameters in the above-mentioned WBM.

Verification

As previously mentioned, the outcome of the Holtrop & Mennen model is the sum of the calm water resistance and added resistance due to wind: $\Sigma(R_{cw} + R_{AA})$. For the verification of presented WBM 6 data points are available originating from the ship's sea trial runs. Three of these data points are when the ship had a course direction of 60° and the other three are with a course direction of 240°. The conditions of each run are listed in Tables 5.3 and 5.4.

Table 5.3: Sea trial parameters, course direction $\Psi = 60°$

Parameter	Run 1	Run 2	Run 3
Main engine output [%]	100	85	70
Speed through water [kts]	16.15	15.70	14.90
Relative wind speed [m/s]	19.90	16.00	14.20
Relative wind direction [°]	8.4	3.8	7.0

Table 5.4: Sea trial parameters, course direction $\Psi = 240°$

Parameter	Run 4	Run 5	Run 6
Main engine output [%]	100	85	70
Speed through water [kts]	16.75	16.17	15.36
Relative wind speed [m/s]	7.10	5.20	4.20
Relative wind direction [°]	264.7	17.3	329.6

The R_{cw} and R_{AA} for each of these runs is calculated and compared with the measured value during the run. The mean errors from this comparison are depicted in Figures 5.2a & 5.2b, with the values listed in Tables 5.5 & 5.6. For clarification reasons, each run is labeled with a distinctive color. The different resistances $\Sigma(R_{cw} + R_{AA})$, R_{cw}, and R_{AA} are labeled respectively with a circle, square, and triangle.

As can be noticed, the resistance prediction with a course direction of 240° is more accurate than the 60°. Moreover, the prediction of the additional wind resistance has a maximum error of 1.8%. The prediction of

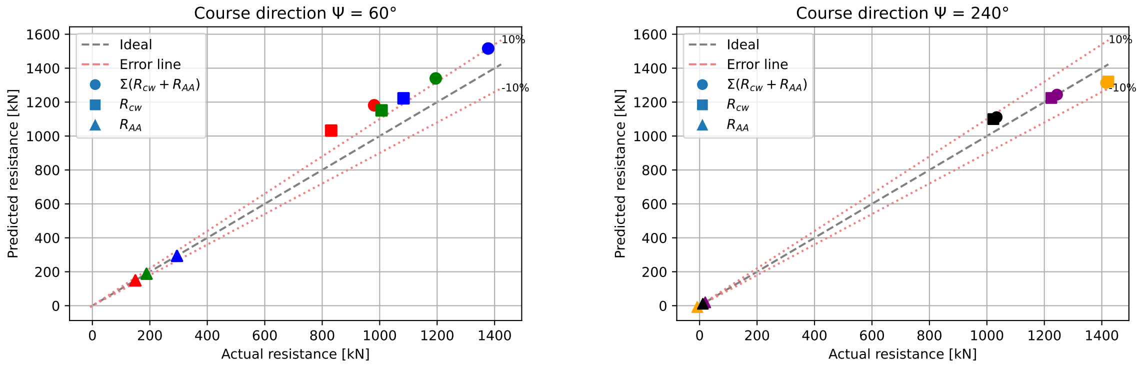

(a) Course direction $\Psi = 60°$; **blue** = run 1, **green** = run 2, **red** = run 3

(b) Course direction $\Psi = 240°$; **orange** = run 4, **purple** = run 5, **black** = run 6

Figure 5.2: Verification resistance model (WBM)

Table 5.5: Mean percentage error resistance, course direction $\Psi = 60°$

Resistance	**Run 1**	**Run 2**	**Run 3**
$\Sigma(R_{cw} + R_{AA})$	+10.0%	+12.1%	+20.5%
R_{cw}	+12.9%	+14.4%	+24.2%
R_{AA}	-0.4%	-0.0%	-0.4%

Table 5.6: Mean percentage error resistance, course direction $\Psi = 240°$

Resistance	**Run 4**	**Run 5**	**Run 6**
$\Sigma(R_{cw} + R_{AA})$	-7.2%	-0.0%	+7.5%
R_{cw}	-7.1%	-0.0%	+7.6%
R_{AA}	-1.8%	-0.4%	+0.7%

the calm water resistance fluctuates the most but within a 15% error when indicating run 3 as an outlier. No explanation was found for the difference in resistance between the two course directions and the relatively high error of run 3. The overall mean absolute percentage error is 9.6% which is deemed acceptable. With the presented arguments, the WBM is verified.

5.3.2. Artificial neural network - BBM

Next, the BBM within the GBM will be presented (Figure 4.4). This BBM is represented by an ANN, converting selected inputs into a desired output. First, the Spearman correlation analysis is discussed which is used for the network's input selection. Secondly, the training procedure together with the determination of the ANN architecture is presented. When the ANN architecture is chosen, a cross-validation is performed to demonstrate the prediction capabilities of the model.

The ANN is constructed using Keras. Keras is an open-source high-level neural networks API written in Python that runs on top of the TensorFlow library (Keras, 2023).

Prior to the determination of the ANN architecture, the model inputs are selected from the available data in the BDNs. The BDNs contain over 100 different data types. Because the prediction of fuel consumption needs to be both accurate and representative of future (unknown) situations, a first selection is made of potential model input parameters. This selection is based on the following assumptions:

- The goal is to predict fuel consumption with an operating WASP system, which will influence engine characteristics in a way that is currently unknown. Thus, parameters strongly related to the operating engine are left out of consideration

- Environmental parameters can be predicted for future situations by means of weather models, and are therefore taken into account

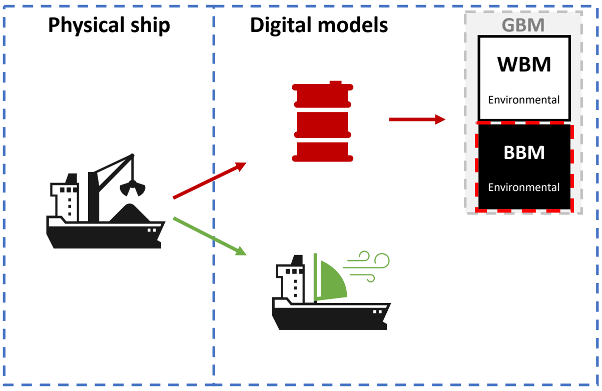

Ref. Figure 4.4: The black-box artificial neural network (red-dashed box) within the gray-box fuel consumption model

- Voyage characteristics such as ship speed and rudder position are considered in this study as they are route-dependent and can be chosen for future voyages

Applying the above-mentioned filtering, resulted in 12 potential model input parameters. For the final input selection, a Spearman correlation analysis is performed for these 12 parameters with regard to their correlation with the fuel consumption of the main engine. The derived correlation coefficient assesses the strength and direction of the relationship between two variables (Sedgwick, 2014). Parkes et al. (2018) have proven that the Spearman correlation analysis is an effective method for feature selection regarding a fuel consumption model. The results are listed in Table 5.7. In terms of engine output, the engine torque is discarded and the brake power is selected. The reason for this is that both parameters have nearly the same correlation factor, and considering WASP implementation, power is a more suitable parameter than torque.

Table 5.7: Spearman correlation coefficients for determination of ANN inputs

Data types	Correlation with fuel consumption main engine	Selection
Brake power output	0.787	✓
Engine torque output	0.789	✗
Ship's heading	-0.082	✗
Rudder angle	-0.241	✓
Rudder rate of turn	0.002	✗
Relative wind direction	0.131	✓
Relative wind speed	0.226	✓
Speed over ground	-0.068	✗
Speed through water	0.142	✓
Speed difference	-0.170	✓
Total power diesel generators	0.041	✗
Sea water temperature	-0.174	✓
Fuel consumption main engine	1.000	—

From the Spearman correlation analysis, 7 parameters from the BDNs are selected. The output of the resistance model, $\Sigma(R_{cw} + R_{AA})$, is added as model input, which results in a total **8** model inputs for the ANN. This inclusion of the resistance as ANN input gives the model its gray box characteristic, and in this case serially coupled. The 8 model inputs are:

- Brake power output
- Rudder angle
- Relative wind direction
- Relative wind speed
- Speed through water (ship speed)
- Speed difference
- Sea water temperature
- Sum of calm water and air resistance (result WBM)

The next step is to determine the architecture of the ANN, i.e., the activation function, training algorithm, and the number of hidden layers and neurons. For the activation function per neuron, the Rectified Linear Unit (ReLU) is chosen. ReLU is a widely used activation function in artificial neural networks, particularly in deep learning models (Agarap, 2018). The fundamental idea behind ReLU is that for any input value, it outputs the same value if it's positive, and zero otherwise. Equation 5.5 shows the mathematical formulation of the ReLU function. ReLU introduces non-linearity to the network, allowing it to learn complex patterns and representations. One of the key advantages of ReLU is its computational efficiency, as the activation is simply thresholding at zero (Agarap, 2018).

$$f(x) = \max(0, x) \tag{5.5}$$

For the training algorithm, the Adam optimizer is chosen. Adam, which stands for Adaptive Moment Estimation, is a widely used optimization algorithm to train deep neural networks and is suitable for problems that are large in terms of data amount (Brownlee, 2021). Adam combines the advantages of two other optimization methods, namely the Adaptive Gradient Algorithm (AdaGrad) and the Root Mean Square Propagation (RMSProp). It maintains two moving averages for each parameter: the first moment (mean) and the second moment (uncentered variance) (Kingma & Ba, 2017). These moving averages are utilized to adaptively adjust the learning rates for each parameter during training. Adam is relatively easy to configure with default configuration settings already capable of solving initial problems, which also results in less computational power compared to other training algorithms (Brownlee, 2021; Kingma & Ba, 2017). The mean squared error (MSE) is used as the loss function during the validation monitoring. The batch size per epoch is set to 16 data points, which lowers the required memory space and accelerates the network's training process.

The default learning rate of the Adam optimizer is used during model training, which is 0.001. The maximum number of epochs during training is set to 500, with an early stopping condition of 35. This denotes that the training phase is stopped when there is no improvement observed after 35 epochs during the validation within the training phase. Moreover, the dropout value is set to 0.2, indicating that during every epoch 20% of the neurons are randomly deselected which helps to avoid potential over-fitting of the model. The dropout process also generalizes the network, making it more capable of handling data that is not in the training set. A visualization of the dropout process, in general, is depicted in Figure 5.3.

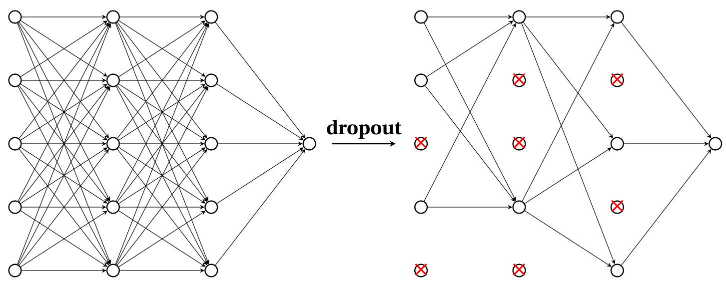

Figure 5.3: Dropout procedure in general, applied during the training phase of an ANN

The 5,678 data points left after the preprocessing are used for the construction of the ANN. First, 500 data points are randomly extracted from the data set to be used later-on for the cross-validation. The remaining 5178 data points are used for the training and intermediate validation process to find the most suitable ANN architecture in terms of hidden layers and neurons. These remaining data points are divided into a training set and a validation set, in a ratio of 90% - 10%. This division of the training and validation data set is done by specifying a certain random state (rs), where rs represents the division parameter. The data splitting is shown in Figure 5.4. During the training phase, the training data set is used to adjust the weights of the neurons. The validation set is used to monitor the loss of the constructed ANN during the training phase and adjust the training settings if necessary.

Within the ANN architecture, the most critical parts are the number of hidden layers and neurons per hidden layer. In the work of Parkes et al. (2018) the hidden layers and neurons are indicated as the main drivers for the total network accuracy. Often a trade-off is made between complexity and accuracy. As there is no one truth for the number of neurons in a hidden layer, several guidelines are provided to determine the

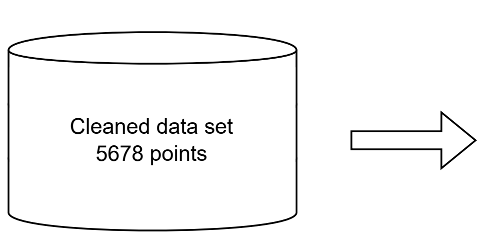

Figure 5.4: Data splitting into training set, validation set (during training), and test set (for cross-validation)

number of neurons per hidden layer depending on the prediction goal (da Silva et al., 2017; Rachmatullah et al., 2021). Zwart (2020) uses the Fletcher-Gloss method described in da Silva et al. (2017) to determine the number of neurons. Equation 5.6 shows this method. Herein is n the number of model inputs, n_1 is the number of neurons in the hidden layer, and n_2 the number of outputs.

$$2\sqrt{n} + n_2 \leq n_1 \leq 2n + 1 \tag{5.6}$$

Most of the literature found with regard to ANN for fuel consumption predictions have 1 hidden layer (Bal Beşikçi et al., 2016; Du et al., 2019; Hu et al., 2019; Pedersen & Larsen, 2009, 2009). This is generally done to lower the complexity of the total network while maintaining sufficient accuracy. Nevertheless, some references also mention the use of multiple hidden layers with beneficial outcomes regarding prediction accuracy (Fam et al., 2022; Parkes et al., 2018; Radonjic & Vukadinovic, 2014). Parkes et al. (2018) state that the accuracy of the network is mainly determined by the number of hidden layers & neurons, and with an increasing number of units, more complex relations can be modeled by the ANN. Nevertheless, a network with too few layers and neurons can be unable to model all the (complex) relationships if necessary. For these reasons, it is chosen to investigate a one and two hidden layer configuration, resulting in 209 possible configurations. The investigated ANN configurations, including the resultant configuration, are depicted in Figure 5.5.

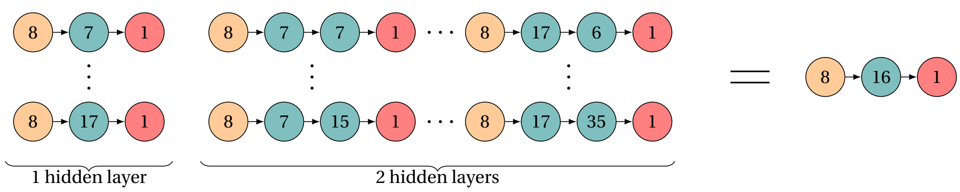

Figure 5.5: Investigated ANN configurations with 1 input layer (yellow), 1 or 2 hidden layers (green), and 1 output layer (red)

The resultant ANN configuration with the highest accuracy is a network with **1** hidden layer containing **16** neurons. The structure of this network is depicted in Figure 5.6. The characteristics of the ANN, together with the training parameters are listed in Table 5.8.

The ANN is trained with the training-validation division of rs=49 and has a resulting mean absolute percentage error (MAPE) of 1.7%. Table 5.9 shows the other results of the ANN. To give an idea, the range of data output is between 900 and 1700 liters of fuel per hour. Figure 5.7 shows the decrease of the MSE and MAPE during the training phase of the network. One thing to notice here is that the network makes better predictions on the validation set (10%) than on the training set (90%). In general, the validation error is higher than the training error, but in some cases, the current situation occurs. Only during the training phase regularization of the data is applied which introduces a relatively small regularization loss (Rosebrock, 2022). Moreover, the error of the training phase is measured during each epoch, whereas the error of the validation is measured after each epoch (Rosebrock, 2022). Because data regularization is not applied during validation, and training-validation errors are measured at different moments, a minor shift in error plots can be observed. Nevertheless, performing an additional cross-validation can potentially justify the accuracy of the adopted network.

Cross-validation

Three additional networks of the same composition (1 hidden layer of 16 neurons) are constructed and cross-validated with the test set containing the 500 data points that were set aside. The distinction between these

Table 5.8: ANN characteristics and used training parameters

Characteristic - parameter	Value
Training algorithm	Adam
Activation function	ReLU
Number of inputs	8
Number of outputs	1
Number of hidden layers	1
Neurons in hidden layer	16
Dropout	0.2
Test set	500 data points
Training - validation set	90% - 10%
Batch size	16 data points
Max number of epochs	500
Learning rate	0.001
Patience	35 epochs
Monitor loss function	MSE

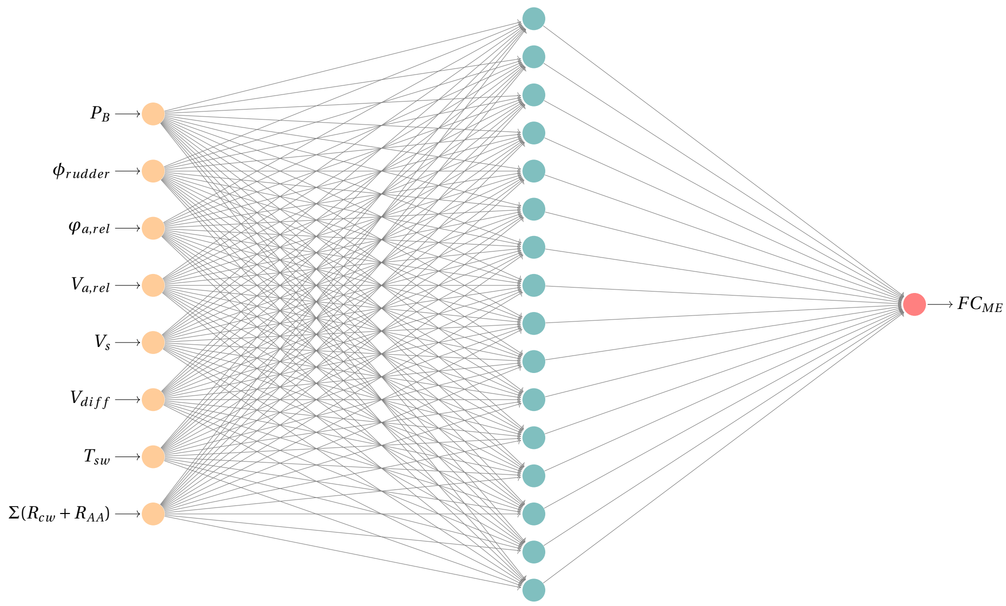

Figure 5.6: Structure ANN model with an input layer with 8 neurons (yellow), 1 hidden layer with 16 neurons (green), and an output layer with 1 neuron (red)

Table 5.9: ANN (rs=49) resulting errors

Error	Value
Mean squared error [$(l/h)^2$]	947.89
Root mean squared error [l/h]	30.79
Mean absolute error [l/h]	23.53
Mean absolute percentage error [%]	1.7

four networks is made by randomly selecting a different rs value which alters the training process and thus results in a network with different weights per neuron. These networks have not seen these data points yet, and by using this constant test data set, cross-validation can be performed. Cross-validation is a common practice in constructing a reliable ANN by proving that the achieved network accuracy is independent of a coincidentally convenient data split with which it was trained (Parkes et al., 2018; Pedersen & Larsen, 2009, 2009; Radonjic & Vukadinovic, 2014). The MAPE per network is listed in Table 5.10, including the overall MAPE with corresponding standard deviation.

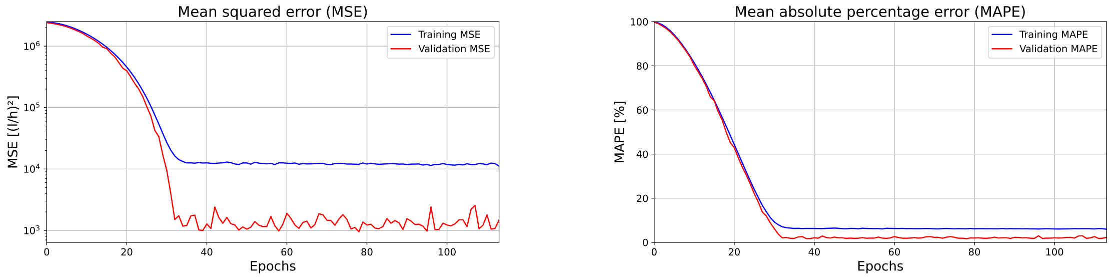

(a) Mean squared error (MSE) plotted on logarithmic scale

(b) Mean absolute percentage error (MAPE)

Figure 5.7: Network errors during training phase (rs=49)

Table 5.10: Cross-validation using test data set between four models with equal configuration

Random state	MAPE
49	1.8%
59	2.1%
61	1.9%
80	1.9%
Overall	1.9%
Standard deviation	+/- 0.1%

The confidence interval is a common practice in statistics to indicate if the adopted method is within a desired accuracy (Carney et al., 1999). The minimum desired confidence interval for machine learning, and especially ANNs, is generally 90% (Carney et al., 1999). The constructed ANN is well within this interval, with an overall MAPE of 1.9% indicating the high accuracy of the network.

To summarize, the ANN model inputs are selected through first filtering together with a Spearman correlation analysis. This resulted in 7 data types from the BDNs. The output of the Holtrop & Mennen model, the sum of calm water resistance and wind resistance, is also added as model input, bringing the number of ANN inputs to 8 and giving the FCM its gray box characteristic. The model has 1 output, the fuel consumption of the main engine. For the training algorithm of the ANN is the Adam optimizer selected. For the activation function per neuron, the ReLU is selected. An investigation is needed in order to determine the number of hidden layers and neurons per hidden layer. As literature in the same field of research has shown already acceptable accuracy for 1 hidden layer, with occasional improvements with multiple hidden layers, the options of 1 and 2 layers are investigated. The number of neurons is based on the Fletcher-Gloss method (Equation 5.6), which provides a range of neurons based on the number of inputs and outputs.

This resulted in an ANN model with 1 hidden layer, with 16 neurons. This network is then cross-validated with 3 other networks composed of the same structure, but which are trained with a different training-validation data division. The cross-validation is performed with the test-data set which was set aside before the training phase, thus the models have not seen this data during their own training and validation. The MAPE of the 4 different network cross-validation is 1.9% with a standard deviation of +/- 0.1%. This lies within the minimum desired confidence interval of 90% generally used in machine learning.

5.4. WASP models - WBM

Now the model representing the ship is completed and cross-validated, the models representing the WASP systems can be constructed (see Figure 4.5). The available wind data in the BDNs is measured at a different height than it would potentially be used by the respective WASP system, resulting in a correction of the wind speed for this height difference. This will first be discussed. Further on, the construction of the models for three different WASP systems are presented based on the literature mentioned in Section 4.4.2.

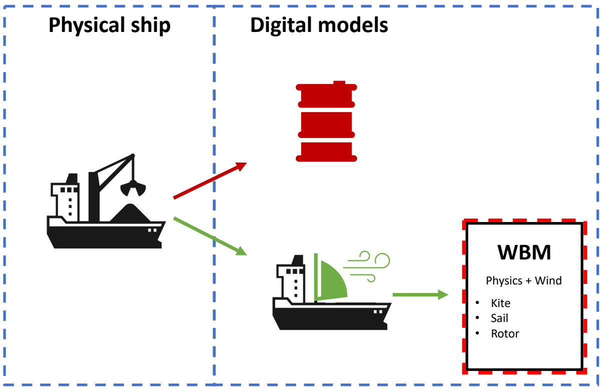

Ref. Figure 4.5: The WBMs of a kite, sail, and rotor (red-dashed box) representing the green ship technologies

5.4.1. Wind speed conversion

The wind sensor, situated on the mast on the bridge deck of BDNs, measures wind speed and direction. Since wind speed fluctuates with altitude (Figure 5.8), the measured wind speed isn't directly applicable to wind propulsion calculations. To obtain the accurate wind speed necessary for calculating the propulsion force of the respective WASP system, the measured wind speed must be converted to the wind speed encountered at the effective height of the WASP system, using Equation 5.7 based on the power-law of the wind profile (Hsu et al., 1994).

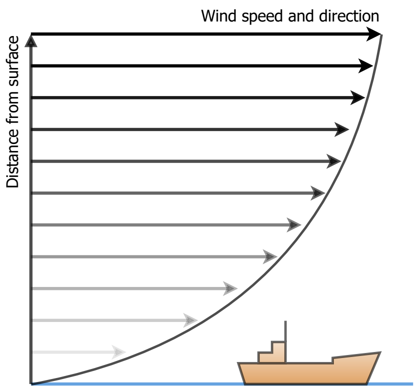

Figure 5.8: Varying wind speed profile over height

$$V_{z_{WASP}} = V_{z_{measured}} \cdot \left(\frac{z_{WASP}}{z_{measured}}\right)^P \tag{5.7}$$

The wind speed is measured at a height of 54.75 meters above the keel. In order to get the measured height above the waterline ($z_{measured}$), the current draft is subtracted from the 54.75 meters. The effective area of where the wind will work on the WASP system (z_{WASP}) depends on the respective system and will be provided in the next sections. The power-law exponent (P) is a spatial parameter depending on the surroundings of the specific situation (e.g., at sea, open or undulating terrain). Hsu et al. (1994) conducted research into this exponent for the wind profile over the ocean under near-neutral stability conditions. They concluded from their experiments that an exponent of $P = 0.11$ is an accurate approximation for the wind profile over the sea. This is also in line with the recommended procedures and guidelines provided by the ITTC (2021) with regard to this wind speed conversion.

5.4.2. Towing kite

The first WASP model that will be discussed is the towing kite. Towing kites for ship propulsion represents an environmentally friendly approach to harnessing wind energy for maritime transport. The towing kite is deployed at the bow area and generates additional propulsion force by towing the vessels forward. The benefits of using a towing kite are mostly linked to the little required deck space and the option for a fully autonomous system (Fritz, 2013). The constructed model is based on the research of Bentin et al. (2018). The resultant propulsion force by the towing kite is approximated with equation 5.8.

$$F_{kite} = 0.5\epsilon\rho_a V_a^2 S_{wi} F_{norm,kite} \tag{5.8}$$

The relative wind speed (V_a) acts on the effective wind surface of the kite (S_{wi}). Here $F_{norm,kite}$ is the normalized propulsion force of the towing kite as a function of only the relative wind direction and elevation angle (δ), and can be calculated with Equation 5.9. This normalized propulsion force is plotted for all wind directions in Figure 5.9 to show the effective wind angles for a towing kite.

$$F_{norm,kite} = \left(\cos\left(\frac{180° - \varphi_{a,rel}}{2}\right)\right)^2 \cdot (\cos(\delta))^2 \tag{5.9}$$

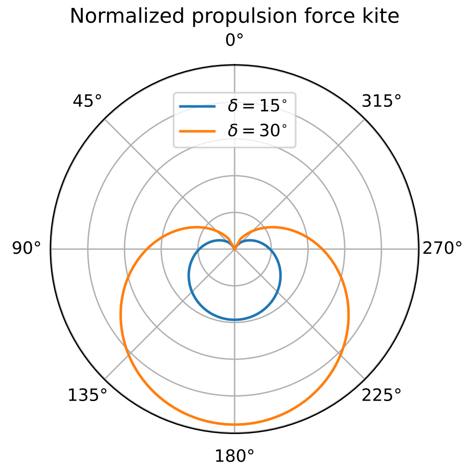

Figure 5.9: Normalized propulsion force directions towing kite for two elevation angles (δ); 0° = headwind, 180° = tailwind

The efficiency of wind energy transfer from the wind field onto the towing kite is represented by ϵ. Literature regarding the dynamics of towing kites shows that there is no 'simple' parameter just representing an energy transfer efficiency. In the book chapter by Fritz (2013) on towing kite applications regarding ship propulsion, a similar equation as Equation 5.8 is provided, but instead of an efficiency parameter a resultant force coefficient is given (C_R). This force coefficient strongly depends on the lift and drag characteristics of the installed kite, and is usually provided by the manufacturer. Unfortunately, this information is not publicly available and thus brings it back to an estimation of the energy transfer efficiency ϵ. For this case-study the energy efficiency is set to 0.5. The minimum required wind speed to deploy the towing kite is set to 10 knots. This is based on the required wind speeds for kite surfers.

Configurations

There are four kite configurations investigated during the case-study, referred to as: *Kite300*, *Kite800*, *Kite1280* and *Kite2500*. These configurations vary in kite sail area, which are respectively: 300 m^2, 800 m^2, 1,280 m^2 and 2,500 m^2. The characteristics per kite configuration are listed in Table 5.11.

Table 5.11: Selected towing kite configurations

Kite characteristic	Kite300	Kite800	Kite1280	Kite2500
Kite sail area [m^2]	300	800	1,280	2,500
Height [m]	77.6	150	250	400
Elevation angle [°]	15	30	30	30

The *Kite300* is chosen because in the work of Dadd (2013) a 300 m^2 kite with a 300 meter long line was investigated for ship propulsion purposes. Dadd (2013) found through varying the elevation angle, an optimum in kite propulsion power with an elevation angle of 15°. In the work of Bentin et al. (2018) on which the kite model is based, an 800 m^2 at a height of 150 meters above the sea is investigated. On the website of GloMEEP (2019) a short overview of possible towing kites for ship propulsion purposes is provided including estimations of power generation and installation costs. GloMEEP is an international collaborating project established within the IMO aiming to support and provide insights into implementing energy-efficient measures for global shipping. GloMEEP (2019) indicate that a 1280 m^2 and 2500 m^2 kite are feasible, and for that reason, both of these kites are also taken into account in this investigation. Figure 5.10 shows a schematic view of the elevation angle and height.

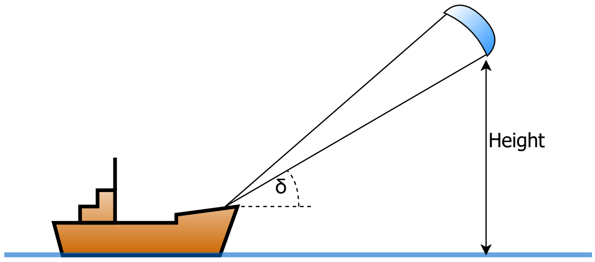

Figure 5.10: Kite configuration parameters: elevation angle (δ) and sailing height

It is assumed that the kite system is a fully autonomous system, including kite deployment and retrieving. An electric motor, included in the kite system, controls the flight and logistics. Such a fully autonomous system is also considered in the book chapter by Fritz (2013). The power usage of the electric motor is estimated at 2 kW with an electric efficiency of 0.95.

5.4.3. DynaRig sail

The next WASP system is the DynaRig. The DynaRig sail is characterized by a square rig configuration, featuring freestanding masts and yards that are rigidly connected to the mast structure. The sails are positioned between the curved yards, ensuring a seamless deployment with no gaps between them. This arrangement enables the sails on each spar to function collectively as a single, integrated sail plan (Perkins et al., 2004).

As with the kite model, the DynaRig sail model is also based on the modeling methods described by Bentin et al. (2018), together with the research conducted by Reche-Vilanova et al. (2021). The resultant propulsion force by the sail is calculated with Equation 5.10. Here, the sail surface is represented by A_S. The normalized propulsion force $F_{norm,sail}$ is derived from the relative wind angle $\varphi_{a,rel}$ and the lift and drag coefficients (C_L and C_D). These coefficients characterize a specific sail. $F_{norm,sail}$ is calculated with Equation 5.11.

$$F_{sail} = 0.5 A_S \rho_a V_a^2 F_{norm,sail} \tag{5.10}$$

$$F_{norm,sail} = C_L \sin(\varphi_{a,rel}) - C_D \cos(\varphi_{a,rel}) \tag{5.11}$$

Aerodynamics

The lift and drag coefficients of a sail can be determined through various methods, such as wind tunnel tests, numerical calculations, and full-scale tests (IMO, 2021). These three options are also accepted by the IMO as reliable methods to be used for classification validations. As addressed by Reche-Vilanova et al. (2021), several wind tunnel tests regarding DynaRig sails have been performed over the last years (Bordogna, 2020; Perkins et al., 2004; Smith et al., 2013).

Perkins et al. (2004) investigated through wind tunnel and scale model tests, the force coefficients of DynaRig sails for a mega sailing yacht. The characteristics of these DynaRig sails are optimized with regard to a sailing yacht hull shape, making the results inapplicable for transport vessels due to deviating hydrodynamic requirements. Smith et al. (2013) investigated the applicability of DynaRig sails for a 10,000 DWT chemical tanker. Although this research is focused on a transport vessel, their methodology which includes interaction effects, is only valid for sail-ship arrangements which are comparable to their specific case-study. Bordogna (2020) conducted wind tunnel tests for three different DynaRig sail configurations and only investigated the lift and drag coefficients of the respective sail without interaction effects. For this reason, the derived force coefficients by Bordogna (2020) are used for this DynaRig model. The sails were virtually trimmed during Bordogna's experiments to optimize for the maximum thrust per apparent wind angle. Figure 5.12 shows the polar plot of the normalized propulsion force of the DynaRig sail using the lift and drag coefficients by Bordogna (2020).

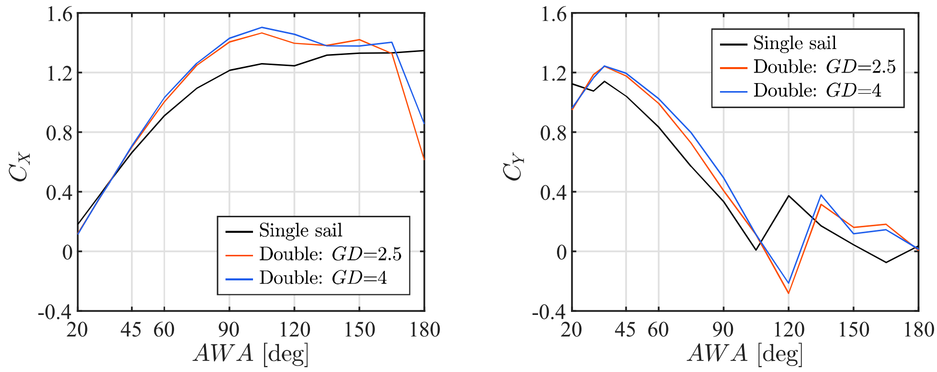

Figure 5.11: Lift and drag coefficients (resp. C_X and C_Y) as a function of the apparent wind angle (AWA), used for the DynaRig model (Bordogna, 2020)

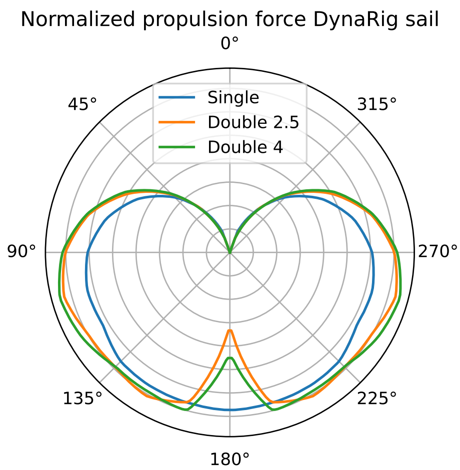

Figure 5.12: Normalized propulsion force directions DynaRig sail with aerodynamic coefficients by Bordogna (2020); 0° = headwind, 180° = tailwind

Windage mast

When DynaRig sails are installed but no wind is present, the sails are reefed to reduce additional air resistance. It is assumed that for the DynaRig sails non-retractable masts are installed which generate additional air resistance. This additional resistance can be calculated per mast with Equation 5.12. The mast is assumed to have a circular cross-section with diameter D_{mast} and height H_{mast}. The mast's drag coefficient $C_{d,mast}$ is assumed to be 0.5, based on the drag coefficient of a sphere (Hall, 2023).

$$R_{windage} = 0.5\rho_a V_a^2 H_{sail} D_{mast} C_{d,mast} \tag{5.12}$$

Configurations

Bordogna (2020) investigated three different sail configurations: 1 sail, 2 sails with a gap distance ratio (GDR) of 2.5, and 2 sails with a GDR of 4. The GDR is defined as the ratio of the distance between two sails and the chord length of a sail ($GDR = GD/chord$). These configurations will referred to as *DynaRig single*, *DynaRig double 2.5*, and *DynaRig double 4*. The investigated sails have an aspect ratio of 1.85 ($AR = H_{sail}/chord$) and a camber of 10% with regard to the sail's chord length. Figure 5.13 illustrates the gap distance, chord, camber, and sail height.

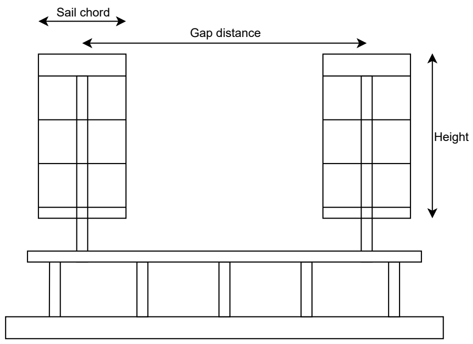

(a) Sail chord, gap distance and height (Bordogna, 2020)

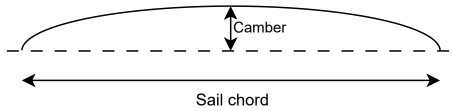

(b) Sail camber; top view of a DynaRig sail

Figure 5.13: Dimensional visualization of a DynaRig sail

The hatch covers of the bulk carrier are spaced 25 meters apart (center-to-center). The potential masts need to be positioned in the gaps between the hatch covers. The chosen gap distance for the case study is 50 meters, which means there are 2 hatch covers between 2 sails. The resulting sail characteristics with this gap distance are provided in Table 5.12.

Table 5.12: Selected DynaRig sail configurations

Sail characteristic	Single	Double 2.5	Double 4
Gap distance ratio [-]	-	2.5	4
Chord length [m]	20	20	12.5
Height sail [m]	37.1	37.1	23.2
Camber [%]	10	10	10

5.4.4. Flettner rotor

The last WASP system which will be modeled is a Flettner rotor. The cylinder of a Flettner rotor is being rotated with the aid of an electric motor. The surrounding air attaches to the cylinder surface and is led into a curve, creating a low and high air pressure side around the cylinder. Consequently, this air pressure difference creates lift. This phenomenon is also known as the Magnus effect and is visualized in Figure 5.14 (Witzgall, 2023).

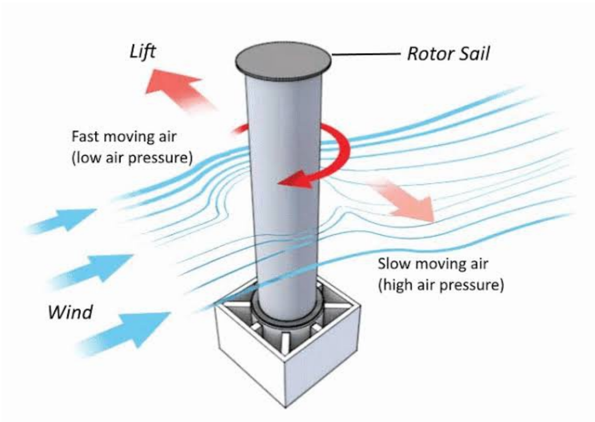

Figure 5.14: Magnus effect induced by the rotating of a Flettner rotor (AnemoiMarine, 2023)

Unlike with the kite and DynaRig model, an already constructed model of a Flettner rotor adopted by Witzgall (2023) will be used. In collaboration with the DT4GS project, Witzgall (2023) used a non-linear regression method to develop a surrogate rotor model based on seven distinctive studies conducted in the field of Flettner rotor lift and drag coefficients. A Matlab script is available where user-defined inputs generate a data file containing the rotor's aerodynamic characteristics (lift and drag coefficients) including the corresponding power demand of the electric motor. This power demand is calculated with Equation 5.13, where the friction coefficient is assumed to be constant ($C_f = 0.007$). The surrogate model is based on experimentally obtained data, resulting in a validation range in which the model is valid. This validation range is listed in Table 5.13.

$$P_{rotor,s} = 0.5\rho_a \cdot V_{a,rel}^3 S_{rotor} C_f \tag{5.13}$$

Table 5.13: Validity range of used surrogate rotor model

Parameter	Validity range
Spin ratio	$0 \leq SR \leq 5$
Reynolds number	$1.0e^5 \leq Re \leq 2.3e^6$
Aspect ratio	$2 \leq AR \leq 8$
Diameter end plate - rotor ratio	$1 \leq D_e/D \leq 8$

Windage rotor

As with the DynaRig sail, the rotor also generates additional air resistance when it is not generating propulsion force. The same calculation is performed to derive this additional resistance but then with rotor parameters:

$$R_{windage} = 0.5\rho_a V_a^2 H_{rotor} D_{rotor} C_{d,rotor} \tag{5.14}$$

Also, the rotor's drag coefficient (when it is not operating) is set to 0.5. This value is also used by Reche-Vilanova et al. (2021) for the rotor's additional air resistance.

Configurations

For the case-study 2 rotor configurations are investigated: the installation of 1 rotor and 4 rotors. The configuration of 4 rotors consists of four times the same rotor as used for the configuration of 1 rotor. Currently, standard rotors for transport vessels vary in diameter from 3 up to 5 meters (AnemoiMarine, 2023; Norsepower, 2023). With a bigger rotor, the potential generated thrust increases due to a greater effective wind area. Nevertheless, the purchase and installation costs also increase with a bigger installation. For this research, it is chosen to investigate the biggest feasible rotor because the goal is to reduce the CO_2 emissions (i.e., fuel consumption).

The maximum diameter for the investigated rotor depends on the available deck space (spatial assessment). The gap between 2 hatch covers is 9 meters. Thus, a rotor with a diameter of 5 meters is spatially feasible. Four locations on the deck are selected for potential rotor installation regarding the second configuration. Feasible heights corresponding with a rotor diameter of 5 meters are 24, 30, and 35 meters (AnemoiMarine, 2023; Norsepower, 2023). Because reducing CO_2 is the goal of this research the 35 meter high rotor is selected for the case-study. The polar plot with the normalized propulsion force of the selected rotor dimensions is depicted in Figure 5.15.

However, a potential height limitation arises by selecting this rotor. The 35 meters of the rotor height is more than the 25 meters of the ship's superstructure measured from deck level, which potentially is a problem with bridges during sailing. To solve this issue, it is assumed that the installed rotors are equipped with a folding-deployment system (see Figure 5.16a). For this research, it is assumed that this folding system is only utilized to overcome the height limitation and not in case the rotor is not operating.

It is common practice to equip a rotor with an end plate larger than the rotor itself. Research on different rotor-end plate ratios found a beneficial ratio of 2 for high aspect ratio rotors, aligning with industry standards (Mancini et al., 2016; NSRSAIL, 2015). Thus, a 10-meter end plate diameter is selected. With the rotor dimensions set, data is retrieved. Matlab inputs for one rotor are listed in Table 5.14, with visualization in Figure 5.16b. Configurations are denoted as *1x Rotor H35D5* and *4x Rotor H35D5*.

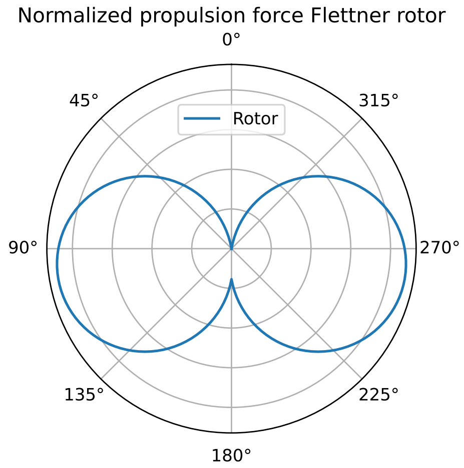

Figure 5.15: Normalized propulsion force directions rotor; 0° = headwind, 180° = tailwind

(a) Rotor folding-deployment system

(b) Dimensions of one rotor

Figure 5.16: Overview of chosen rotor (AnemoiMarine, 2023)

Table 5.14: Input values to generate the data file containing rotor aerodynamic coefficients and power demand

Input	Value range
Relative wind angle [°]	$\varphi_{a,rel} = 0:10:180$
Relative wind speed [m/s]	$V_{a,rel} = 0:3:30$
Spin ratio [-]	$SR = 0:0.5:4$
Rotor height [m]	35
Diameter rotor [m]	5
Diameter end plate [m]	10

The resulting rotor data file contains the generated thrust per relative wind angle and speed and the corresponding electric motor power demand. This data file is then integrated into the Python script to be used as WBM. The rotor WBM, as with the models of the kite and DynaRig sail, only takes as inputs wind speed and direction. However, two additional operational conditions are added to the model within the Python script:

1. A SR optimization step is added which investigates which SR generates the highest thrust for a given wind speed
2. If the rotor's power demand is higher than the reduction of the ship's brake power, the rotor is turned off

The rotor model itself does not have an optimization regarding thrust and SR. This optimization is added to the model, resulting in the following investigation: when the model receives the wind input it first iterates over all the possible spin ratios in order to find the maximum possible thrust for a given SR. The maximum rotor rotation is set to 180 rpm, which corresponds to industry standards of such a rotor (Norsepower, 2023). Within this optimization, it is assumed that the electric motor is capable of handling the potential high changes in rotor rotational speed.

The other added condition is a check between the reduction of brake power due to rotor thrust generation and the corresponding power demand. If the power demand is higher than brake power gain (e.g., weak wind conditions), the rotor will not be used to prevent unnecessary fuel consumption.

5.5. Conclusion on model construction

This chapter has elaborated on the construction of the digital models, along with the adopted preprocessing framework that aligns with the respective model requirements. By presenting both the preprocessing framework and model construction, RQ4 is addressed: *'To what extent can data from bunker delivery notes be incorporated into the selected digital models?'*

Two types of data are used for the model construction: the operational data which is provided as BDNs and ship characteristics which are provided in various PDF files. These separate data types are integrated into a Python script and preprocessed. As a first step, the data selection takes place. Because an operating vessel is being considered, the minimum ship speed is set to 6 knots. With this selection 43.7% of the data points are disregarded. After the preprocessing 5,678 data points are left to be used for the model construction and case-study. These data points represent 5,678 hours of the vessel during operational conditions in the period of Q3 2022 to Q3 2023.

The FCM representing the ship is modeled as a GBM consisting of a resistance prediction model (white box part) and an artificial neural network (black box part). The outcome of the resistance model is the sum of the ship's calm water resistance, calculated with the Holtrop and Mennen (1982) method, and the added wind resistance, calculated according to the adopted method of Andersen (2013). Due to the lack of wave data, the total ship resistance can't be derived. The resistance model is verified with 6 known data points from the vessel's available sea trial report.

Next, this resistance sum is used as one of the 8 inputs of the ANN which gives the FCM its gray box characteristic. The other seven inputs are selected through a Spearman correlation analysis and consist of the ship's brake power, environmental-related parameters, and route-dependent parameters found in the BDNs. From the investigation of 209 possible configurations, with the restricting of a maximum of two hidden layers, the most suitable network architecture resulted in a configuration of one hidden layer consisting of 16 neurons. Moreover, a cross-validation is performed with three additional networks with the same architecture but training with a different data split. Cross-validation is a common practice in machine learning to justify that the resultant configuration is independent of a coincidentally convenient data split regarding its training and validation data. The overall MAPE of the network is 1.9% with a standard deviation of 0.1%. This lies in the confidence interval of 90% adopted in machine learning.

Three different WASP systems (towing kite, DynaRig sail, Flettner rotor) are modeled as WBMs. These models only require wind data as input to predict their potential propulsion force. The available wind speed is measured with a wind sensor at a certain height. However because the wind profile differs over height, a wind speed conversion needs to be performed before it is used as model input.

The kite model is based on the work of Bentin et al. (2018) in which a wind energy transfer coefficient represents the aerodynamics of the kite model. Four kite configurations are selected based on found literature and industry standards to be investigated in this research.

The DynaRig model is based on the research conducted by Bentin et al. (2018) and Reche-Vilanova et al. (2021). Herein, the lift and drag coefficients originating from experiments conducted by Bordogna (2020) are used because of their applicability to other ships instead of solely to the used experimental set-up. Accounting for the available deck space (feasibility assessment) the resulting sail configurations are 1 sail (*DynaRig single*), 2 sails with a GDR of 2.5 (*DynaRig double 2.5*), and 2 sails with a GDR of 4 (*DynaRig double 4*).

For the Flettner rotor, a surrogate model developed by Witzgall (2023) within the DT4GS project is used. Two rotor configurations are investigated: installing 1 rotor with a height of 35 meters and a diameter of 5 meters (*1x Rotor H35D5*) and installing 4 of the previously mentioned rotors (*4x Rotor H35D5*). As with the DynaRig sails, the feasibility assessment showed that a rotor with a diameter of 5 meters is spatially possible.

Now the models representing the ship itself and the green ship technologies are constructed. The integration of both models needs to be performed to achieve one green ship DM. The framework adopted for this integration is presented in the next chapter.

6

Model integration & case-study

In order to achieve one green ship DM, the constructed models presented in Chapter 5 need to be combined (red-dashed box, Figure 4.6). This chapter presents the adopted framework for this integration and answers RQ5: *'To what extent can the output of the digital models be integrated into one green ship DM?'* This framework is based on the chosen data source, BDNs. The required adjustments to this framework are also discussed in case another data source will be used.

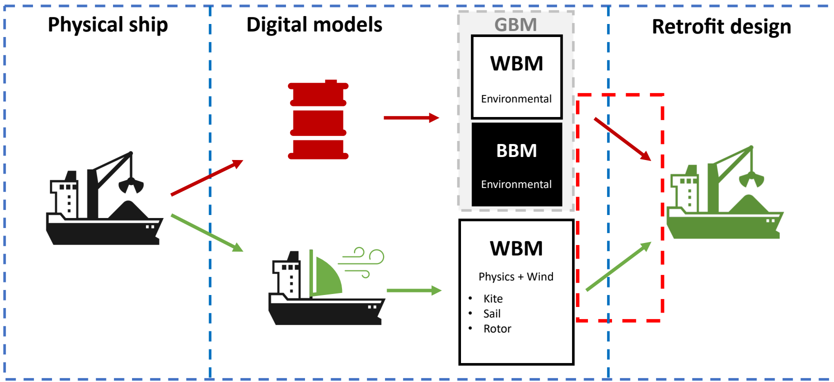

Ref. Figure 4.6: Integration of models representing ship and WAPS systems (red-dashed box) into one green ship DM

6.1. Model integration framework

The goal of the green ship DM is to calculate the fuel consumption in case of an operating WASP. Comparing this with the fuel consumption without a WASP results in potential fuel reduction which provides an insight into the WASP's environmental and financial benefits. The output of the WASP's WBMs is propulsion force and possible power demand. One of the inputs of the ANN in the FCM is the ship's brake power. Thus, the ship's brake power including WASP force needs to be determined.

Bentin et al. (2018) also investigated the potential fuel reduction due to operating WASP systems by reducing the ship's brake power with the WASP's propulsion power. The authors calculate the WASP's propulsion power by multiplying the WASP's propulsion force with the ship speed (Equation 6.1).

$$P_{WASP} = F_{WASP} \cdot V_s \tag{6.1}$$

However, this calculation is only valid in the case that the ship is **only** propelled by the respective WASP system, hence, the achieved ship speed is the result of **only** the WASP system. In this research the implementation of wind-**assisted** ship propulsion is investigated, thus the procedure of Bentin et al. (2018) can not be used here and another method needs to be adopted.

Instead of reducing the ship's brake power with the WASP's potential propulsion power, the WASP's propulsion force is implemented with the propeller thrust demand in the ship's force balance to overcome the experienced resistance. This force balance (Equation 6.2) is visualized in Figure 6.2. Using this force balance a new working point of the propeller is derived, which is also known as the propeller-matching procedure. Vigna and Figari (2023) have performed this matching procedure including an operating Flettner rotor in order to derive the ship's brake power. Even though Vigna and Figari did not consider an existing ship, their method is applicable to this situation. The adopted integration framework will be based on this procedure.

$$\underbrace{R_T = (1-t)\cdot T}_{\text{Without operating WASP}} \quad \Rightarrow \quad \underbrace{R_T = (1-t)\cdot T + F_{WASP}}_{\text{Including operating WASP}} \tag{6.2}$$

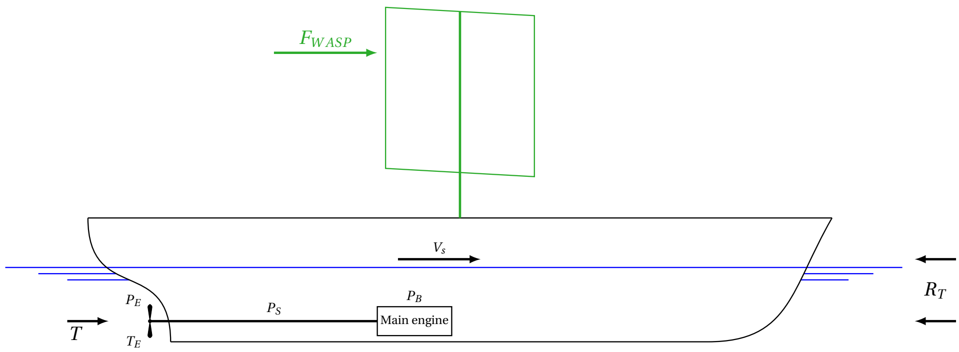

Figure 6.1: Ship's force balance including WASP represented by a green sail

The established model integration framework for this research is depicted in Figure 6.2. The output of the WASP WBMs is firstly transformed into brake power, and next integrated into the FCM to predict the corresponding fuel consumption. The required steps for this integration are depicted in orange and will be discussed in the following sections. This presented framework is based on evaluating the known data from the BDNs. Necessary adjustments to this framework for future data sets are presented in Section 6.5.

6.2. Matching

To derive the new working point of the propeller, Equation 6.2 of the force balance is rewritten to the forward equilibrium equation including the terms of the propeller characteristics and hull demand resulting from the required ship speed (Vigna & Figari, 2023). This results in Equation 6.3.

$$\underbrace{\frac{K_T}{J^2} - \frac{R_T}{\rho_{sw}\cdot(1-t)(1-w)^2\cdot V_s^2\cdot D_p^2} = 0}_{\text{Without operating WASP}} \quad \Rightarrow \quad \underbrace{\frac{K_T}{J^2} - \frac{R_T - F_{WASP}}{\rho_{sw}\cdot(1-t)(1-w)^2\cdot V_s^2\cdot D_p^2} = 0}_{\text{Including operating WASP}} \tag{6.3}$$

The first term in Equation 6.3 represents the characteristics of the installed propeller. The second term represents the hull demand to achieve the desired ship speed V_s. To solve this equation, the total ship resistance needs to be determined. Unfortunately the constructed Holtrop & Mennen model does not calculate the total resistance R_T. However, the BDNs provide sufficient data to calculate R_T. By determining the advance ratio J with Equation 6.4, the propeller thrust coefficient K_T can be found by interpolating the propeller curves (Appendix D).

Next, the total resistance is calculated with Equation 6.5 using Equation 6.6 of the propeller thrust. Because the bulk carrier does not have a gearbox, the main engine rotation (n_e) from the BDNs is assumed to be equal to the propeller rotation (n_p). To verify this assumption, the total resistance is derived with this calculation for the six sea trial data points, and compared with the known value of R_T provided in the sea trial report. This verification is provided in Table 6.1. As the maximum found error with this calculation is 5.0%

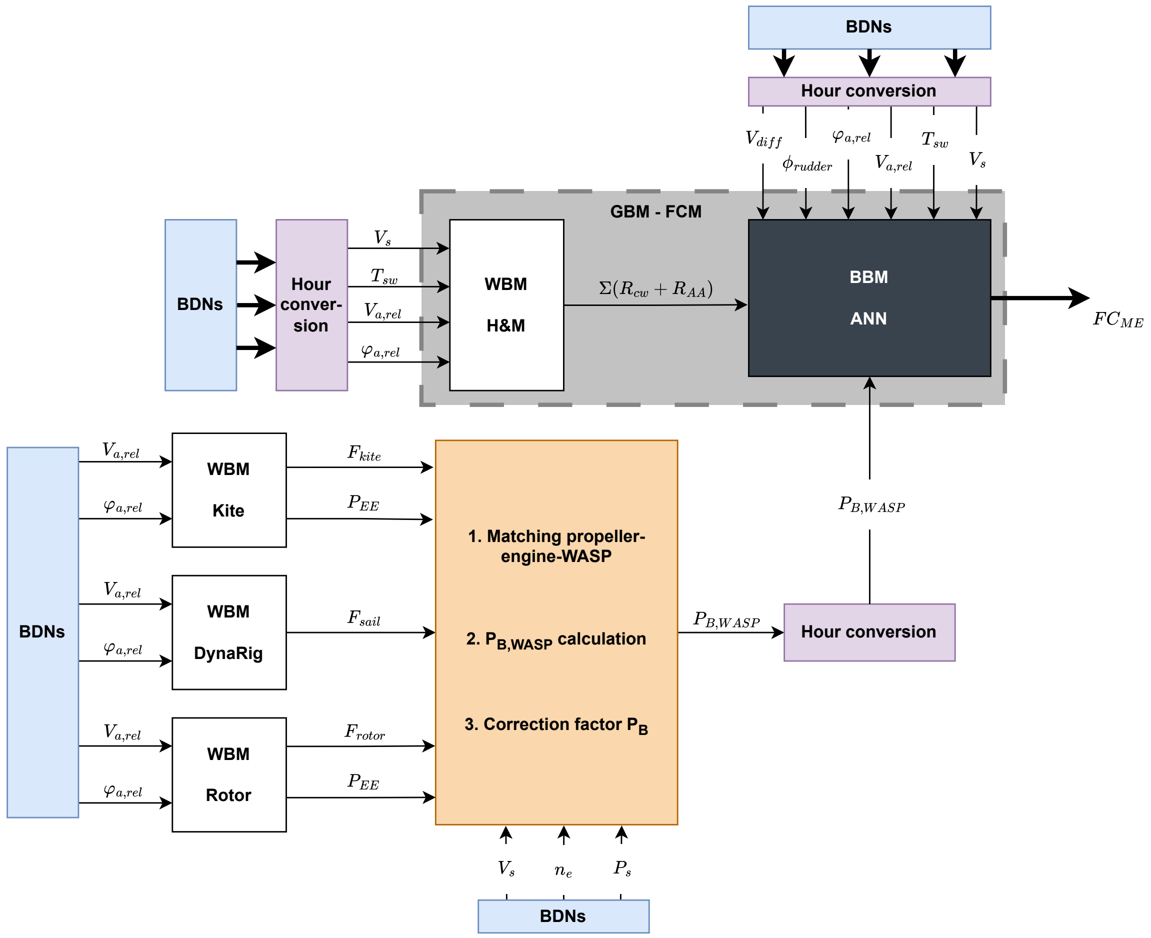

Figure 6.2: Schematic overview of digital models including, the adopted model integration framework (orange), the preprocessed operational data in 5 minute scale (blue), and the data hour conversion step (purple)

(run 6), the propeller rotation assumption is deemed to be acceptable for this calculation.

$$J = \frac{V_A}{n_p D_p} = \frac{(1-w)\cdot V_s}{n_p D_p} \tag{6.4}$$

$$R_T = (1-t) K_T \rho_{sw} n_p^2 D_p^4 \tag{6.5}$$

$$T = K_T \rho_{sw} n_p^2 D_p^4 \tag{6.6}$$

Table 6.1: Verification of total resistance calculation within integration framework with the sea trial data

Parameter	Run 1	Run 2	Run 3	Run 4	Run 5	Run 6
V_s [kts]	16.15	16.75	15.70	16.17	14.90	15.36
n_e [rpm]	68.50	69.00	65.20	65.60	61.30	61.80
η_S [-]	0.99	0.99	0.99	0.99	0.99	0.99
η_R [-]	1.03	1.03	1.03	1.03	1.03	1.03
R_T measured [kN]	1477.06	1417.52	1296.80	1246.72	1085.41	1036.63
R_T calculated [kN]	1472.15	1419.03	1285.67	1247.00	1117.58	1088.08
ΔR_T [%]	-0.3	+0.1	-0.9	+0.0	+3.0	+5.0

In the case of an increase of air resistance due to the windage of non-retractable masts or rotors, the resistance R_T is higher than the previous situation without installed rotors or masts. This additional air resistance is added to the derived total resistance. Next, using the propeller open water characteristics (Appendix D) the new propeller working point is derived, which includes the values for the advance ratio J (Equation 6.4), propeller thrust coefficient K_T (Equation 6.6) and propeller torque coefficient K_Q (Equation 6.7). These propeller characteristics relate to each other in the open water efficiency of the respective propeller (Equation 6.8).

$$Q = K_Q \rho_{sw} n_p^2 D_p^5 \tag{6.7}$$

$$\eta_0 = \frac{K_T}{K_Q} \cdot \frac{J}{2\pi} \tag{6.8}$$

6.3. Brake power calculation

With the parameters of the propeller working point known, the required brake power for that situation can be calculated using Equation 6.9. The new propeller rotation (n_p) is calculated using Equation 6.4. The relative-rotative efficiency (η_R) is calculated with Equation 6.10 (Holtrop & Mennen, 1982).

$$P_B = \frac{2\pi \rho_{sw} D_p^5 n_p^3 K_Q}{\eta_S \eta_{GB} \eta_R} \tag{6.9}$$

$$\eta_R = 0.9922 - 0.05908(Ae/Ao) + 0.07424(C_P - 0.0225 lcb) \tag{6.10}$$

6.4. Correction factor

Because the current brake power is recorded in the BDNs, a correction factor (cf) can be calculated per data point to improve accuracy in the power computation. This cf can be seen as a variable value for all the efficiencies used in the brake power calculation (i.e., $\eta_S, \eta_{GB}, \eta_R$). Equation 6.11 is used to calculate the cf per data point. The calculated brake power (P_B) is derived using: the advance ratio corresponding with the previously mentioned total resistance calculation; the propeller torque coefficient which can be derived with the advance ratio (using Equation 6.7); and finally Equation 6.9. The correction factor is then multiplied by the ship's brake power with operating WASP.

$$cf = \frac{P_B \text{ (BDNs)}}{P_B \text{ (calculated)}} \tag{6.11}$$

The obtained brake power is transformed into a power measure per hour, as presented in the preprocessing framework. Finally, the brake power is ready to be used for the ANN to predict the ship's fuel consumption with operating WASP. Table 6.2 shows the cf values for the six sea trial runs in order to provide an insight into the value range of this cf.

Table 6.2: Correction factor values of sea trial report data

	Run 1	Run 2	Run 3	Run 4	Run 5	Run 6
V_s [kts]	16.15	16.75	15.70	16.17	14.90	15.36
η_S [-]	0.99	0.99	0.99	0.99	0.99	0.99
η_R [-]	1.03	1.03	1.03	1.03	1.03	1.03
P_B measured [kW]	14877	15212	12726	12943	10478	10704
P_B calculated [kW]	15253	15618	13170	13434	10952	11238
cf [-]	0.975	0.974	0.966	0.963	0.957	0.952

6.5. Integration adjustments for future data set

The presented integration framework is adopted with regard to the available data from the BDNs. In the case of using data regarding sailing trips in the future, two of the presented steps need to be adjusted due to the lack of specific data. First, the total resistance calculation used in the matching procedure can not be performed. If additional wave data is available or a prediction of these, then the Holtrop & Mennen method can be used to predict the necessary total ship resistance. The other adjustment is the cf calculation. This calculation is only performed because the measured P_B is available and will therefore be skipped for future data sets.

6.6. Case-study

With the model integration completed, the green ship DM is ready to be used for the case-study. The nine selected WASP configurations (4x kite, 3x DynaRig, 2x rotor) will be evaluated on the operational data regarding the periods Q3 2022 till Q3 2023, using the selected assessment methods presented in Section 4.5. The feasibility assessment is already performed during the selection of WASP configurations. The results of this evaluation are presented in the next chapter.

6.7. Conclusion on modeling integration framework

This chapter presented the integration of the FCM and WASP models, resulting in one green ship DM to be used for the case-study and providing the answer for RQ5: *'To what extent can the output of the digital models be integrated into one green ship DM?'*

The output of the WASP models is propulsion force and power demand if applicable. One of the inputs of FCM is the ship's brake power. The integration of the models is performed by transforming the WASP's propulsion force into the ship's brake power in the case of an operating WASP system. This transformation is done by adding this propulsion force into the ship's force balance and deriving the new working point of the propeller. This is also known as the propeller matching procedure. Vigna and Figari (2023) have performed this procedure to derive the ship's brake power with an operating Flettner rotor. This derived brake power with WASP is then used as input in the FCM which predicts the fuel consumption of the bulk carrier with the respective operating WASP system.

The steps in the adopted integration framework are based on the available BDNs. In a future situation in which data for later predictions will be used, some alterations are required to the presented framework. The ship's total resistance calculation, performed in this framework, will not be valid anymore and needs to be replaced with a prediction method. Moreover, a brake power correction calculation is disregarded in case of future situations. This correction calculation, which can be seen as a dynamic efficiency term, can now be performed because the brake power is recorded in the BDNs.

With the integration framework completed, the models will form the final green ship DM for the the case-study. This is performed for the bulk carrier with the available data from the BDNs regarding the periods Q3 2022 to Q3 2023.

7
Results

This chapter presents the results of the performed case-study, which drive the potential retrofit decision by the shipowner and directly answers RQ6: *'To what extent does the output of the green ship DM directly impact the retrofit design?'*.

7.1. Overall savings Q3 2022 - Q3 2023

With the model integration completed, the retrofit potential for the bulk carrier can be examined based on the available data. For each WASP configuration, the monetary, fuel, and CO_2 savings are calculated, over the 5,678 sailing hours (≈ 237 sailing days). A fuel price of $618.50/mt-fuel is used in this calculation. The results are provided in Table 7.1. The percentage reduction is applicable for all the listed savings as it is all directly linked to the same variable: fuel consumption. The savings are calculated as the difference between the predicted fuel consumption by the green ship DM of the bulk carrier with and without WASP. The MAPE between the actual (BDNs) and the predicted fuel consumption (green ship DM), both without WASPs, is 0.3%. This indicates the high accuracy of the model and verifies the use of the model. By calculating the difference between both values predicted by the green ship DM, the result will lay in the same accuracy domain. If the difference would be calculated between the actual fuel consumption recorded in the BDNs and the predicted consumption with WASP by the green ship DM, potential uncertainties regarding the used sensors are introduced of which no information is available.

Table 7.1: Total WASP system savings during 5,678 sailing hours

WASP configuration	Fuel savings [mt]	$-savings [K$]	CO_2 savings [mt]	Percentage savings [%]
Kite300	1,031	637	3,240	-12.5
Kite800	1,048	648	3,293	-12.7
Kite1280	1,070	662	3,364	-13.0
Kite2500	1,129	698	3,549	-13.7
DynaRig single	1,145	708	3,599	-13.9
DynaRig double 2.5	1,148	710	3,610	-14.0
DynaRig double 4	1,068	660	3,357	-13.0
1x Rotor H35D5	1,197	740	3,762	-14.6
4x Rotor H35D5	1,598	989	5,025	-19.4

Furthermore, Table 7.2 shows the resulting reductions per sailing hour based on the sailing conditions between Q3 2022 and Q4 2023. The potential monetary savings per hour are required for the payback period calculation of the financial assessment presented in Section 7.3. A first impression of the overall results shows that the CO_2 reduction potential is within the range of 12% to 20% regarding the investigated WASP configurations. This is in line with the literature study conducted by Bouman et al. (2017) into CO_2 reduction by green ship technologies. Comparing a single configuration of each WASP system (1 kite, 1 sail, 1 rotor), shows that the rotor is the most beneficial to apply in terms of savings potential. The kite configurations progressively increase in saving potential with increasing kite sail area. The difference between the 2 double DynaRig configurations is due to the smaller sail in the double 4 configuration (Section 5.4.3).

Table 7.2: Total WASP system savings per sailing hour

WASP configuration	Fuel savings [kg/h]	\$-savings [\$/h]	CO_2 savings [kg/h]	Percentage savings [%]
Kite300	182	112	571	-12.5
Kite800	184	114	580	-12.7
Kite1280	188	117	592	-13.0
Kite2500	199	123	625	-13.7
DynaRig single	202	125	634	-13.9
DynaRig double 2.5	202	125	636	-14.0
DynaRig double 4	188	116	591	-13.0
1x Rotor H35D5	211	130	663	-14.6
4x Rotor H35D5	281	174	885	-19.4

7.2. Environmental assessment

7.2.1. EEXI

The main environmental assessment tool selected for this research is the EEXI. Through the EEXI, the ship's impact on the environment is assessed in terms of the ship's design. The EEXI calculation according to the IMO is provided in Equation 7.1.

$$EEXI = \frac{P_{ME} \cdot C_f \cdot sfc_{ME} + P_{AE} \cdot C_F \cdot sfc_{AE} - P_{WASP} \cdot C_F \cdot sfc_{ME}}{f_i \cdot f_c \cdot f_l \cdot f_w \cdot f_m \cdot DWT \cdot V_{ref}} \tag{7.1}$$

Here the main engine specifications at 75% MCR (P_{ME} and sfc_{ME}) and fuel conversion factor (C_f) are provided by the available engine reports of the bulk carrier. There are no auxiliary engine specifications available. These are calculated in accordance with the guidelines provided by the IMO (2022b). The ship's reference speed is obtained from the available speed-power curve, at 75% MCR draught condition. The correction factors f_i till f_m are all set to 1 because these are not applicable for the used bulk carrier (IMO, 2022b). The values of the mentioned parameters are listed in Table 7.3.

Table 7.3: Parameters used for the EEXI calculation

Parameter	Value
P_{ME} [kW]	11,467
C_f [mt-CO_2/mt-fuel]	3.114
sfc_{ME} [g/kWh]	162.56
P_{AE} [kW]	631.25
sfc_{AE} [g/kWh]	255.4
DWT [mt]	209,472
V_{ref} [kts]	14.20

The power reduction due to an operating WASP (P_{WASP}) is calculated with Equation 4.3, according to the procedure presented in Section 4.5.1. The global wind probability matrix provided by the IMO (2021) is used for this calculation. Examining the sailing route of the bulk carrier during the period Q3 2022 - Q3 2023 showed that the vessel had sailed approximately 90% on the same shipping routes on which the wind matrix is based (Figure 4.8). This indicates that this wind prediction method has sufficient accuracy regarding this ship's operational area. The ship's current, required, and resulting EEXI values per investigated WASP configuration are provided in Table 7.4.

All the investigated WASP configurations decrease the ship's EEXI value as suspected and consequently comply with the required EEXI value. Moreover, as with the overall results in Section 7.1 installing a rotor results in the highest CO_2 reduction. The *4x Rotor H35D5* configuration is simply a factor 4 environmental beneficial in terms of design potential, as the result of Equation 4.3.

Table 7.4: New EEXI value per installed WASP configuration

WASP configuration	EEXI [g/(mt-nm)]	Reduction [%]
Required value (max)	2.370	-
No WASP (current)	2.120	-
Kite300	2.112	-0.4
Kite800	2.101	-0.9
Kite1280	2.085	-1.6
Kite2500	2.044	-3.6
DynaRig single	2.054	-3.1
DynaRig double 2.5	2.052	-3.2
DynaRig double 4	2.095	-1.2
1x Rotor H35D5	2.029	-4.3
4x Rotor H35D5	1.754	-17.2

7.2.2. CII

The ship's operational aspect is evaluated by calculating the corresponding CII. The traveled distance and total fuel consumption during the selected 11 months are listed in Table 7.5. As mentioned in Section 4.5 this will not be the official CII value as it is required to use a whole calendar year for that calculation. Nevertheless, this CII calculation provides a useful indication of the vessel's operational impact. The required CII values including the rating for the years 2023, 2024, and 2025 corresponding to the used bulk carrier are depicted in Figure 7.1.

Table 7.5: Sailing distance and predicted fuel consumption (without WASP system) per period for CII calculation

Period	Distance travelled [nm]	Fuel consumption [liters]
Q3 2022	12,447	2,591,950
Q4 2022	18,597	3,161,470
Q1 2023	8,601	1,490,790
Q2 2023	10,295	1,799,420

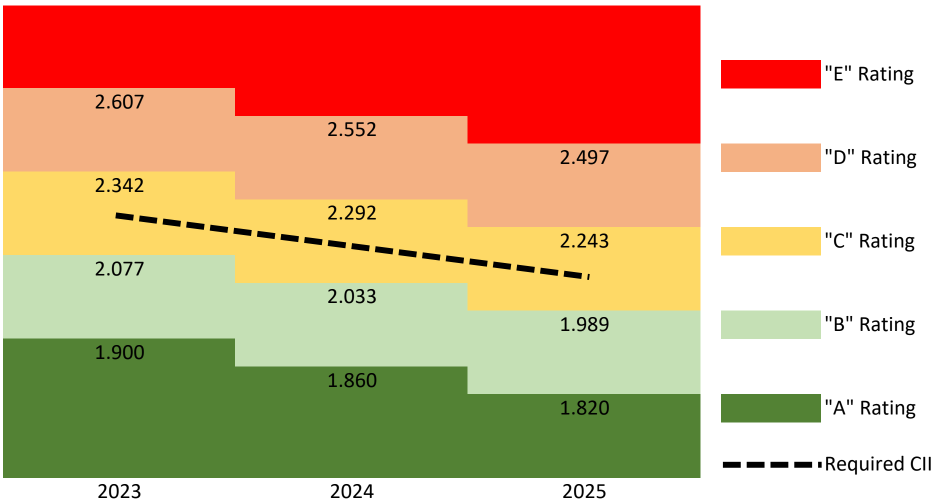

Figure 7.1: Attained CII values of the investigated bulk carrier; required CII values for 2023, 2024, and 2025 are respectively 2.212, 2.166, 2.119

For the calculations of the attained CII per installed WASP configuration, a fuel oil density of 0.8352 g/cm^3 is used. The fuel consumption is predicted with the constructed green ship DM. The results are provided in Table 7.6, including color labeling per CII corresponding to its rating for the year 2023.

The bulk carrier is currently above the required CII, in the C-rating. All the WASP configurations bring the bulk carrier in the B-rating regarding the year 2023, whereas both rotor configurations also comply with the B-rating regarding the year 2024 and *4x Rotor H35D5* extend B-compliance for the year 2025.

Table 7.6: CII approximation per WASP configuration of 11 months during Q3 2022 - Q2 2023

WASP configuration	Attained CII [g/(mt-nm)]
Required (2023)	2.212
No WASP	2.248
Kite300	2.059 (-8.4%)
Kite800	2.056 (-8.6%)
Kite1280	2.051 (-8.8%)
Kite2500	2.039 (-9.3%)
DynaRig single	2.035 (-9.5%)
DynaRig double 2.5	2.035 (-9.5%)
DynaRig double 4	2.052 (-8.8%)
1x Rotor H35D5	2.020 (-10.2%)
4x Rotor H35D5	1.931 (-14.1%)

7.3. Financial assessment

Lastly, the financial assessment is performed by calculating the payback period per WASP configuration. Each financial parameter in the payback period calculation (Equation 4.4) will be discussed next before the payback period per configuration is determined.

A: $-saving per sailing hour by WASP

The $-savings per hour is the driving parameter of the payback period. This saving directly determines how financially beneficial the respective system is. The $-savings per hour of each investigated WASP configuration are provided in Table 7.2, based on the BDNs.

B: Purchase & installation

For the purchase and installation costs, the estimations provided by GloMEEP (2019) are used. Besides information on energy-efficient measures for global shipping, GloMEEP also provides reliable estimations of purchase and installation costs of WASP systems (i.e., kite, sails, and rotors). Table 7.7 shows the estimation costs for a towing kite.

Table 7.7: Purchase costs estimation towing kite (GloMEEP, 2019)

Kite sail area [m^2]	Costs [K$]
160	280
320	480
640	920
1,280	1,755
2,500	2,590

The estimation of implementation costs for DynaRig sails (fixed sails) is $170,000 to $300,000 per installed mast. Thus, for the *DynaRig single* configuration the costs are between $170,000 and $300,000, and for the *DynaRig double 2.5* and *DynaRig double 4* the costs are between $340,000 and $600,000.

The estimation of implementation costs for rotors is $400,000 to $950,000 per installed rotor. Because the biggest rotor dimensions currently available are used for this research, the costs are estimated in the higher range from GloMEEP (2019). Thus for one rotor: $700,000 to $950,000, and for 4 rotors: $2,800,000 to $3,600,000.

C: Out of service costs & dry docking

Unfortunately, no evident information or estimations are available online for the costs regarding taking the ship out of service for retrofitting and dry docking. This is mainly due to the fact shipping companies and maintenance docks only provide such information through a direct offer. Consequently, this expense will not be taken into account in the payback period calculation of this research. However, it does not mean it can be neglected when considering WASP installation.

D: Operational & maintenance costs

The costs regarding operations and maintenance of the respective WASP system are in general provided by the manufacturer. For this research, these costs are estimated to be annually at 2% of the WASP installation costs, which is in line with research conducted by van der Kolk et al. (2019) who did a technological and economical assessment of WASP systems for transport vessels.

Payback period

Next, the payback period (P), without costs 'C', per WASP configuration can be calculated, based on the operational data. The results in different time scales are provided in Table 7.8, in which the time is considered as the vessel in operational condition (i.e., minimal ship speed of 6 knots). To obtain the total payback period accounting for all, one must include the term $\frac{C}{A}$ to the provided payback period results with their known value for 'C'.

Table 7.8: Payback period (P) of WASP configurations expressed in operating time, without costs 'C'

WASP configuration	P [hrs]	P [days]	P [years]
Kite300	4,091	170	0.5
Kite800	10,121	422	1.2
Kite1280	15,596	650	1.8
Kite2500	22,128	922	2.5
DynaRig single	1,368 ∼ 2,419	57 ∼ 101	0.2 ∼ 0.3
DynaRig double 2.5	2,735 ∼ 4,850	114 ∼ 202	0.3 ∼ 0.6
DynaRig double 4	2,943 ∼ 5,220	123 ∼ 218	0.3 ∼ 0.6
1x Rotor H35D5	5,437 ∼ 7,411	227 ∼ 309	0.6 ∼ 0.8
4x Rotor H35D5	16,696 ∼ 21,702	696 ∼ 904	1.9 ∼ 2.5

The resulting payback periods show that both *Kite2500* and *4x Rotor H35D5* take the longest time to be financially profitable. The DynaRig configurations are on average the best option in terms of payback period.

7.4. Conclusion on case-study results

The results of the performed bulk carrier case-study are presented in this chapter. These results represent the required information identified for a possible retrofit design, and aim to answer RQ6: *'To what extent does the output of the green ship DM directly impact the retrofit design?'*

The fuel savings per WASP configuration are predicted with the green ship DM over the selected periods. The range of saving potential is between 12% and 20%, with the *4x Rotor H35D5* configuration showing to have the highest reduction potential. The four kite configurations progressively increase in saving potential logically with increasing kite area. The DynaRig sail configuration with the same dimensions (*DynaRig single* and *DynaRig double 2.5*) both show similar reduction results. The lower reduction potential of the *DynaRig double 4* is due to its smaller sail dimensions. The fuel difference is calculated with the green ship DM for both the situations with and without installed WASP configuration. The MAPE between the predicted fuel consumption without WASP (by the green ship DM) and the actual fuel consumption without WASP (by BDNs) is 0.3% indicating the high accuracy of the model and verifying its use.

The environmental assessment of the green ship DM is performed with the EEXI and CII. For all the investigated WASP configurations the bulk carrier's EEXI value is reduced. This reduction represents the estimated design CO_2 emissions per transported tonne over a nautical mile. The *4x Rotor H35D5* resulted in the highest estimated design emission reduction. This is also noticed with the CII calculation. Under the current circumstances (based on 11 months of operational data) the *4x Rotor H35D5* brings the bulk carrier in the CII B-rating for years 2023 to 2025. For solely the year 2023, all the investigated WASP configurations result in a B-rating, indicating the ship's compliance regarding its environmental impact due to operations.

Additionally, a financial assessment is performed. The payback period per WASP configuration is derived to provide a time-related indication for a potential retrofit. For this calculation, the overall $-savings result during the investigated period is divided by the total number of operation hours, resulting in a $-savings per operating hour per WASP configuration. Together with estimations of retrofit-related costs, the payback period is calculated. Even though not all costs are known, the first estimation showed that on average the DynaRig configurations are the best option in financial terms. The *Kite2500* and *4x Rotor H35D5* have the longest payback period.

In conclusion, both the environmental and financial impact per WASP configuration regarding the bulk carrier are investigated. These assessments drive the potential retrofit decision by the ship owner. The environmental assessment showed that installing the *4x Rotor H35D5* will lead to the highest CO_2 reduction in both a design and operational view. Nevertheless, this is also the configuration with the highest payback time. Moreover, the DynaRig configurations are on average the most financially attractive, without taking into account dry-docking and out-of-service costs. The final decision will depend on the requirements set by the ship owner.

8 Conclusions

This research proposed and investigated the use of a data-driven design method for ship retrofit modeling to reduce CO_2 emissions. WASP models are evaluated with adopted environmental assessment tools together with a financial assessment. The conclusions of this research are presented in this chapter. First, the answers to the six research questions supporting the main objective are presented, as stated in Chapter 1. Next, the conclusion of the main research objective is provided.

8.1. Conclusions on research questions

8.1.1. RQ1: What is the state-of-the-art in data-driven ship design for green ships?

Green ship design refers to the goal of designing environmentally friendly ships while maintaining safe operational conditions. The design of green ships introduces new risks in terms of safety and logistics, compared to traditional ship design. Therefore, newly developed design techniques are required to mitigate these potential risks. With its capabilities of handling big data together with complex simulation characteristics, DT-supported design is identified as a favorable method for green ship design.

A literature investigation showed that scientific research into maritime DT applications is currently in the early stages of development. Only conceptual DTs or DTs covering a vessel's subsystem are found regarding new-build ships. Furthermore, publications of DT applications for retrofit design are not available. A research gap of DT-supported design for both new-build ships and retrofitting is identified. The potential for retrofitting is investigated in this research.

8.1.2. RQ2: Which steps are involved in constructing a DT for retrofit design?

To correctly answer this question the definition of a DT needs to be defined clearly. A DT consists of a physical and virtual product connected through a two-way automated data flow. The steps involved in constructing a DT for retrofit are identified as the following:

1. Determining the DT objective. By formulating its objective, the overlap between the required and feasible digital models can be identified. These models depend on respectively the objective and the available data on which the models will be based.

2. Establish the data acquisition system. This determines the availability and quality of the data. Regarding a DT, utilizing operational data acquisition systems, such as IMO's DCS, is considered to be convenient as it provides a solid source of operational data during the ship's whole lifetime.

3. Adopt a data preprocessing framework. Applying techniques, such as feature selection and noise identification will result in high-quality data in the right format to be used for model construction.

4. Selection modeling approaches. There are various ways to construct virtual models depending on the data amount and the objective. Regarding data science in general, the three main approaches are BBM, WBM, and GBM. A trade-off should guide the choice between these options.

5. Perform model training. In the case of statistical-based models (BBM or GBM), model training is required to calibrate and achieve acceptable accuracy.
6. Verify and validate (V&V) the virtual models. Performing a V&V-procedure, the accuracy, and consequently, the reliability of the total system is ensured. This can be done through a case-study or by applying model tests.
7. Integration of the virtual part with the physical part. After this step, the virtual and physical parts are directly linked and represent each other. Following the adopted DT definition, the result of this integration is the DT.

8.1.3. RQ3: What is the most suitable green ship digital model using bunker delivery notes for CO_2 reduction?

The final green ship digital model is composed of a model part representing the ship, and a model part representing the green ship technology. The model(s) within these parts depend on the available data. This results in a FCM representing the ship, and three types of WASP models representing the green ship technology part.

Literature showed the available data in the BDNs is feasible to construct a ship resistance model and an ANN, respectively characterized as a WBM and a BBM. Combining both models results in one gray box FCM. The three WASP systems (towing kite, DynaRig sail, and Flettner rotor) are modeled as WBMs using the available wind data in the BDNs.

The evaluation of the CO_2 emission reduction by these WASP systems will be performed using environmental assessment tools adopted by the IMO. This assessment involves the design and operational CO_2 emissions.

8.1.4. RQ4: To what extent can data from bunker delivery notes be incorporated into the selected digital models?

A preprocessing framework is adopted regarding the BDNs. This framework is the result of investigating the data requirements of the chosen digital models. The main identified driver of the resulting data is the data selection. As the environmental assessment is linked to the ship in operational conditions, the ship speed is set to a minimum speed. In this research the minimum speed is set to 6 knots, consequently eliminating more than 40% of the data in the BDNs.

Ship characteristics and environmental data are integrated into the selected resistance model, the white box part within the FCM. These data types are presented in the accepted procedures on which the resistance model is based. The output of this model is used as one of the inputs of the ANN, providing the gray box characteristic of the FCM.

A Spearman correlation analysis including chosen criteria is used to identify data types within the BDNs that are strongly linked to the fuel consumption of the ship's main engine. The identified data types are selected as inputs for the ANN, the black box part within the FCM. The output of the total FCM is fuel consumption per hour.

The three WASP models only require wind data to determine the potential propulsion force generated by the WASP system. The wind speed in the BDNs is recorded by a wind sensor at a certain height. Due to the varying wind profile over height, this speed needs to be converted with regard to the effective height of the respective WASP system. This conversion is performed for each system before the propulsion force is calculated.

8.1.5. RQ5: To what extent can the output of the digital models be integrated into one green ship DM?

The constructed WASP models provide a propulsion force of the respective operating WASP system. One of the inputs of FCM is the ship's brake power. To combine both models into one green ship DM, the WASP's propulsion force is transformed into a new ship's brake power by integrating this force into the ship's force balance. Herein the propeller's new working point is derived via the propeller-engine matching procedure, resulting in the new ship's brake power. This new brake power is used as input into the FCM. With this integration, the green ship DM is constructed with which the fuel consumption per operating WASP configuration can be predicted.

The adopted integration framework is based on the available data in the BDNs. Some calculations within the framework depend on specific data. When the green ship DM is used with data originating from other sources, some steps need to be alternated. This indicates that the integration is flexible when treated carefully.

8.1.6. RQ6: To what extent does the output of the green ship DM directly impact the retrofit design?

With the green ship DM, the saving potential per WASP configuration can be evaluated during the selected period. This indicates the environmental and financial benefits in terms of CO_2 emissions and fuel costs of this period.

The environmental assessment tools EEXI and CII represent respectively the ship's estimated design and operational environmental impact. Evaluating the EEXI and CII reduction as a result of a certain WASP configuration provides the environmental justification for a retrofit design. Moreover, as the CII is a yearly evaluation of the ship's performance, the final DT can provide continuous operational evaluation.

The financial assessment per WASP configuration through the green ship DM provides insight into the payback period of the system. This payback period is based on the potential $-savings per configuration. Together with the environmental benefits, the ship owner can decide if a certain retrofit is environmentally necessary and financially beneficial. Such a choice can be made through a trade-off with this information.

8.2. Conclusion on main objective

The main objective of this research was:

"To what extent can available operational ship data be used to improve future green ship design by reducing CO_2 emissions?"

Incorporating operational data into ship design resulted in the investigation of a DT-supported design method. The beneficial characteristics of a DT are its capability to handle large amounts of data and perform virtual simulations. The risks introduced by environmentally friendly ship design can be reduced by applying such a data-driven method. Within the field of green ship technologies to reduce CO_2 emissions, WASP systems are evaluated for DT design. With the lifetime ability of a DT, operational data collected by an already mandatory data acquisition system is selected as the data source for the modeling construction. The selected source is the IMO's BDNs which provide HF operational data and have proven to be feasible for modeling construction. A green ship DM is constructed which incorporates ship characteristics, route-dependent, and environmental data to predict the fuel consumption with an operating WASP system. The fuel consumption can be compared to the situation without an installed WASP system, resulting in potential CO_2 emission reduction (environmental) and its payback period (financial). Together with adopted environmental assessment tools by the IMO using the constructed green ship DM, enables the ship owner to make a trade-off for a potential retrofit design.

9

Discussion & recommendations

In this chapter, the adopted methodology and recommendations are discussed. First, the contribution to scientific research is presented, highlighting the novelties within the work. This is followed by an evaluation of the methodology and choice of data source. Additionally, assumptions and necessary changes concerning the transformation towards a DT for operational use are provided. Lastly, the author's vision of developing a DT for new-build design using retrofit DTs is presented.

9.1. Scientific contribution

In this research, a DT-supported method has been selected with a chosen data source to investigate environmentally friendly ship design. The performed literature investigation identified a literature gap for both new-build DTs and retrofit DTs. Together with the available data and personal vision of the design DT development (Section 9.5), a DT for retrofit design is selected for this research. As identified by Mauro and Kana (2023) computer models are often falsely labeled as Digital Twins. In order to prevent contributing to this error in nomenclature, this research strictly followed the DT definitions by Kritzinger et al. (2018) and Grieves (2014), to identify the steps toward the development of a DT-supported retrofit design (Figure 3.9). Following this definition resulted in the construction of a green ship DM which supports the DT for retrofit purposes.

The first proposed step in constructing this green ship DM is to find the overlap in models regarding the objective and available data (Figure 4.2). The objective is to reduce CO_2 emissions which led to the IMO's environmental assessment tools EEXI and CII. The BDNs fulfilled the role of the available operational data. The BDNs are one of the mandatory IMO's DCS methods, that have not been used for research purposes yet, only for the ship's yearly mandatory CII calculation. By proving BDNs as a feasible data source for DTs, an incoming HF data flow consisting of operational ship data is guaranteed. The proposed framework for constructing a green ship DM for retrofit design (Figure 4.9) consists of constructing a model representing a ship and one representing the green ship part that is integrated into one green ship DM (Figure 4.3). This DM can predict the ship's fuel consumption with an operating WASP system using route-dependent and environmental data. By linking this output with the selected tools EEXI & CII, together with a financial assessment, advice for possible retrofit design is provided.

9.2. Methodology evaluation

9.2.1. Modeling framework evaluation

During the data preprocessing filtering stage, no interpolations were performed for invalid data points. This resulted in 5.2% of the data points being disregarded due to noise identification in this data set. Moreover, a time conversion was performed on the data, transforming the respective points from a sampling time of 5 minutes into 1 hour. Also, no interpolation was implemented in the case that an hour is incomplete. This resulted in a data loss of 1.1%. Even though in both cases the data loss is a fraction of the total amount, interpolation can help prevent unnecessary loss.

For the hour conversion of the feature ‘wind direction’, a weighted average was taken over the respective hour. This wind direction is only used as input for the ANN, not for the WASP models. But no one-truth is found to correctly average the wind direction over a given time.

The focus of this research lies in the integration of operational data into a retrofit design. The constructed WASP models are at a high level. For example, the aerodynamics in the towing kite model are approximated by only one value; the wind energy transfer efficiency ϵ. To get more accurate predictions of the WASP system’s propulsion force, more refined WASP models should be used.

One of the foremost assumptions within this research is regarding the fuel consumption prediction by the green ship DM with an operating WASP system. The FCM is validated with high accuracy for known sailing conditions regarding given inputs. One of these inputs is the ship’s brake power. During the case-study only the value for the brake power is changed to investigate the influence of an installed WASP system, assuming that the resulting fuel consumption corresponds to that situation. To correctly verify this assumption, model or full-scale tests need to be executed including installing the respective WASP system. Only in this way, the verification loop of the proposed method can be closed. Additionally, by conducting these verification tests, the extrapolation capabilities of the presented method are investigated.

9.2.2. BDNs evaluation

The bunker delivery notes as a data source have proven to be feasible for the selected modeling construction. The numerous amount of data points regarding route-dependent and environmental information are used for the fuel prediction. Nevertheless, no information is available about the method and quality of the sensors used for the data collection. Without having this information, no certainty can be provided about the potential errors within these values due to sensor sensibility or recording method.

Despite the many different recorded data types, no data regarding waves, trim, and draft were available. By incorporating these types of data within the constructed resistance model, a more reliable estimation of the ship’s resistance, and even the total resistance can be determined. The water depth, which can be used in speed loss due to shallow water effects (Fan et al., 2020) is present in the BDNs but incomplete and consists of multiple anomalies. Therefore, it is disregarded in this research.

Moreover, data from one month (March 2023) is missing, which is probably the result of human error. Unfortunately, this resulted in an incomplete calculation for the CII using 11 months, instead of the required 12 consecutive months.

9.2.3. Assessment evaluation

Two environmental assessment tools by the IMO were in this research: the EEXI and the CII. The EEXI is calculated following its procedure. Because the current EEXI value of the bulk carrier is known, the calculation could be verified. By using the EEXI, an acceptable and mandatory evaluation of the ship’s environmental impact is provided in terms of ship design. One of the reasons for using the EEXI in this research is its focus on CO_2 reduction through design, making it a logical choice as a measure linked to design. Moreover, by adopting an international mandatory measure, the compliance of the retrofit is highly acceptable.

Due to the aforementioned missing data of one month, only an incomplete prediction of the CII can be provided instead of performing the actual calculation. The CII calculation is sensitive to minor changes in its parameters which indicates that more accurate values for distance and fuel conversion, together with information about the sensors would improve the reliability of the derived CII value. Additionally, since no values from previous years or calculations are available, verification cannot be performed. Nevertheless, by demonstrating the feasibility of the calculation with the proposed framework, the resulting DT is future-proofed, given that the BDNs will be collected throughout the vessel’s entire lifetime.

9.3. Data changes when using future data set

The presented design approach is based on the available data set and also evaluates the vessel during that period. With the simulation performance ability, and convenience of DT to be of use during the whole lifetime, data sets containing information for future situations will be used after retrofitting. The changes in certain calculations within the model integration, associated with applying this new data set, are already discussed in section 6.5, covering the ship's total resistance and brake power. Other recommendations for future state data sets and the determination of required data types are provided in the next sections.

9.3.1. Environmental data

A good estimation of the wind direction and speed is crucial for the DT as it covers the installation of WASP systems. It is used to determine the WASP system's propulsion force and therefore the prediction of the ship's fuel consumption. The IMO's global wind probability matrix can be used in the case that the next route is still unknown and a first prediction is requested. A recent report by EMSA (2023) showed that when a wind probability matrix is used based on the intended sailing route, a difference in EEXI value of more than 10% is found for the respective vessel. This indicates the higher prediction accuracy when using more detailed wind models. From the selected wind probability density matrix a probability density function can be derived which can be used for prediction.

The speed difference and temperature of seawater can utilize currently known data to derive the probability density function. Subsequently, a Monte Carlo simulation can be used to construct the dataset. This method is described and successfully executed in the work of Fan et al. (2020) to construct a data set with environmental data linked to a selected shipping route. The data of both these parameters can also first be categorized per sailing route before the probability density is derived, to increase prediction accuracy.

9.3.2. Route-dependent data

The ship's speed and rudder angle are both route-dependent parameters, which result from the ship owner. By selecting a sailing route including a (maximum) sailing time, the ship's heading and speed are determined.

9.4. Recommendations - future work

This section presents the recommendations for future work.

In this research, no interaction effects between the WASP system and the ship itself are taken into account. Even though these effects are ignored in the IMO's calculation for the EEXI with WASP (IMO, 2021) as considered to be of significance only during unsafe operations, they are not to be neglected when considering the installation of a WASP system. Examples of such effects are:

- Change in center of gravity. Thies and Ringsberg (2023) showed the influence of the longitudinal position of the WASP systems on the potential power reduction resulting in differences up to 4%.
- Induced trimming moment due to WASP, resulting in changes of the aero-hydrodynamic performance of the vessel and influences the WASP lift and drag coefficients (Smith et al., 2013).
- Heel angle due to WASP which influences the ship's course-keeping ability. In the last decade, a new type of rudder has been developed that improves the ship's maneuvering capabilities; the gate rudder (Stark et al., 2022). As depicted in Figure 9.1, this rudder is composed of two rudder blades located aside from the propeller. Originally designed as an ESD that generates underwater lift, the gate rudder also compensates for the induced heel angle and reduces the ship's leeway (IMO, 2023c).

It is proposed that the installation of a gearbox or controllable pitch propeller is necessary due to the fluctuating nature of propulsion force by the wind. Because the wind is not constantly acting at the same speed in the same direction, the propeller power demand will also fluctuate if a constant ship speed is desired. It is believed that a gearbox or a CPP could mitigate the power fluctuations endured by the main engine.

Besides the necessary changes in the data set as discussed in the previous section, other implementations are identified with regard to the transformation towards an operational applicable DT:

- Applying route optimization for the most beneficial wind propulsion is a convenient next field to investigate to transform the resulting design DT for operational use. Bentin et al. (2018) showed that the shortest sailing route is not necessarily the most efficient one when considering wind propulsion.

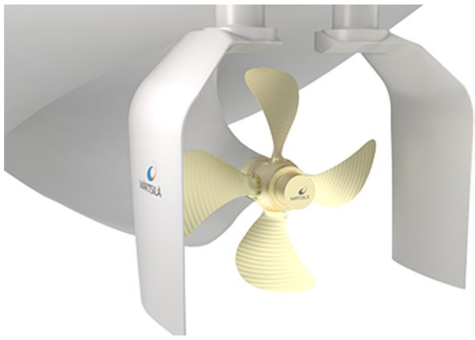

Figure 9.1: Gate rudder design by Wartsila (2020)

- Incorporating maintenance data, such as propeller and hull cleaning, to extend the DT operational performance by taking into account the performance degradation as a result of maintenance checks.
- Besides the CII measure, the EEOI calculation can be integrated to assess specific future routes or trips.

Moreover, the presented method is focused on the model integration of ship and green ship technologies (WASP systems), providing results linked to a potential retrofit decision. Another perspective could be to construct a similar framework that optimizes for the specific WASP systems and the respective dimensions. With a selected environmental or financial objective, the output could potentially provide the corresponding dimensions for a given WASP system.

9.5. Proposed DT design framework, from retrofit to new-builds

It is a complex task to compose a DT for a new-build vessel because there is no data reference data available in order to construct and train the respective DT. As previously mentioned in Section 2.5.1 at this moment only theoretical frameworks for new-build designs are available (Sapkota et al., 2021; Xiao et al., 2022). DTs that support the operational phase of a vessel have been researched more extensively. During this phase, operational data is collected from that ship and used with the DT to improve future operations. It is suggested that this operational data also can be used to identify design improvements for the respective vessel which can result in design decisions for a potential retrofit operation. A design methodology applying a DT for retrofitting is proposed by the author which is believed to form a basis for a DT design model of new build vessels. A visual representation of the proposed methodology is depicted in Figure 9.2.

Reasoning for this proposed method: it is possible to retrieve operational data of a particular vessel that is functioning as a living lab (bulk carrier X-1), by using onboard installed sensors (IoT). With this data, a DT of that vessel can be composed and trained to achieve the required accuracy. Now with a DT of bulk carrier X-1 at an acceptable level, design improvements of this vessel can be investigated through simulations performed which can lead to a new version of the respective DT (following adopted definition: DM of bulk carrier X-1.v2). If the output of this improved DM has proven to achieve the desired retrofitting goals then it can be used for the retrofit design for bulk carrier X-1 to X-1.v2. After the retrofitting the DM represents the respective ship and becomes the DT of bulk carrier X-1.v2 (following DT definition). This DT can be standardized into a DT of the vessel series (DT of bulk carriers X-series). With further standardization of the X-series DT, a DT for the general vessel type (in this case bulk carriers) can be created.

Whereas retrofitting was at the start of the DT application, the shift goes towards new-build by using the knowledge from the first retrofit DT (bulk carrier X-1) as a basis. With the acceptable and validated DT of the general ship type (DT bulk carrier), a new build series of that ship type (bulk carriers Y-series) can be constructed using the DT, or with another standardization step a general DT for a ship can be made (DT vessel) that can be the basis for new build ships of other types (e.g. oil tankers).

The previously mentioned steps are depicted as a block scheme in Figure 9.3, where the red-dashed box indicates where the proposed DT for retrofitting of Section 3.8 fits into this story, and on which part of this vision this thesis has been working on.

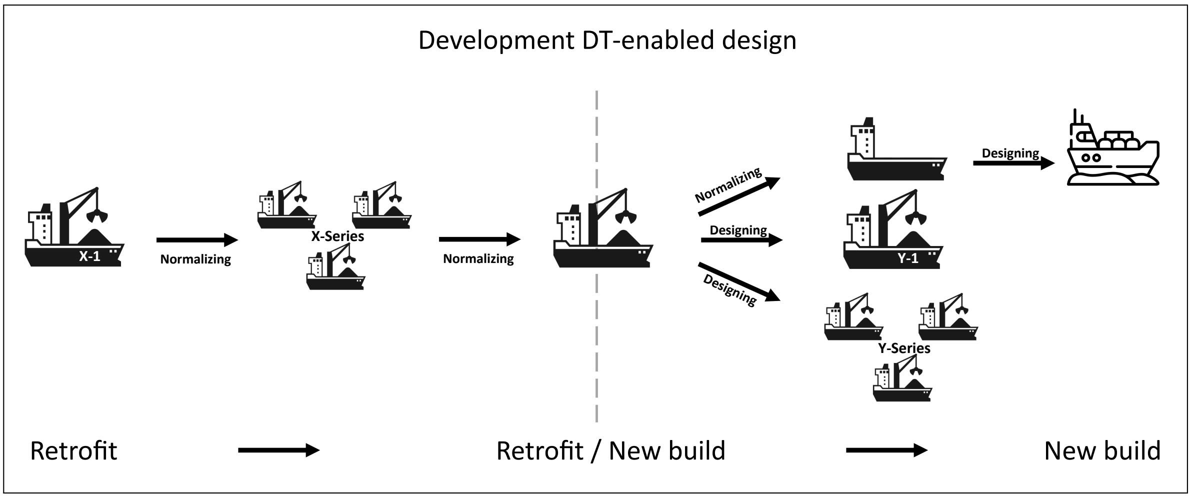

Figure 9.2: Visual representation of proposed DT design framework, from retrofit to new-builds

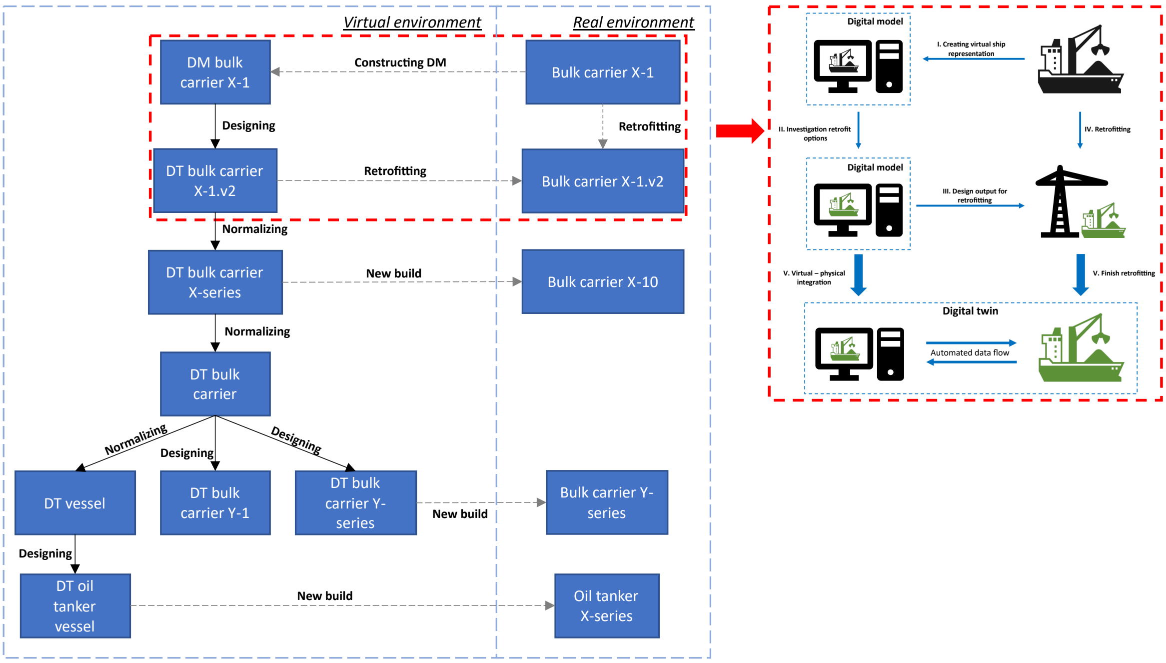

Figure 9.3: Block scheme of proposed DT design framework, from retrofit to new-builds. The red-dashed box indicates the retrofit phase within the framework

A

Available operational data bulk carrier

- DateTimeStamp: Date and time of recorded data.
- ME_REV_COUNTER: Main Engine Revolution Counter.
- ME_RPM: Main Engine RPM.
- ME_RPM_TM: Main Engine RPM torque meter.
- RPM DIFF: Difference in RPM values.
- MCR %: Percentage of Maximum Continuous Rating for the engine.
- FUEL_PUMP_INDEX: Index related to fuel pump operations.
- SHAFT_PWR: Shaft power.
- TORQUE: Torque produced by the engine.
- TINJ: Fuel oil temperature as injected in the engine.
- FO_VISCOSITY: Fuel Oil Viscosity.
- FO_VISCOSITY_2: Fuel Oil viscosity additional data source.
- HEADING_GYRO: Ship's heading using gyroscopic instrumentation.
- RUDDER_ANGLE_INDICATOR: Angle indicator for the ship's rudder position.
- RUDDER_ROT: Rudder rate of turn.
- WIND_DIR: Wind direction.
- WIND_TRUE_OR_RELATIVE: True or relative wind direction.
- WIND_SPEED: Wind speed.
- SoG: Speed Over Ground.
- SPEED_THROUGH_WATER: Speed of the ship through the water.
- SPEED_DIFF: Speed difference.
- WATER_DEPTH: Depth of the water.
- TC_1_RPM: RPM of m/e turbocharger No1.
- TC_2_RPM: RPM of m/e turbocharger No2.

- PWR_G1, PWR_G2, PWR_G3: Power generated by Diesel Generators G1, G2, and G3.
- DG_PWR_TOTAL: Total power generated by all Diesel Generators.
- FM_COUNTER_ME_GE_FO_IN_FLOW: Fuel meter counter for total Fuel Oil supplied to the Main Engine and Diesel generators.
- FM_COUNTER_GE_FO_IN_FLOW: Fuel meter counter for Gas Engine Fuel Oil Inflow.
- FM_COUNTER_GE_FO_OUT_FLOW: Fuel meter counter for Gas Engine Fuel Oil Outflow.
- DG_Fuel, ME_Fuel: Fuel consumption for Diesel Generators and Main Engine.
- ME_SFOC, DG_SFOC: Specific Fuel Oil Consumption for Main Engine and Diesel Generators.
- TOTAL_DG_PWR: Total power generated by Diesel Generators.
- T_IN_ME_GE_FO_FLOW, T_IN_ME_GE_MGO_FLOW: Fuel temperature measurements for Main Engine Fuel Oil Flow and Diesel Generator MGO Flow.
- T_IN_ME_FO_LOW: Temperature measurement for Main Engine Fuel Oil Low.
- T_FO_SERV, T_FO_SETT: Fuel Oil temperatures in Service and settling tanks.
- TCL_C_01, TCL_C_02, ... , TCL_C_06: Cooling water temperature of each cylinder unit.
- TBTB_TC_01, TBTB_TC_02: Temperature before turbo blower for T/C No1 and No2.
- TATB_TC_01, TATB_TC_02: Temperature after turbo blower for T/C No1 and No2.
- T_ER: Engine room ambient temperature.
- SCAV_PRESS, SCAV_TEMP: Scavenge air pressure and temperature.
- T_IN_AC_01, T_IN_AC_02, T_OUT_AC_01, T_OUT_AC_02: Inlet and Outlet temperatures of air cooler No1 and No2.
- T_IN_GE_DO_FLOW: Temperature measurement for Diesel Generator Diesel Oil Flow.
- TCW_IN_AC_01, TCW_OUT_AC_01, TCW_OUT_AC_02: Temperature measurements for Cooling Water.
- TSW_IN: Temperature of Seawater Inlet.
- TEMPERATURE_ME_THRUST_PAD: Temperature of Main Engine Thrust Pad.
- TEMPERATURE_STERN_TUBE_BRG, TEMPERATURE_STERN_TUBE_BRG_P: Temperatures of Stern Tube Bearings.
- TEMPERATURE_INTERM_SHAFT_BRG_1: Temperature of Intermediate Shaft Bearing 1.
- T_IN_ME_CO_FLOW: Temperature measurement for Main Engine Cylinder Oil Flow.
- TBTB_G1_1-3, TBTB_G1_4-6, ... , TBTB_G3_1-3, TBTB_G3_4-6: Temperature before turbo blower of diesel generator No1 (cylinder units 1,2,3 and units 4,5,6). Same for each D/G.
- TATB_G1, TATB_G2, TATB_G3: Temperature after turbo blower of diesel generator No1 (cylinder units 1,2,3 and units 4,5,6). Same for each D/G.
- TCL_C_01_G1, ... , TCL_C_06_G3: Cooling water Temperature of diesel generators 1,2,3.
- T_FW_LT: Temperature of Fresh Water Low Temperature cooling system.
- FM_BO_IN_FLOW: Fuel meter reading for Boiler Oil Inflow.
- LONG_DEGREES, LONG_MINUTES, LONG_LETTER: Longitude coordinates.

- LAT_DEGREES, LAT_MINUTES, LAT_LETTER: Latitude coordinates.
- SPEED_TRANSVERSE_TW_LOG, SPEED_OVER_GROUND_LOG: Transverse speed through water indicated on speed log, speed over-ground indicated on speed log.
- RUN_HR001, RUN_HR002: Running hours data for specific components.

B

Holtrop & Mennen method

The frictional resistance is calculated according to the ITTC-1957 friction formula:

$$R_F = 0.5 C_f \rho_{sw} S V_s^2 \tag{B.1}$$

The parameters in this equation are the frictional resistance coefficient C_f, sea water density ρ_{sw}, wetted hull surface area S and the ship speed V_s. The C_f is calculated with the respective Reynolds number R_n:

$$C_f = \frac{0.075}{(\log_{10}(R_n) - 2)^2} \tag{B.2}$$

Where R_n is calculated with Equation B.3, including an interpolation for the kinematic viscosity (ν) of the seawater depending on the seawater temperature using the seawater properties tables provided by the ITTC (2011).

$$R_n = \frac{V_s L_{oa}}{\nu(T_{sw})} \tag{B.3}$$

The hull form factor $(1 + k_1)$ is derived with Equation B.4:

$$(1 + k_1) = c_{13}\{0.93 + c_{12}(B/L_R)^{0.92497} \cdot (0.95 - C_P)^{-0.521448} \cdot (1 - C_P + 0.0225 lcb)^{0.6906}\} \tag{B.4}$$

The longitudinal center of buoyancy lcb, is derived from the available trim tables of the ship depending on the loading condition during sailing. L_R represents the length of a run and is determined with Equation B.5:

$$L_R = L_{oa} \cdot \left(\frac{1 - C_P + 0.06 C_P lcb}{4 C_P - 1} \right) \tag{B.5}$$

Where C_P is the ship's prismatic coefficient. For the resistance of the appendages, only the rudder is taken into account. R_{APP} is calculated with Equation B.6:

$$R_{APP} = 0.5 \rho_{sw} V_s^2 S_{APP} (1 + k_2) C_f \tag{B.6}$$

The rudder surface area S_{APP} is derived from the available ship drawings together with the CAD program Rhino 3D. For the appendage resistance factor $(1 + k_2)$, the average rudder value provided by Holtrop and Mennen (1982) is used.

The wave resistance R_W is determined with Equation B.7:

$$R_W = c_1 c_2 c_5 \nabla \rho_{sw} g \exp\{m_1 F_n^d + m_2 \cos(\lambda F_n^{-2})\} \tag{B.7}$$

The ship's displacement volume ∇ is derived from the ship's loading condition tables. λ represents a ship dimensional parameter, depending on C_P, B and L_{oa}. The Froude number F_n is calculated with Equation B.8:

$$F_n = \frac{V_s}{\sqrt{g \cdot L_{oa}}} \tag{B.8}$$

The bulk carrier used for this case-study does not have a bulbous bow, resulting in no additional pressure resistance due to a bulbous bow R_B.
The additional pressure resistance of an immersed transom stern R_{TR} is determined by Equation B.9:

$$R_{TR} = 0.5 \rho V_s^2 A_{TR} c_6 \tag{B.9}$$

The immersed stern area A_{TR} is derived from the loading condition tables together with the ship's drawings. The model-ship correlation resistance R_A is calculated with Equation B.10:

$$R_A = 0.5 \rho_{sw} V_s^2 S C_A \tag{B.10}$$

The correlation allowance coefficient C_A is derived with Equation B.11:

$$C_A = 0.006(L + 100)^{-0.16} + 0.00205 + 0.003\sqrt{L/7.5} C_B^4 c_2 (0.04 - c_4) \tag{B.11}$$

Here, C_B represents the ship's block coefficient.

Coefficients directly linked to the ship's characteristics (e.g., C_B and C_P) are determined with its main particulars. The regression parameters m_i and c_i are derived according to the regression procedure provided by Holtrop and Mennen (1982).

C
Errors of ANN training phase

Table C.1: Error during training and validation of network with random state 49

	Training				Validation			
Epoch	MSE (Loss)	MAE	MAPE	RMSE	MSE (Loss)	MAE	MAPE	RMSE
0	2465045	1542.911	99.90734	1570.046	2407702	1522.971	99.7922	1551.677
1	2439333	1535.354	99.46459	1561.837	2370851	1512.13	99.15735	1539.757
2	2392084	1521.201	98.62144	1546.636	2308417	1493.625	98.08627	1519.348
3	2325454	1501.089	97.43295	1524.944	2242351	1473.701	96.92786	1497.448
4	2243975	1475.698	95.89913	1497.99	2161063	1448.341	95.41381	1470.055
5	2149979	1445.637	94.05566	1466.281	2066658	1417.764	93.54046	1437.588
6	2045755	1411.399	91.97051	1430.299	1966512	1384.812	91.55906	1402.324
7	1933605	1373.395	89.64317	1390.541	1849043	1344.37	89.06075	1359.795
8	1815802	1332.001	87.07497	1347.517	1734790	1303.915	86.58681	1317.114
9	1694043	1287.537	84.32903	1301.554	1613990	1259.564	83.88136	1270.429
10	1569353	1240.282	81.4179	1252.738	1464814	1201.416	80.2218	1210.295
11	1443992	1190.491	78.29713	1201.662	1350278	1154.619	77.27266	1162.015
12	1319501	1138.409	75.02881	1148.695	1234533	1105.594	74.26373	1111.095
13	1195806	1084.248	71.62934	1093.529	1108355	1048.756	70.68819	1052.784
14	1075484	1028.23	68.07657	1037.055	959872.9	976.7413	66.03416	979.731
15	958597.4	970.5698	64.38745	979.0798	912799.9	951.6981	64.13921	955.4056
16	846121.3	911.4315	60.51674	919.8485	767473.6	873.8305	59.18518	876.0557
17	739108.5	851.041	56.58914	859.7142	668762.1	815.9794	55.36193	817.7787
18	637540.4	789.704	52.58406	798.4612	541578.1	734.4239	49.89729	735.9199
19	542858.2	727.5676	48.52253	736.7891	438580.4	661.4337	45.22932	662.254
20	456326	665.033	44.34515	675.519	395514.2	627.9933	42.93793	628.8992
21	377051.3	602.7091	40.25414	614.045	314469	559.9208	38.39895	560.7753
22	305529.5	540.3512	36.05595	552.7473	246214.5	495.3458	34.12618	496.2001
23	242658.5	478.9187	31.96496	492.6038	199190.8	445.0794	30.54033	446.308
24	188293.2	418.4686	27.91095	433.9277	150367.4	386.4856	26.48891	387.7724
25	142927	360.4114	23.96447	378.0569	103824.6	320.6783	22.05906	322.2182
26	105500.9	305.2525	20.37506	324.8091	73312.76	268.4575	18.27778	270.7633
27	75756.54	252.8708	16.82294	275.239	42709.21	203.6389	13.7998	206.6621
28	54080.51	207.6421	13.90936	232.5522	33590.65	178.8206	11.96212	183.2775
29	37952.76	167.577	11.24412	194.8147	17032.36	125.3085	8.834179	130.5081
30	26915.27	136.174	9.264318	164.0587	9474.951	91.22058	6.22761	97.33936
31	20237.81	115.0056	7.982321	142.2597	3970.977	54.81116	3.756348	63.01569
32	16289.53	99.78314	7.057193	127.6304	1504.95	28.21555	2.046987	38.79368
33	14218.54	91.80384	6.643385	119.2415	1734.62	32.57359	2.221003	41.64877

Continued on next page...

Table C.1: Error during training and validation of network with random state 49 (continued)

	Training				Validation			
Epoch	MSE (Loss)	MAE	MAPE	RMSE	MSE (Loss)	MAE	MAPE	RMSE
34	13241.74	88.66911	6.44786	115.0728	1175.756	25.36149	1.815253	34.2893
35	12567.7	85.33105	6.315306	112.1058	1204.816	25.98852	1.802023	34.71046
36	12597.84	84.64973	6.361451	112.2401	1723.275	32.61747	2.450715	41.51235
37	12435.26	83.61054	6.244515	111.5135	1775.921	35.56344	2.613762	42.14168
38	12747.54	84.64504	6.320094	112.905	1021.375	24.03058	1.724608	31.95897
39	12505.16	84.00899	6.301022	111.8265	997.1124	23.62039	1.705549	31.57709
40	12591.67	83.9418	6.305784	112.2126	1277.67	28.01414	2.073043	35.74451
41	12391.74	83.51994	6.269414	111.3182	1075.906	25.72665	1.876774	32.80101
42	12333.87	83.54472	6.22465	111.058	2399.346	36.27323	2.888673	48.98312
43	12498.56	84.23117	6.359606	111.797	1621.959	31.45574	2.179924	40.27355
44	12614.97	83.4091	6.379491	112.3164	1306.373	27.08141	1.963614	36.14378
45	12979.87	84.57397	6.466314	113.9292	1626.963	32.29425	2.385154	40.33563
46	12706.54	83.52042	6.365864	112.7233	1286.775	28.43021	2.09014	35.87165
47	12072.18	82.13336	6.213559	109.8735	1229.66	29.87412	2.073615	35.06651
48	11843.17	81.70641	6.154614	108.8263	1013.953	24.89205	1.784978	31.84262
49	12554.19	83.315	6.321984	112.0455	1142.892	26.70129	1.92831	33.80669
50	12554.5	82.81116	6.305888	112.0469	1048.533	24.68557	1.808209	32.38106
51	11970.77	81.94626	6.154331	109.411	1132.345	25.45002	1.854929	33.65034
52	12859.45	82.79678	6.391356	113.3995	1397.36	29.51368	2.153755	37.38128
53	12456.08	81.98456	6.297845	111.6068	1216.267	25.9405	1.860848	34.87502
54	12252.37	82.51878	6.276321	110.6904	1154.127	26.36362	1.919727	33.97245
55	12144.63	82.45028	6.217895	110.2027	1165.382	25.17392	1.919028	34.1377
56	12323.44	82.36961	6.233577	111.011	1680.355	31.94098	2.399673	40.99214
57	11826.9	80.90738	6.097336	108.7515	1186.414	26.33049	1.925174	34.44437
58	12587.49	82.4952	6.37571	112.194	981.1069	24.80891	1.783866	31.32263
59	12600.55	82.90771	6.320329	112.2522	1267.268	27.17869	2.007885	35.59871
60	12407.91	81.85837	6.295652	111.3908	1905.919	35.12192	2.612103	43.65683
61	12340.29	82.60125	6.282541	111.0869	1570.803	29.38385	2.202402	39.63336
62	12520.21	83.45216	6.323977	111.8937	1227.672	26.66749	1.882527	35.03815
63	11949.14	82.6492	6.218721	109.3121	1080.805	26.11579	1.852623	32.8756
64	12227.87	82.61594	6.236753	110.5797	1349.865	28.31828	1.930986	36.74051
65	12097.54	81.84842	6.200966	109.9888	1417.261	29.06462	2.151345	37.64652
66	12118.62	82.01231	6.187086	110.0846	1093.003	25.88125	1.906609	33.0606
67	12214.62	82.21523	6.223451	110.5198	1246.992	29.10003	2.094693	35.31277
68	12335.41	82.71176	6.287487	111.0649	1867.362	33.0472	2.533066	43.21299
69	12365.41	82.36063	6.232543	111.1999	1799.274	34.97041	2.583108	42.41785
70	11862.48	81.16592	6.134624	108.915	1466.796	31.70445	2.252866	38.29877
71	11798.08	81.2743	6.092391	108.619	1454.633	31.48542	2.273426	38.13966
72	12266.17	82.22111	6.228018	110.7528	1213.469	26.24786	1.861372	34.83487
73	12343.68	82.24567	6.31265	111.1021	1535.286	31.56249	2.334212	39.18272
74	12296.31	82.00042	6.230773	110.8887	1810.756	36.66492	2.602189	42.55298
75	12034.9	81.43852	6.125791	109.7037	1508.339	33.16101	2.306128	38.83735
76	12055.72	81.30484	6.203529	109.7986	1058.533	25.9254	1.880059	32.5351
77	11975.65	81.62991	6.183418	109.4333	1118.392	25.69255	1.860484	33.44238
78	11928.14	81.43571	6.133593	109.216	947.8828	23.53033	1.665458	30.78771
79	12544.69	82.70016	6.306401	112.0031	1374.018	27.92305	1.998327	37.06775
80	12029.87	81.23351	6.139983	109.6808	1224.719	27.25368	1.975834	34.99598
81	12399.18	82.03924	6.211481	111.3516	1263.58	28.18548	2.058177	35.54688
82	12114.77	81.38822	6.188673	110.0671	1091.395	25.86692	1.876306	33.03627
83	11935.91	81.34557	6.169895	109.2516	1068.539	25.75674	1.831972	32.68852
84	12031.15	81.88939	6.191379	109.6866	1156.542	27.55715	1.986781	34.00797
85	12132.67	80.74416	6.152738	110.1484	1566.3	31.79484	2.345935	39.57651

Continued on next page...

Table C.1: Error during training and validation of network with random state 49 (continued)

	Training				Validation			
Epoch	MSE (Loss)	MAE	MAPE	RMSE	MSE (Loss)	MAE	MAPE	RMSE
86	12208.03	81.73286	6.155221	110.49	1309.118	27.06313	1.986923	36.18174
87	12157.72	82.17152	6.265663	110.2621	1449.712	28.58301	2.075412	38.07508
88	11999.52	80.53216	6.128207	109.5423	1331.024	28.50452	2.097234	36.48321
89	12053.41	81.14512	6.219702	109.788	1033.524	24.2972	1.75493	32.14846
90	11843.84	81.59161	6.154737	108.8294	1556.771	30.85354	2.264947	39.45593
91	11993.13	81.89571	6.177685	109.5132	1423.445	31.31364	2.220592	37.72857
92	12030.92	80.69061	6.13379	109.6855	1250.221	28.05018	2.046225	35.35846
93	12081.38	81.45954	6.184548	109.9153	1263.127	29.86472	2.09995	35.5405
94	11581.37	80.30599	6.100221	107.6168	1173.85	25.76344	1.862141	34.26149
95	11824.43	80.8206	6.10697	108.7402	973.8993	26.0721	1.811594	31.20736
96	11408.68	79.85665	6.046716	106.8114	2419.339	37.69418	2.977834	49.18678
97	11888.65	81.1385	6.124252	109.0351	1036.26	24.61612	1.762916	32.191
98	11878.08	81.14796	6.195281	108.9866	1036.033	26.44053	1.913528	32.18747
99	12266.23	81.40548	6.145874	110.753	1315.767	27.80929	1.904194	36.2735
100	11859.52	80.82539	6.077518	108.9014	1226.953	29.22972	2.060315	35.02789
101	11648.57	80.44719	6.041621	107.9286	1186.748	27.14005	1.941234	34.44921
102	11559.88	80.7275	6.070677	107.5169	1280.516	27.98692	2.021923	35.78429
103	11834.63	80.41065	6.106549	108.7871	1485.409	30.05222	2.228671	38.54101
104	11642.06	81.12582	6.120458	107.8984	1489.99	29.35748	2.257865	38.60038
105	12197.45	81.64355	6.208032	110.4421	1151.304	27.18147	1.940116	33.93087
106	11821.26	81.65841	6.177727	108.7256	2200.119	39.23472	2.896	46.90543
107	11835.41	80.89707	6.190419	108.7907	2551.223	38.50597	2.969786	50.50964
108	12247.89	81.79766	6.212924	110.6702	1065.724	25.10595	1.791046	32.64542
109	12101.78	81.33131	6.174579	110.0081	1218.828	29.13507	2.054044	34.91172
110	11769.22	80.19758	6.071659	108.4861	1792.716	35.84558	2.611732	42.34048
111	12482.1	81.85992	6.269865	111.7233	1052.016	24.85032	1.777541	32.43479
112	12247.27	81.42828	6.168074	110.6674	1077.432	25.6265	1.842145	32.82426
113	11166.96	79.89491	5.933844	105.6739	1472.693	29.77963	2.262267	38.37568

D

Propeller curves of bulk carrier case-study

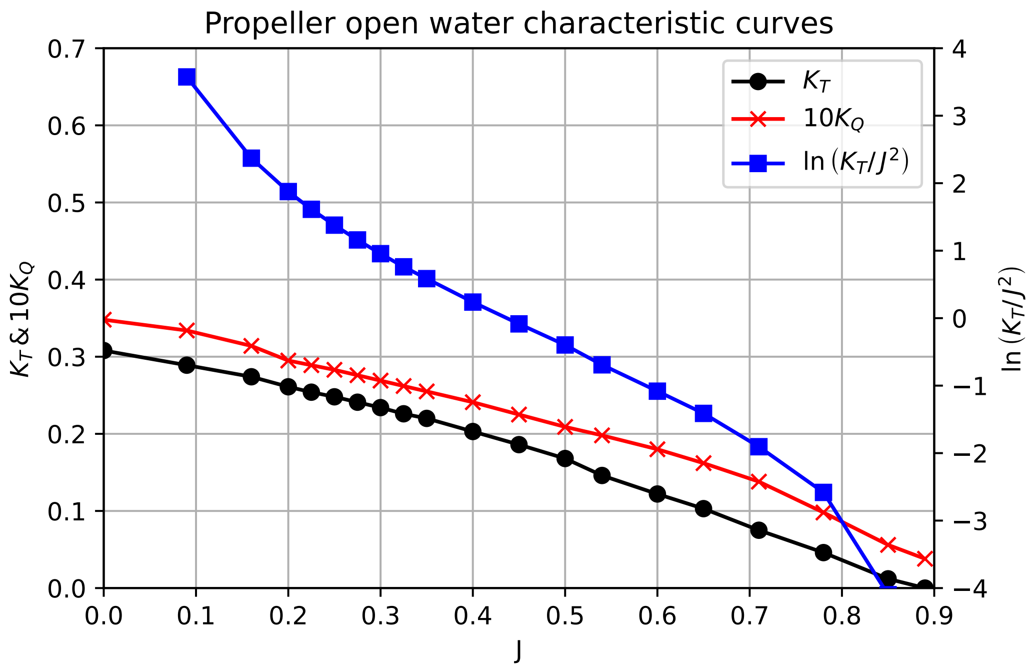

Figure D.1: Open water characteristics of the propeller used in the case-study

Bibliography

Abbas, F., et al. (2022). Master thesis: Vessel performance analysis using high frequency operational data.

Agarap, A. F. (2018). Deep Learning using Rectified Linear Units (ReLU). *arXiv e-prints*. https://doi.org/10.48550/arXiv.1803.08375

Agarwal, M. (2019, April). What is the speed of a ship at sea? https://www.marineinsight.com/guidelines/speed-of-a-ship-at-sea/

Ammar, N. R., & Seddiek, I. S. (2022). Wind assisted propulsion system onboard ships: Case study flettner rotors. *Ships and Offshore Structures*, *17*(7), 1616–1627. https://doi.org/10.1080/17445302.2021.1937797

An, H., Pan, H., & Yang, P. (2022). Research progress of air lubrication drag reduction technology for ships. *Fluids*, *7*(10), 319.

Andersen, I. (2013). Wind loads on post-panamax container ship. *Ocean Engineering*, *58*, 115–134. https://doi.org/10.1016/j.oceaneng.2012.10.008

Andrews, D. (2006). Simulation and the design building block approach in the design of ships and other complex systems. *Proceedings of the Royal Society A: Mathematical, Physical and Engineering Sciences*, *462*(2075), 3407–3433.

AnemoiMarine. (2023, October). Rotor sail technology - anemoi marine. https://anemoimarine.com/rotor-sail-technology/

Anish. (2021, October). What is noon report on ships and how is it prepared? https://www.marineinsight.com/guidelines/what-is-noon-report-on-ships/

Antai, E. E., & Williams, E. (2021). A study to investigate the option of applying a towing kite to an existing tanker vessel as a hybrid propulsion system. *International Research Journal of Modernization in Engineering Technology and Science*, *3*(04).

Aronietis, R., Sys, C., & Vanelslander, T. (2014). Ship retrofit solutions: Economic, energy and environmental impacts. *Soft Comput. Appl., Vol. One: Unified Eng. Concept*, *5*. https://doi.org/10.1201/b17517-8

Arrichiello, V., & Gualeni, P. (2020). Systems engineering and digital twin: A vision for the future of cruise ships design, production and operations. *International Journal on Interactive Design and Manufacturing (IJIDeM)*, *14*. https://doi.org/10.1007/s12008-019-00621-3

Atilhan, S., Park, S., El-Halwagi, M. M., Atilhan, M., Moore, M., & Nielsen, R. B. (2021). Green hydrogen as an alternative fuel for the shipping industry. *Current Opinion in Chemical Engineering*, *31*, 100668.

Autiosalo, J., Vepsäläinen, J., Viitala, R., & Tammi, K. (2019). A feature-based framework for structuring industrial digital twins. *IEEE access*, *8*, 1193–1208.

Bal Beşikçi, E., Arslan, O., Turan, O., & Ölçer, A. (2016). An artificial neural network based decision support system for energy efficient ship operations. *Computers Operations Research*, *66*, 393–401. https://www.sciencedirect.com/science/article/pii/S0305054815000842

Baldi, F., & Gabrielii, C. (2015). A feasibility analysis of waste heat recovery systems for marine applications. *Energy*, *80*, 654–665. https://doi.org/https://doi.org/10.1016/j.energy.2014.12.020

Bateman. (2019). Chapter 7 resistance and powering of ships. *United States Naval Academy*. https://pdf4pro.com/view/chapter-7-resistance-and-powering-of-ships-667e7d.html

Bentin, M., Kotzur, S., Schlaak, M., Zastrau, D., & Freye, D. (2018). Perspectives for a wind assisted ship propulsion. *International Journal of Maritime Engineering, Vol 160*. https://doi.org/10.3940/rina.ijme.2018.a1.439

Benvenuto, G., Campora, U., Laviola, M., & Terlizzi, G. (2017). Simulation model of a dual-fuel four stroke engine for low emission ship propulsion applications. *International Review of Mechanical Engineering (IREME)*, *11*(11). https://www.praiseworthyprize.org/jsm/index.php?journal=ireme&page=article&op=view&path%5C%5B%5C%5D=20493

Bockmann, M. (2022). Shipping emissions rise 4.9% in 2021. https://lloydslist.maritimeintelligence.informa.com/LL1139627/Shipping-emissions-rise-49-in-2021

Bordogna, G. (2020). Aerodynamics of wind-assisted ships : Interaction effects on the aerodynamic performance of multiple wind-propulsion systems. https://api.semanticscholar.org/CorpusID:213469716

Boulland, J. (2021, April). How infrastructure will lay the foundations for alternative fuels. https://marine-offshore.bureauveritas.com/insight/how-infrastructure-will-lay-foundations-alternative-fuels

Bouman, E. A., Lindstad, E., Rialland, A. I., & Strømman, A. H. (2017). State-of-the-art technologies, measures, and potential for reducing ghg emissions from shipping – a review. *Transportation Research Part D: Transport and Environment*, *52*, 408–421. https://www.sciencedirect.com/science/article/pii/S1361920916307015

Brenner, M., Zagkas, V., Harries, S., & Stein, T. (2013). Optimization using viscous flow computations for retrofitting ships in operation. http://hdl.handle.net/2117/332639

Breslin, J. P., & Andersen, P. (1994). *Hydrodynamics of ship propellers*. Cambridge university press.

Brownlee, J. (2021, January). Gentle introduction to the adam optimization algorithm for deep learning. https://machinelearningmastery.com/adam-optimization-algorithm-for-deep-learning/

Brunton, S. L., & Kutz, J. N. (2022). *Data-driven science and engineering: Machine learning, dynamical systems, and control*. Cambridge University Press.

Bucci, V., Sulligoi, G., Chalfant, J., & Chryssostomidis, C. (2021). Evolution in design methodology for complex electric ships. *Journal of Ship Production and Design*, *37*, 1–13. https://doi.org/10.5957/JSPD.08190045

Carl Fredrik, R. (2018). *Ship design under uncertainty* [Doctoral dissertation, NTNU]. http://hdl.handle.net/11250/2563319

Carney, J., Cunningham, P., & Bhagwan, U. (1999). Confidence and prediction intervals for neural network ensembles. *IJCNN'99. International Joint Conference on Neural Networks. Proceedings (Cat. No.99CH36339)*, *2*, 1215–1218 vol.2. https://doi.org/10.1109/IJCNN.1999.831133

Chen, B., Wan, J., Celesti, A., Li, D., Abbas, H., & Zhang, Q. (2018). Edge computing in iot-based manufacturing. *IEEE Communications Magazine*, *56*(9), 103–109. https://doi.org/10.1109/MCOM.2018.1701231

Chirica, I., Presura, A., & Angheluta, C. (2019). Retrofit solutions for green and efficient inland ships. *Journal of Physics: Conference Series*, *1297*, 012009. https://doi.org/10.1088/1742-6596/1297/1/012009

Chou, T., Kosmas, V., Acciaro, M., & Renken, K. (2021). A comeback of wind power in shipping: An economic and operational review on the wind-assisted ship propulsion technology. *Sustainability*, *13*(4), 1880.

Cong, Y., Gan, H., & Wang, H. (2022). Parameter investigation of the pilot fuel post-injection strategy on performance and emissions characteristics of a large marine two-stroke natural gas-diesel dual-fuel engine. *Fuel*, *323*, 124404. https://www.sciencedirect.com/science/article/pii/S001623612201256X

Container XChange. (2019, October). https://www.container-xchange.com/blog/5-green-shipping-initiatives-reduce-ghg/

Container XChange. (2020, January). What is big data in the shipping industry? https://www.container-xchange.com/blog/big-data-in-shipping/

Coraddu, A., Oneto, L., Baldi, F., & Anguita, D. (2015). Ship efficiency forecast based on sensors data collection: Improving numerical models through data analytics. *OCEANS 2015 - Genova*, 1–10. https://doi.org/10.1109/OCEANS-Genova.2015.7271412

Coraddu, A., Oneto, L., Baldi, F., Cipollini, F., Atlar, M., & Savio, S. (2019). Data-driven ship digital twin for estimating the speed loss caused by the marine fouling. *Ocean Engineering*, *186*. https://doi.org/10.1016/j.oceaneng.2019.05.045

Dadd, G. M. (2013). Kite dynamics for ship propulsion. https://api.semanticscholar.org/CorpusID:106836686

Dairi, A., Cheng, T., Harrou, F., Sun, Y., & Leiknes, T. (2019). Deep learning approach for sustainable wwtp operation: A case study on data-driven influent conditions monitoring. *Sustainable Cities and Society*, *50*, 101670.

da Silva, I. N., Spatti, D. H., Flauzino, R. A., Liboni, L. H. B., & dos Reis Alves, S. F. (2017). *Artificial neural networks - a practical course*. Springer International Publishing. https://books.google.nl/books?id=DL_mDAAAQBAJ

de Kat, J., & Mouawad, J. (2019). Green ship technologies. *Sustainable Shipping*.

Demo, N., Tezzele, M., Mola, A., & Rozza, G. (2021). Hull shape design optimization with parameter space and model reductions, and self-learning mesh morphing. *Journal of Marine Science and Engineering*, *9*(2). https://doi.org/10.3390/jmse9020185

DT4GS. (2022, April). https://dt4gs.eu/

Du, Y., Meng, Q., Wang, S., & Kuang, H. (2019). Two-phase optimal solutions for ship speed and trim optimization over a voyage using voyage report data. *Transportation Research Part B: Methodological*, *122*, 88–114. https://www.sciencedirect.com/science/article/pii/S0191261517305738

Duan, Y., Shen, X., & Wang, H. (2023). Dual-branch time–frequency domain anti-interference method for ship radiated noise signal. *Ocean Engineering*, *279*. https://doi.org/10.1016/j.oceaneng.2023.114537

EC. (2015a). Paris agreement. https://climate.ec.europa.eu/eu-action/international-action-climate-change/climate-negotiations/paris-agreement_en

EC. (2015b). Retrofit (retrofitting ships with new technologies for improved overall environmental footprint). https://cordis.europa.eu/project/id/285420/reporting

EC. (2021a). A european green deal. https://commission.europa.eu/strategy-and-policy/priorities-2019-2024/european-green-deal_en

EC. (2021b). Reducing emissions from the shipping sector. https://climate.ec.europa.eu/eu-action/transport-emissions/reducing-emissions-shipping-sector_en

EC. (2023). Fourth annual report from the european commission on co2 emissions from maritime transport (period 2018-2021). https://climate.ec.europa.eu/system/files/2023-03/swd_2023_54_en.pdf

Ehmer, M., & Khan, F. (2012). A comparative study of white box, black box and grey box testing techniques. *International Journal of Advanced Computer Science and Applications*, *3*. https://doi.org/10.14569/IJACSA.2012.030603

Elvekrok, D. R. (1997). Concurrent engineering in ship design. *Journal of Ship Production*, *13*(4), 258–269. https://doi.org/10.5957/JSP.1997.13.4.258

EMSA. (2023, November). New study: Potential of Wind-Assisted Propulsion for Shipping. https://www.emsa.europa.eu/newsroom/latest-news/item/5079-new-study-potential-of-wind-assisted-propulsion-for-shipping.html

Endresen, Ø., Sørgård, E., Behrens, H. L., Brett, P. O., & Isaksen, I. S. A. (2007). A historical reconstruction of ships' fuel consumption and emissions. *Journal of Geophysical Research: Atmospheres*, *112*(D12). https://agupubs.onlinelibrary.wiley.com/doi/abs/10.1029/2006JD007630

Erikstad, S. (2017). Merging physics, big data analytics and simulation for the next-generation digital twins.

Estefan, J. A., et al. (2007). Survey of model-based systems engineering (mbse) methodologies. *Incose MBSE Focus Group*, *25*(8), 1–12.

Evans, J. H. (1959). Basic design concepts. *Journal of the American Society for Naval Engineers*, *71*(4), 671–678. https://onlinelibrary.wiley.com/doi/abs/10.1111/j.1559-3584.1959.tb01836.x

Fafoutellis, P., Mantouka, E. G., & Vlahogianni, E. I. (2020). Eco-driving and its impacts on fuel efficiency: An overview of technologies and data-driven methods. *Sustainability*, *13*(1), 226. https://doi.org/10.3390/su13010226

Fam, M. L., Tay, Z. Y., & Konovessis, D. (2022). An artificial neural network for fuel efficiency analysis for cargo vessel operation. *Ocean Engineering*, *264*, 112437. https://www.sciencedirect.com/science/article/pii/S002980182201719X

Fan, A., Yan, X., Bucknall, R., Yin, Q., Ji, S., Liu, Y., Song, R., & Chen, X. (2020). A novel ship energy efficiency model considering random environmental parameters. *Journal of Marine Engineering & Technology*, *19*(4), 215–228. https://doi.org/10.1080/20464177.2018.1546644

Fan, A., Yang, J., Yang, L., Wu, D., & Vladimir, N. (2022). A review of ship fuel consumption models. *Ocean Engineering*, *264*, 112405. https://www.sciencedirect.com/science/article/pii/S0029801822016936

Feng, S., Xu, S., Yuan, P., Xing, Y., Shen, B., Li, Z., Zhang, C., Wang, X., Wang, Z., Ma, J., & Kong, W. (2022). The impact of alternative fuels on ship engine emissions and aftertreatment systems: A review. *Catalysts*, *12*(2), 138. https://doi.org/10.3390/catal12020138

Fitzgerald, M. E., & Ross, A. M. (2019). Artificial intelligence analytics with multi-attribute tradespace exploration and set-based design [17th Annual Conference on Systems Engineering Research (CSER)]. *Procedia Computer Science*, *153*, 27–36. https://www.sciencedirect.com/science/article/pii/S1877050919307112

Fitzpatrick, P., Jang, J., Kim, B., Kim, J., Lee, J., McStay, P., & Raptakis, G. (2017). Full scale applications of air lubrication for reduction of ship frictional resistance. *SNAME Maritime Convention*.

Foretich, A., Zaimes, G. G., Hawkins, T. R., & Newes, E. (2021). Challenges and opportunities for alternative fuels in the maritime sector. *Maritime Transport Research*, *2*, 100033. https://www.sciencedirect.com/science/article/pii/S2666822X21000241

Fritz, F. (2013). Application of an automated kite system for ship propulsion and power generation. In U. Ahrens, M. Diehl, & R. Schmehl (Eds.), *Airborne wind energy* (pp. 359–372). Springer Berlin Heidelberg. https://doi.org/10.1007/978-3-642-39965-7_20

Gaggero, S., Vernengo, G., & Villa, D. (2022). A marine propeller design method based on two-fidelity data levels. *Applied Ocean Research*, *123*, 103156. https://www.sciencedirect.com/science/article/pii/S0141118722001031

Gao, T., Wang, Y., Pang, Y., & Cao, J. (2016). Hull shape optimization for autonomous underwater vehicles using cfd. *Engineering applications of computational fluid mechanics*, *10*(1), 599–607.

García, S., Ramírez-Gallego, S., Luengo, J., Benítez, J. M., & Herrera, F. (2016). Big data preprocessing: Methods and prospects. *Big Data Analytics*, *1*(1), 1–22.

gCaptain. (2012). Floating on air – dk group receives first order for air cavity system. https://gcaptain.com/floating-group-receives-order/

Giering, J.-E., & Dyck, A. (2021). Maritime digital twin architecture: A concept for holistic digital twin application for shipbuilding and shipping. *at-Automatisierungstechnik*, *69*(12), 1081–1095.

Giernalczyk, M., & Kaminski, P. (2021). Assessment of the propulsion system operation of the ships equipped with the air lubrication system. *Sensors*, *21*(4), 1357. https://doi.org/10.3390/s21041357

Gilbert, P., Walsh, C., Traut, M., Kesieme, U., Pazouki, K., & Murphy, A. (2018). Assessment of full life-cycle air emissions of alternative shipping fuels. *Journal of Cleaner Production*, *172*, 855–866. https://www.sciencedirect.com/science/article/pii/S0959652617324721

GloMEEP. (2019). Kite. https://glomeep.imo.org/technology/kite/

Grieves, M. (2014). Digital twin: Manufacturing excellence through virtual factory replication. *White paper*, *1*(2014), 1–7.

Grieves, M. (2019). Virtually intelligent product systems: Digital and physical twins. *Complex Systems Engineering: Theory and Practice*, *1*, 175–200.

Hall, N. (2023, November). Shape effects on drag. https://www1.grc.nasa.gov/beginners-guide-to-aeronautics/shape-effects-on-drag/

Haranen, M., Pakkanen, P., Kariranta, R., & Salo, J. (2016). White, grey and black-box modelling in ship performance evaluation.

Hirdaris, S., & Cheng, Y. (2012). The role of technology in green ship design. https://doi.org/10.13140/RG.2.1.4242.0564

Hochberg, M. (2020, April). The story of how royal caribbean cut a cruise ship in half and lengthened it. https://www.royalcaribbeanblog.com/2020/04/22/the-story-of-how-royal-caribbean-cut-cruise-ship-half-and-lengthened-it

Hochkirch, K., & Bertram, V. (2010). Engineering options for more fuel efficient ships. *Proceedings of First International Symposium on Fishing Vessel Energy Efficiency*, *1*.

Hochkirch, K., Heimann, J., & Bertram, V. (2013). Hull optimization for operational profile – the next game level. In *Marine v : Proceedings of the v international conference on computational methods in marine engineering* (pp. 81–88). CIMNE. http://hdl.handle.net/2117/332640

Holtrop, J., & Mennen, G. (1982). An approximate power prediction method. *International Shipbuilding Progress*, *29*(335), 166–170.

Hsu, S. A., Meindl, E. A., & Gilhousen, D. B. (1994). Determining the power-law wind-profile exponent under near-neutral stability conditions at sea. *Journal of Applied Meteorology and Climatology*, *33*(6), 757–765. https://journals.ametsoc.org/view/journals/apme/33/6/1520-0450_1994_033_0757_dtplwp_2_0_co_2.xml

Hu, Z., Jin, Y., Hu, Q., Sen, S., Zhou, T., & Osman, M. T. (2019). Prediction of fuel consumption for enroute ship based on machine learning. *IEEE Access*, *7*, 119497–119505. https://doi.org/10.1109/ACCESS.2019.2933630

Huang, D. (2013). Speciality english for fundamentals and concepts in shipbuilding engineering. *National Defense Industry Press, Beijing*.

Huang, L., Pena, B., Liu, Y., & Anderlini, E. (2022). Machine learning in sustainable ship design and operation: A review. *Ocean Engineering*, *266*, 112907. https://www.sciencedirect.com/science/article/pii/S0029801822021904

IMO. (2009). Guidelines for voluntary use of the ship energy efficiency operational indicator (eeoi). https://gmn.imo.org/wp-content/uploads/2017/05/Circ-684-EEOI-Guidelines.pdf

IMO. (2018). Imo's work to cut ghg emissions from ships. https://www.imo.org/en/MediaCentre/HotTopics/Pages/Cutting-GHG-emissions.aspx

IMO. (2021). 2021 guidance on treatment of innovative energy efficiency technologies for calculation and verification of the attained eedi and eex. https://wwwcdn.imo.org/localresources/en/OurWork/Environment/Documents/Air%20pollution/MEPC.1-Circ.896.pdf

IMO. (2022a). 2022 guidelines on the operational carbon intensity rating of ships (cii rating guidelines, g4). https://wwwcdn.imo.org/localresources/en/OurWork/Environment/Documents/Air%20pollution/MEPC.354(78).pdf

IMO. (2022b). Improving the energy efficiency of ships. https://www.imo.org/en/OurWork/Environment/Pages/Improving%20the%20energy%20efficiency%20of%20ships.aspx

IMO. (2023a). 2023 imo strategy on reduction of ghg emissions from ships. https://www.imo.org/en/OurWork/Environment/Pages/2023-IMO-Strategy-on-Reduction-of-GHG-Emissions-from-Ships.aspx

IMO. (2023b). Imo data collection system (dcs). https://www.imo.org/en/ourwork/environment/pages/data-collection-system.aspx

IMO. (2023c). Reduction of ghg emissions from ships - wind propulsion technologies as a key enabler. https://www.wind-ship.org/wp-content/uploads/2023/05/MEPC-80-INF.33-Wind-propulsion-technologies-as-a-key-enabler-RINA-and-IWSA-1.pdf

ITTC. (2011). *Fresh water and seawater properties*. https://www.ittc.info/media/7989/75-02-01-03.pdf

ITTC. (2021). *Preparation, conduct and analysis of speed/power trials*. https://www.ittc.info/media/9874/75-04-01-011.pdf

Jones, D., Snider, C., Nassehi, A., Yon, J., & Hicks, B. (2020). Characterising the digital twin: A systematic literature review. *CIRP Journal of Manufacturing Science and Technology*, *29*, 36–52. https://www.sciencedirect.com/science/article/pii/S1755581720300110

Kamath, Y., Sivaprasad, K., & Jayaram, S. (2019). Application of computing technology in ship recycling. *RINA, Royal Institution of Naval Architects - 19th International Conference on Computer Applications in Shipbuilding*.

Kawakita, C., Sato, S., & Okimoto, T. (2015). Application of simulation technology to mitsubishi air lubrication system. *Mitsubishi Heavy Industries Technical Review*, *52*(1), 50–56.

Keras. (2023). Keras documentation: About keras 3. https://keras.io/about/

Kesieme, U., Pazouki, K., Murphy, A., & Chrysanthou, A. (2019). Biofuel as an alternative shipping fuel: Technological, environmental and economic assessment. *Sustainable Energy & Fuels*, *3*(4), 899–909.

Kim, H., Koo, K. Y., & Joung, T.-H. (2020). A study on the necessity of integrated evaluation of alternative marine fuels. *Journal of International Maritime Safety, Environmental Affairs, and Shipping*, *4*(2), 26–31. https://doi.org/10.1080/25725084.2020.1779426

Kim, H., & Yang, C. (2010). A new surface modification approach for cfd-based hull form optimization. *Journal of Hydrodynamics*, *22*(1), 503–508.

Kim, M., & Park, D.-W. (2015). A study on the green ship design for ultra large container ship. *Journal of the Korean Society of Marine Environment Safety*, *21*(5), 558–570.

Kingma, D. P., & Ba, J. (2017). Adam: A method for stochastic optimization.

Kiran, D. (2022). Chapter twenty-two - machinery replacement analysis. In D. Kiran (Ed.), *Principles of economics and management for manufacturing engineering* (pp. 259–267). Butterworth-Heinemann. https://www.sciencedirect.com/science/article/pii/B9780323998628000029

Klein Woud, J., & Stapersma, D. (2002). *Design of propulsion and electric power generation systems*. IMarEST.

Kondratenko, A. A., Kujala, P., & Hirdaris, S. E. (2023). Holistic and sustainable design optimization of arctic ships. *Ocean Engineering*, *275*, 114095. https://www.sciencedirect.com/science/article/pii/S0029801823004791

Kooij, E. (2022). *Systems modeling in the naval domain* [Master's thesis, TU Delft]. http://resolver.tudelft.nl/uuid:2b291a7c-886d-49bc-8806-c9515e4a2a23

Kritzinger, W., Karner, M., Traar, G., Henjes, J., & Sihn, W. (2018). Digital twin in manufacturing: A categorical literature review and classification [16th IFAC Symposium on Information Control Problems in Manufacturing INCOM 2018]. *IFAC-PapersOnLine*, *51*(11), 1016–1022. https://www.sciencedirect.com/science/article/pii/S2405896318316021

Lai, K.-H., Lun, V. Y., Wong, C. W., & Cheng, T. C. E. (2011). Green shipping practices in the shipping industry: Conceptualization, adoption, and implications. *Resources, Conservation and Recycling*, *55*(6), 631–638.

Land, I. (2022, November). How digital twins are transforming aerospace and defense. https://blogs.synopsys.com/from-silicon-to-software/2022/10/19/digital-twins-aerospace-defense-government

Leaper, R., Renilson, M., & Ryan, C. (2014). Reducing underwater noise from large commercial ships: Current status and future directions. *Journal of Ocean Technology*, *9*, 65–83.

Leifsson, L. Þ., Sævarsdóttir, H., Sigurðsson, S. Þ., & Vésteinsson, A. (2008). Grey-box modeling of an ocean vessel for operational optimization [EUROSIM 2007]. *Simulation Modelling Practice and Theory*, *16*(8), 923–932. https://www.sciencedirect.com/science/article/pii/S1569190X08000488

Li, B., Lv, J., Deng, F., Cui, Y., & Zhang, B. (2023). The energy recovery effect of wave energy utilization system under the rolling motion of ships. *Journal of Waterway, Port, Coastal, and Ocean Engineering*, *149*(2), 04022030.

Li, W. (2023). *Application of digital twins in the design of new green transport vessels* [Master's thesis, TU Delft]. http://resolver.tudelft.nl/uuid:728e8857-1c6d-444d-a1af-06c710095056

Lindstad, E., Stokke, T., Alteskjær, A., Borgen, H., & Sandaas, I. (2022). Ship of the future – a slender dry-bulker with wind assisted propulsion. *Maritime Transport Research*, *3*, 100055. https://doi.org/10.1016/j.martra.2022.100055

Liu, J., & Hekkenberg, R. (2017). Sixty years of research on ship rudders: Effects of design choices on rudder performance. *Ships and offshore structures*, *12*(4), 495–512.

Liu, M., Fang, S., Dong, H., & Xu, C. (2021). Review of digital twin about concepts, technologies, and industrial applications [Digital Twin towards Smart Manufacturing and Industry 4.0]. *Journal of Manufacturing Systems*, *58*, 346–361. https://www.sciencedirect.com/science/article/pii/S0278612520301072

Lo, C., Chen, C., & Zhong, R. Y. (2021). A review of digital twin in product design and development. *Advanced Engineering Informatics*, *48*, 101297. https://www.sciencedirect.com/science/article/pii/S1474034621000513

Lu, R., & Ringsberg, J. W. (2020). Ship energy performance study of three wind-assisted ship propulsion technologies including a parametric study of the flettner rotor technology. *Ships and Offshore Structures*, *15*(3), 249–258. https://doi.org/10.1080/17445302.2019.1612544

Maimun, A., Khairuddin, J., & Siow, C. (2019). Review of systems engineering methods, techniques and tools for ship design as large and complex systems.

MAN. (2018). Basic principles of ship propulsion. https://www.man-es.com/docs/default-source/document-sync/basic-principles-of-ship-propulsion-eng.pdf

Mancini, S., De Marco, A., Pensa, C., Calise, G., & De Luca, F. (2016). Flettner rotor concept for marine applications: A systematic study. *International Journal of Rotating Machinery*, *2016*, 12. https://doi.org/10.1155/2016/3458750

Marine Digital. (2020). Data analytics in maritime/shipping. https://marine-digital.com/article_data_analytics_in_maritime

Matsui, S. (2022). A new mathematical hull-form with 10-shape parameters for evaluation of ship response in waves. *Journal of Marine Science and Technology*, *27*(1), 508–521.

Mauro, F., & Kana, A. (2023). Digital twin for ship life-cycle: A critical systematic review. *Ocean Engineering*, *269*, 113479. https://doi.org/10.1016/j.oceaneng.2022.113479

Mewis, F., & Deichmann, F. (2013). Power-and cost-savings for container vessels by hydrodynamic energy saving devices. *Proceedings of the 4th International Ship Efficiency Conference, Hamburg Germany*.

Mjalli, F. S., Al-Asheh, S., & Alfadala, H. (2007). Use of artificial neural network black-box modeling for the prediction of wastewater treatment plants performance. *Journal of Environmental Management*, *83*(3), 329–338. https://www.sciencedirect.com/science/article/pii/S0301479706001228

Montáns, F. J., Chinesta, F., Gómez-Bombarelli, R., & Kutz, J. N. (2019). Data-driven modeling and learning in science and engineering [Data-Based Engineering Science and Technology]. *Comptes Rendus Mécanique*, *347*(11), 845–855. https://www.sciencedirect.com/science/article/pii/S1631072119301809

Moore, R. (2018, April). Grimaldi ferries to undergo lengthening and battery refits. https://www.rivieramm.com/news-content-hub/news-content-hub/grimaldi-ferries-to-undergo-lengthening-and-battery-refits-25242

Mosedale, E. (2020, July). Is the ship design spiral holding you back? https://blogs.sw.siemens.com/simcenter/ship-design-spiral-simcenter/

Mouzakitis, S., Kontzinos, C., Tsapelas, J., Kanellou, I., Kormpakis, G., Kapsalis, P., & Askounis, D. (2023, September). Enabling maritime digitalization by extreme-scale analytics, ai and digital twins: The vesselai architecture. https://doi.org/10.1007/978-3-031-16075-2_16

Naaijen, P., Koster, V., & Dallinga, R. (2006). On the power savings by an auxiliary kite propulsion system. *International Shipbuilding Progress*, *53*, 255–279.

Natsume, Y. (2021, December). Gaussian process models. https://towardsdatascience.com/gaussian-process-models-7ebce1feb83d

Ni, B., & Zeng, L. (2019). Ship design process. In W. Cui, S. Fu, & Z. Hu (Eds.), *Encyclopedia of ocean engineering* (pp. 1–8). Springer Singapore. https://doi.org/10.1007/978-981-10-6963-5_36-1

Nikolopoulos, L., & Boulougouris, E. (2020). A novel method for the holistic, simulation driven ship design optimization under uncertainty in the big data era. *Ocean Engineering*, *218*, 107634. https://www.sciencedirect.com/science/article/pii/S002980182030634X

Nissen, P. (1989). Retrofitting of ccg icebreaker louis s. st. laurent.

Noor, C. M., Noor, M., & Mamat, R. (2018). Biodiesel as alternative fuel for marine diesel engine applications: A review. *renewable and sustainable energy reviews*, *94*, 127–142.

Norsepower. (2023). Norsepower rotor sail™. https://www.norsepower.com/technical-info/

Nowacki, H. (2010). Five decades of computer-aided ship design [Computer aided ship design: Some recent results and steps ahead in theory, methodology and practice]. *Computer-Aided Design*, *42*(11), 956–969. https://www.sciencedirect.com/science/article/pii/S0010448509001985

NSRSAIL. (2015). Factsheet flettner freighter. https://www.nsrsail.eu/

Pan, P., Sun, Y., Yuan, C., Yan, X., & Tang, X. (2021). Research progress on ship power systems integrated with new energy sources: A review. *Renewable and Sustainable Energy Reviews*, *144*, 111048.

Papanikolaou, A. (2002). Developments and potential of advanced marine vehicles concepts. *Bulletin of the KANSAI Society of Naval Architects, Japan*, *55*, 50–54.

Papanikolaou, A. (2010). Holistic ship design optimization [Computer aided ship design: Some recent results and steps ahead in theory, methodology and practice]. *Computer-Aided Design*, *42*(11), 1028–1044. https://www.sciencedirect.com/science/article/pii/S0010448509001973

Papanikolaou, A. (2014, September). *Ship design - methodologies of preliminary design*. https://doi.org/10.1007/978-94-017-8751-2

Papanikolaou, A. (2019). *A holistic approach to ship design* (Vol. 1). Springer.

Park, S., Cho, J., Park, J., & Song, S. (2017). Numerical study of the performance and nox emission of a diesel-methanol dual-fuel engine using multi-objective pareto optimization. *Energy*, *124*, 272–283. https://www.sciencedirect.com/science/article/pii/S0360544217302037

Park, Y.-S., & Lek, S. (2016). Chapter 7 - artificial neural networks: Multilayer perceptron for ecological modeling. In S. E. Jørgensen (Ed.), *Ecological model types* (pp. 123–140, Vol. 28). Elsevier. https://www.sciencedirect.com/science/article/pii/B9780444636232000074

Parkes, A., Sobey, A., & Hudson, D. (2018). Physics-based shaft power prediction for large merchant ships using neural networks. *Ocean Engineering*, *166*. https://doi.org/10.1016/j.oceaneng.2018.07.060

Patzer, D. (2021, April). Machine learning a systems engineering perspective. https://towardsdatascience.com/machine-learning-a-systems-engineering-perspective-1be9d13040e7

Pavlov, G. A., Yun, L., Bliault, A., & He, S.-L. (2020). *Air lubricated and air cavity ships*. Springer.

Pedersen, B. P., & Larsen, J. (2009). Modeling of ship propulsion performance. *World Maritime Technology Conference WMTC2009*.

Pedersen, B., & Larsen, J. (2009). Prediction of full-scale propulsion power using artificial neural networks [Prediction of Full-Scale Propulsion Power using Artificial Neural Networks ; Conference date: 01-01-2009]. *COMPIT '09*, 537–550.

Perera, L., & Mo, B. (2016). Emission control based energy efficiency measures in ship operations. *Applied Ocean Research*, *60*, 29–46. https://doi.org/10.1016/j.apor.2016.08.006

Pérez Fernández, R. (2021). What the shipbuilding future holds in terms of cad/cam/cim systems. https://doi.org/10.5957/SOME-2021-004

Peri, D., Rossetti, M., & Campana, E. F. (2001). Design optimization of ship hulls via cfd techniques. *Journal of ship research*, *45*(02), 140–149.

Perkins, T., Dijkstra, G., & Roberts, D. (2004). The maltese falcon: The realization [Paper: P2004-6 Proceedings]. *Proceedings of the HISWA Symposium 2004*. http://resolver.tudelft.nl/uuid:c4aab97b-1fd7-4598-8c0b-845b799209b3

Petersen, J., Jacobsen, D., & Winther, O. (2012). Statistical modelling for ship propulsion efficiency. *Journal of Marine Science and Technology*, *17*(1), 30–39. https://doi.org/10.1007/s00773-011-0151-0

Prins, H., Flikkema, M., Schuiling, B., Xing-Kaeding, Y., Voermans, A., Müller, M., Coache, S., Hasselaar, T., & Paboeuf, S. (2016). Green retrofitting through optimisation of hull-propulsion interaction – grip [Transport Research Arena TRA2016]. *Transportation Research Procedia*, *14*, 1591–1600. https://www.sciencedirect.com/science/article/pii/S2352146516301259

Rachmatullah, M. I. C., Santoso, J., & Surendro, K. (2021). Determining the number of hidden layer and hidden neuron of neural network for wind speed prediction. *PeerJ Computer Science*, *7*, e724. https://doi.org/10.7717/peerj-cs.724

Radonjic, A., & Vukadinovic, K. (2014). Application of ensemble neural networks to prediction of towboat shaft power. *Journal of Marine Science and Technology*, *20*. https://doi.org/10.1007/s00773-014-0273-2

Radosavljevic, D. (2022). Simulation-driven ship design. *DIGITAL INDUSTRIES SOFTWARE*. https://static.sw.cdn.siemens.com/siemens-disw-assets/public/6LguukHruu2cXE5J67D5kb/en-US/Siemens%20SW%20Simulation%20driven%20ship%20design%20White%20Paper.pdf

Reche-Vilanova, M., Hansen, H., & Bingham, H. B. (2021). Performance Prediction Program for Wind-Assisted Cargo Ships. *Journal of Sailing Technology*, *6*(01), 91–117. https://doi.org/10.5957/jst/2021.6.1.91

Reinhold, K., Järvis, M., & Prause, G. (2019). Occupational health and safety aspects of green shipping in the baltic sea. *Entrepreneurship and Sustainability Issues*, *7*, 10–24. https://doi.org/10.9770/jesi.2019.7.1(1)

RINA. (2020). What does it mean to be a retrofit ship of the future? *Naval Architect*, *2020-August*(August), 41–43. https://www.scopus.com/inward/record.uri?eid=2-s2.0-85096160506&partnerID=40&md5=8b3b8d2a8dad2b7d82b0bf83c9155b48

Ritari, A., Huotari, J., & Tammi, K. (2023). Marine vessel powertrain design optimization: Multiperiod modeling considering retrofits and alternative fuels. *Proceedings of the Institution of Mechanical Engineers, Part M: Journal of Engineering for the Maritime Environment*, 14750902221145747. https://doi.org/10.1177/14750902221145747

Rosebrock, A. (2022, January). Why is my validation loss lower than my training loss? https://pyimagesearch.com/2019/10/14/why-is-my-validation-loss-lower-than-my-training-loss/

Rudzki, K., & Tarelko, W. (2016). A decision-making system supporting selection of commanded outputs for a ship's propulsion system with a controllable pitch propeller. *Ocean Engineering*, *126*, 254–264. https://www.sciencedirect.com/science/article/pii/S002980181630395X

Rutkowski, G. (2016). Study of green shipping technologies-harnessing wind, waves and solar power in new generation marine propulsion systems. *TransNav: International Journal on Marine Navigation and Safety of Sea Transportation*, *10*(4), 627–632.

Saber. (2022). Saber for automotive systems. https://www.synopsys.com/verification/virtual-prototyping/saber/saber-automotive-systems.html

Sánchez-Sotano, A., Cerezo-Narváez, A., Abad-Fraga, F., Pastor-Fernández, A., & Salguero-Gómez, J. (2020). Trends of digital transformation in the shipbuilding sector. In *New trends in the use of artificial intelligence for the industry 4.0*. IntechOpen.

Sapkota, M. S., Apeh, E., Hadfield, M., Haratian, R., & Adey, J., Robert amd Baynham. (2021). An approach for adaptive model performance validation within digital twinning. *Internation Journal of Computational Methods and Experimental Measurements*, *9*(3), 213–225.

Schuler, M. (2015, July). World's first 'widened' containership re-enters service – ship photos of the day. https://gcaptain.com/worlds-first-widened-containership-re-enters-service-ship-photos-of-the-day

Sedgwick, P. (2014). Spearman's rank correlation coefficient. *Bmj*, *349*.

Shafto, M., Conroy, M., Doyle, R., Glaessgen, E., Kemp, C., LeMoigne, J., & Wang, L. (2010). Modeling, simulation, information technology and processing roadmap.

Sherbaz, S., & Duan, W. (2012a). Operational options for green ships. *Journal of Marine Science and Application*, *11*(3), 335–340.

Sherbaz, S., & Duan, W. (2012b). Propeller efficiency options for green ship. *Proceedings of 2012 9th International Bhurban Conference on Applied Sciences Technology (IBCAST)*, 155–161. https://doi.org/10.1109/IBCAST.2012.6177547

Shevchenko, N. (2020, December). An introduction to model-based systems engineering (mbse). https://insights.sei.cmu.edu/blog/introduction-model-based-systems-engineering-mbse/

Shi, W., Xiao, Y., Chen, Z., McLaughlin, H., & Li, K. X. (2018). Evolution of green shipping research: Themes and methods. *Maritime Policy & Management*, *45*(7), 863–876.

Sinay. (2022, April). What are 7 types of cargo ships? https://sinay.ai/en/what-are-7-types-of-cargo-ships/

Singer, D., Doerry, N., & BUCKLEY, M. (2009). What is set-based design? *Naval Engineers Journal*, *121*, 31–43. https://doi.org/10.1111/j.1559-3584.2009.00226.x

Skulstad, R., Li, G., Fossen, T. I., & Zhang, H. (2023). Constrained control allocation for dynamic ship positioning using deep neural network [All Open Access, Hybrid Gold Open Access]. *Ocean Engineering*, *279*. https://doi.org/10.1016/j.oceaneng.2023.114434

Smith, T., Newton, P., Winn, G., & Grech La Rosa, A. (2013). Analysis techniques for evaluating the fuel savings associated with wind assistance.

Spinelli, F., Mancini, S., Vitiello, L., Bilandi, R. N., & De Carlini, M. (2022). Shipping decarbonization: An overview of the different stern hydrodynamic energy saving devices. *Journal of Marine Science and Engineering*, *10*(5), 574.

Stachowski, T., & Kjeilen, H. (2017). Holistic ship design – how to utilise a digital twin in concept design through basic and detailed design. *International Conference on Computer Applications in Shipbuilding*.

Stark, C., Xu, Y., Zhang, M., Yuan, Z., Tao, L., & Shi, W. (2022). Study on applicability of energy-saving devices to hydrogen fuel cell-powered ships. *Journal of Marine Science and Engineering*, *10*(3). https://doi.org/10.3390/jmse10030388

Statista. (2021). *Energy density of maritime fuels in 2020, by fuel type (in megajoule per liter) [graph]*. Statista. https://www.statista.com/statistics/1279431/energy-density-of-maritime-fuels/

Sun, W., Liu, X., Zheng, A., Wei, J., & Chen, J. (2022). A data-driven strategy model to incorporate expertise experience in hull form design and optimization. *ISOPE International Ocean and Polar Engineering Conference*, ISOPE–I.

Sun, X. (2015). Research on operational energy efficiency for inland river ships with involvement of navigation environment. *China: Wuhan University of Technology*.

Sun, X., Ning, J., Liang, X., Jing, G., Chen, Y., & Chen, G. (2022). Effect of direct water injection on combustion and emissions characteristics of marine diesel engines. *Fuel*, *309*, 122213. https://www.sciencedirect.com/science/article/pii/S0016236121020883

Sunaryo, S., & Pahalatua, D. (2015). Green ship recycle yard design. *Journal of Naval Architecture and Marine Engineering*, *12*(1), 15–20.

Swider, A., Wang, Y., & Pedersen, E. (2018). Data-driven vessel operational profile based on t-sne and hierarchical clustering. *OCEANS 2018 MTS/IEEE Charleston*, 1–7.

Tadros, M., Ventura, M., & Guedes Soares, C. Numerical simulation of a two-stroke marine diesel engine. In: 2015, 609–617. https://doi.org/10.1201/b18855-80

Tadros, M., Ventura, M., & Soares, C. G. (2023). Review of current regulations, available technologies, and future trends in the green shipping industry. *Ocean Engineering*, *280*, 114670.

Tadros, M., Ventura, M., & Guedes Soares, C. (2021). Design of propeller series optimizing fuel consumption and propeller efficiency. *Journal of Marine Science and Engineering*, *9*(11), 1226. https://doi.org/10.3390/jmse9111226

Tao, F., Cheng, J., Qi, Q., Zhang, M., Zhang, H., & Sui, F. (2018). Digital twin-driven product design, manufacturing and service with big data. *The International Journal of Advanced Manufacturing Technology*, *94*, 3563–3576.

Tao, F., Zhang, H., Liu, A., & Nee, A. Y. C. (2019). Digital twin in industry: State-of-the-art. *IEEE Transactions on Industrial Informatics*, *15*(4), 2405–2415. https://doi.org/10.1109/TII.2018.2873186

Tepper, N. (2011). Exploring the use of model-based systems engineering (mbse) to develop systems architectures in naval ship design.

Thies, F., & Ringsberg, J. W. (2023). Retrofitting wasp to a ropax vessel—design, performance and uncertainties. *Energies*, *16*(2), 673.

Tibco. (2023). What is a neural network? https://www.tibco.com/reference-center/what-is-a-neural-network

Tiseo. (2023). Topic: Shipping emissions worldwide. https://www.statista.com/topics/11288/shipping-emissions-worldwide/#topicOverview

Tissera, M. D., & McDonnell, M. D. (2016). Deep extreme learning machines: Supervised auto-encoding architecture for classification. *Neurocomputing*, *174*, 42–49. https://doi.org/https://doi.org/10.1016/j.neucom.2015.03.110

Toossi, R. (2013). Marine vehicles. https://www.thermalfluidscentral.org/encyclopedia/index.php/Marine_Vehicles

Uyanık, T., Karatuğ, Ç., & Arslanoğlu, Y. (2020). Machine learning approach to ship fuel consumption: A case of container vessel. *Transportation Research Part D: Transport and Environment*, *84*, 102389. https://www.sciencedirect.com/science/article/pii/S1361920920305769

Van Bruinessen, T., Smulders, F., & Hopman, H. (2014). Towards a different view on ship design.

van der Kolk, N., Bordogna, G., Mason, J., Bonello, J.-M., Vrijdag, A., Broderick, J., Larkin, A., Smith, T., Akkerman, I., Keuning, J., & Huijsmans, R. (2019). Wind-assist for commercial ships: A techno-economic assessment.

Van Os, J. (2018, October). *The Digital Twin throughout the Lifecycle* (Vol. Day 2 Thu, October 25, 2018).

Vesting, F., Gustafsson, R., & Bensow, R. E. (2016). Development and application of optimisation algorithms for propeller design. *Ship Technology Research*, *63*(1), 50–69. https://doi.org/10.1080/09377255.2016.1145916

Vigna, V., & Figari, M. (2023). Wind-assisted ship propulsion: Matching flettner rotors with diesel engines and controllable pitch propellers. *Journal of Marine Science and Engineering*, *11*(5). https://doi.org/10.3390/jmse11051072

Voermans, A., & Cales, T. (2020). Insight into energy saving devices - future marine propulsion systems - lecture slides. *TU Delft - Wärtsilä*.

Wang, H. (2014). The end of the era of heavy fuel oil in maritime shipping. *The International Council on Clean Transportation (ICCT)*. http://www.theicct.org/blogs/staff/end-era-heavy-fuel-oil-maritime-shipping

Wang, H., & Hon, G. (2011). Reducing greenhouse gas emissions from ships. https://theicct.org/sites/default/files/publications/ICCT_GHGfromships_jun2011.pdf

Wartsila. (2020). GATE RUDDER™ manoeuvring device - Wärtsilä. https://www.wartsila.com/marine/products/propulsors-and-gears/energy-saving-technology/gate-rudder-tm

Wei, Y., Sun, G., & Wan, D. (2023). Hull form optimization using bayesian optimization framework. *The 33rd International Ocean and Polar Engineering Conference*.

Wilkins, J. (2016, October). *Retrofit your way to industry 4.0*. https://www.eurekamagazine.co.uk/content/blogs/guest-blog-retrofit-your-way-to-industry-4-0

Witzgall, F. (2023). *Aerodynamic modelling of wind-assisted ship propulsion* [Master's thesis, Institut Supérieur de l'Aéronautique et de l'Espace] [Thesis completed at French Alternative Energies and Atomic Energy Commission (CEA)].

Woodyard, D. (2009). *Pounder's marine diesel engines and gas turbines*. Butterworth-Heinemann.

Wu, X., Feng, Y., Xu, G., Zhu, Y., Ming, P., & Dai, L. (2023). Numerical investigations on charge motion and combustion of natural gas-enhanced ammonia in marine pre-chamber lean-burn engine with dual-fuel combustion system. *International Journal of Hydrogen Energy*, *48*(30), 11476–11492. https://www.sciencedirect.com/science/article/pii/S0360319922019280

Xiao, W., He, M., Wei, Z., & Wang, N. (2022). Swlc-dt: An architecture for ship whole life cycle digital twin based on vertical–horizontal design. *Machines*, *10*(11), 998. https://doi.org/10.3390/machines10110998

Yang, T., Yang, Z., Zhang, Y., & Yuan, C. (2019). Research progress on ship speed optimisation for energy efficiency improvement. *Navigation of China*, *42*(3), 130–134.

Yasar, K., & Wigmore, I. (2023, March). What is black box ai? definition from techtarget. https://www.techtarget.com/whatis/definition/black-box-AI

Yoo, S.-L., & Kim, K.-I. (2023). Deep learning-based prediction of ship transit time. *Ocean Engineering*, *280*. https://doi.org/10.1016/j.oceaneng.2023.114592

Yuan, J., & Nian, V. (2018). Ship energy consumption prediction with gaussian process metamodel [Cleaner Energy for Cleaner Cities]. *Energy Procedia*, *152*, 655–660. https://www.sciencedirect.com/science/article/pii/S1876610218307719

Zhang, H., Li, G., Hatledal, L. I., Chu, Y., Ellefsen, A. L., Han, P., Major, P., Skulstad, R., Wang, T., & Hildre, H. P. (2022). A digital twin of the research vessel gunnerus for lifecycle services: Outlining key technologies. *IEEE Robotics Automation Magazine*, 2–15. https://doi.org/10.1109/MRA.2022.3217745

Zhao, Y., Fan, Y., Fagerholt, K., & Zhou, J. (2021). Reducing sulfur and nitrogen emissions in shipping economically. *Transportation Research Part D: Transport and Environment*, *90*, 102641. https://www.sciencedirect.com/science/article/pii/S1361920920308269

Zwart, R. (2020). *Trim optimization for ships in service* [Master's thesis, TU Delft]. http://resolver.tudelft.nl/uuid:599cfbd1-489f-406f-8ddf-64416fd7a53b